

# Magnetic nanoparticulate catalysts in flow processes

Smugowski, Hubert Jakub

*Award date:*
2011

*Awarding institution:*
University of Bath

# Magnetic nanoparticulate catalysts in flow processes

Hubert Smugowski

A thesis submitted for the degree of Doctor of Philosophy
University of Bath
Department of Chemical Engineering
September 2011

# -ACKNOWLEDGMENTS-

*I would like to thank Dr. Urszula Laska and*
*Dr. Pawel Plucinski for all their help.*

*Thanks are also due to Prof. Gareth Price, Dr. Chris Frost,*
*Dr. Sofia Pascu and Mr. Rory Arrowsmith.*

*I would like to thank John Bishop, Fernando Acosta, Robert Brain, and*
*Ursula Potter for their technical support.*
*Most of all I would like to thank all my friends and colleagues.*

**List of contents**

**List of figures**

**List of schemes**

**List of tables**

**Abbreviations**

9BP - 9-bromophenanthrene

AAS - Atomic Absorption Spectroscopy

App. - Appendix

R-BINAP - (*R*)-(+)-(1,1'-Binaphthalene-2,2'-diyl)bis(diphenylphosphine)

R-BINAS - Sulfonated (*R*)-(+)-(1,1'-Binaphthalene-2,2'-diyl)bis(diphenylphosphine)

DMIT - dimethyl itaconate

EDX - Energy-Dispersive X-ray spectroscopy

Eq. - Equation

ee - enantiomeric excess

GC - Gas Chromatography

IR - Infrared Spectroscopy

MNP - magnetic nanoparticles

NB - nitrobenzene

NMR - Nuclear Magnetic Resonance

R-P-Phos - (R)-(+)-2,2',6,6'-Tetramethoxy-4,4'-bis(diphenylphosphino)-3,3'-bipyridine)

P-Xyl-Phos - (R)-(+)-2,2',6,6'-Tetramethoxy-4,4'-bis(di(3,5-xylyl)phosphino)3,3'bi-pyridine)

S/C - substrate to catalyst ratio

sec - section

TEM - Transmission Electron Microscopy

TLC - Thin Layer Chromatography

XPS - X-ray Photoelectron Spectroscopy

**Symbols**

$c_0$ - initial concentration [kmol $m^{-3}$]

$d$ - capillary diameter [m]

$m_{cat}$ - mass of catalyst [g]

$(-r_A)$ - rate of reaction [kmol $g_{cat}^{-1}$ $s^{-1}$]

$Re$ - Reynolds number [-]

$u_s$ - superficial velocity [$m^3$ $m^{-2}$ $s^{-1}$]

$\upsilon$ - volumetric flow rate [$m^3$ $s^{-1}$]

$X$ - conversion [-]

$\eta$ - dynamic viscosity [N s $m^{-2}$]

$\rho$ - density [kg $m^{-3}$]

$\tau$ - residence time [s]

$\upsilon_L$ – volumetric flow of liquid [$cm^3$ $min^{-1}$]

$\upsilon_G$ - volumetric flow of gas [$cm^3$ $min^{-1}$]

n – rotation rate [$min^{-1}$]

$\beta$ – saturation [-]

**Abstract**

Homogeneous catalysts are highly efficient but their separation and recovery from the products can be problematic. Conversely, heterogeneous systems can suffer from lower catalytic activities, generally due to limited mass transport of reactants to the solid surface of the catalyst. The separation of (nano)catalyst is a difficult chemical process and the heavy metals contamination in the product is undesirable and must be limited to ppm. Approach to overcome these drawbacks is described in this work. Iron oxide magnetic nanoparticles were evaluated as a support for different catalysts as an example of semi-homogenous catalytic systems and these were described in the first part of this work. A range of catalysts supported onto magnetic nanoparticles was utilized in different catalytic reactions, including: hydrogenation, oxidation, epoxidation. A variety of coatings, including alumina, carbon, and silica were used in order to establish the way of protecting nanoparticles from aggregation. Silica was chosen to be the best protecting material. The second part of this thesis covers the investigations carried out to design and construct a capillary reactor with magnetically entrapped and manipulated nanoparticle catalysts for continuous hydrogenation and Suzuki C-C coupling reaction. For both reactions, high conversion was achieved, and no noticeable loss of catalyst was observed. Other potentially highly valuable new technology for performing chemical synthesis was described in this thesis, which includes hydrogenation of nitrobenzene, dimethyl itaconate and tandem Knoevenagel condensation - hydrogenation process in a microreactor, with a thin layer of nanocatalysts entrapped and moved by the external magnetic field. The possibility of trapping and moving nanocatalyst without any separation devices inside the reactor opens new avenues in the area of catalytic flow chemistry. The preparation of multi-modal imaging agents using magnetic nanoparticles was also studied. Silica coated magnetic nanoparticles were modified with quantum dots, showing possibility of preparation of fluorescent probe. MNPs were also radiolabeled using copper-64, which suggest potential of this material as multimodal imaging agent. Initial *in vitro* experiments suggested that the nanoparticles have potential to enter cells and to act as MRI/PET imaging agents.

**Introduction**

Charles H. Duell, the commissioner of the United States Patent and Trademark Office 1899, is famous for purportedly saying *"Everything that can be invented has been invented."* [1]. That statement has been proven wrong many times. One area which has the potential to develop many significant inventions was introduced in the lecture by Richard Feynman, "Plenty of Room at the Bottom" [2]. The lecture was presented at the annual meeting of the American Physical Society, in the California Institute of Technology (Caltech). During this talk, the foundations of nanoscience were declared, and groundbreaking possibilities were presented for producing small scale materials. This speech was revolutionary and inspiring.

In the preface of the book Nanochemistry by Geoffrey A. Ozin and Andre C. Arsenauly [3], it is written *"In the beginning there was Nano……"* . Nowadays, this word is no longer reserved for the world of science, it has entered into public consciousness. Nanoscience is challenging, amazing, and multi-disciplinary, it is hardly surprising that during the past decade nanoscience research has rapidly progressed across the globe.

In the preface of his book about nanoparticles, Janson H. Fendler stated *"small is not only beautiful but also eminently useful"* [4]. Enormous interest in nanoscience has brought exponentially increasing numbers of research publications. The incredible rush in this area of science can be explained by the unique properties of nanomaterials. Nanoscience accelerated after two major developments: the birth of clusters science, and secondly the construction of the scanning tunnelling microscope. Huge potential is being found in the properties of new nanomaterials like fullerens, carbon nanotubes, semiconductor nanocrystals, metal oxide nanoparticles and quantum wires and dots.

K. Eric Dexler wrote in his book about the coming Era of Nanotechnology, *"It looks like it is not the end of nano-scientific discoveries, which are like an engine, driving to the next industrial revolution. It could have more influence on our lives than the two greatest inventions in that domain: the replacement of sticks and stones by metals and cements, and the harnessing of electricity"* [5].

Grunes [4], in his article in Chemical Communications stated that catalysis is the main area of interest in nanotechnology and nanoscience. This is because of two

main problems: firstly, the variable activity and selectivity presented by heterogeneous catalysis, and secondly the problems presented during separation by homogeneous catalysis. The solution of these problems will be presented through the application of "semi-heterogeneous catalysis" which is called in the literature the frontier between homogeneous and heterogeneous catalysis [6].

In this work, I will present modern materials, especially magnetic nanoparticles, and their properties and possibilities for use in modern catalysis.

# CHAPTER 1

## Catalysts supported on magnetic nanoparticles

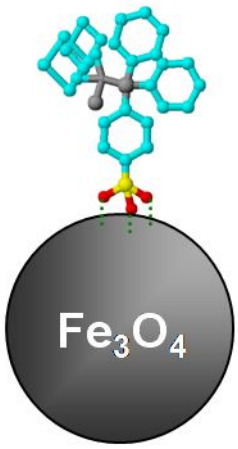


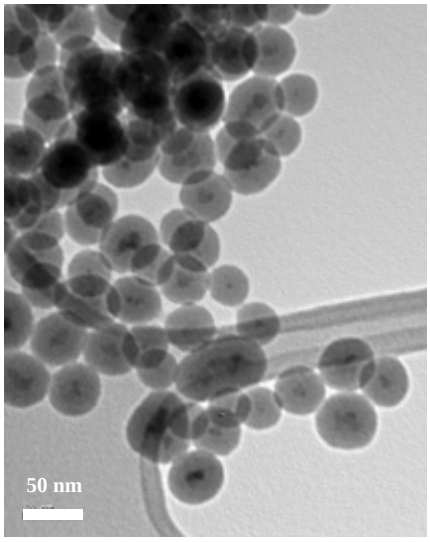

## 1.1 Catalysis and catalysts

In many chemistry books, reviews, and articles there is particular emphasis on the wonder of the catalysis phenomena. Hagen [8] called catalysis the key to chemical transformation, while Thomas and Thomas [9] described it as the occupant of a pivotal position in the chemical, physical and biological sciences. Herrmann [10] estimated that 90 % of all commercially produced chemical products involve catalysts at some stage in the process of their manufacture. Bell [11] stated that everything that modern society requires is owed to the invention of catalysis: inexpensive transportation fuels, lubricants, high strength polymers, drugs for 'incurable' diseases, stain resistant fibres, and others.

The term "catalysis" was introduced as early as 1836 by Berzelius in order to explain various decompositions and transformations of reactions [8]. He associated catalysts with substances endowed with some mysterious quality, and talked of a catalytic force. Berzelius hypothesized that a catalyst possesses magical powers that influence the affinity of chemicals. A more appropriate definition, which is still valid nowadays, was proposed by Ostwald (1895) *"a catalyst accelerates a chemical reaction without affecting the position of equilibrium"* [8]. A catalyst is defined as a substance, that increases the rate of attainment of chemical equilibrium without undergoing chemical change itself [9]: a substance which changes the kinetics but not the thermodynamics [12]. Catalysts work by providing an (alternative) mechanism involving a different transition state and lower activation energy. The effect of this is that more molecular collisions have the energy needed to reach the transition state. Hence, catalysts can perform reactions that, albeit thermodynamically feasible, would not run without the presence of a catalyst, or perform them much faster, more specificly, or at lower temperatures. This means that catalysts reduce the amount of energy needed to initiate a chemical reaction. Catalysts cannot make energetically unfavourable reactions possible — they have no effect on the chemical equilibrium of a reaction because the rate of both the forward and the reverse reaction are equally affected. The net free energy change of a reaction is the same whether a catalyst is used or not; the catalyst just makes it easier to activate. According to the catalyst definition, it is supposed to remain unchanged after a chemical reaction, and be characterized by easy recovery and reuse. It is

desirable from both an economical and an environmental viewpoint [13]. Catalysts can be either heterogeneous or homogeneous. Heterogeneous catalysts are in a different phase from the reactants, *e.g.* a solid catalyst in a liquid reaction mixture, whereas homogeneous catalysts are in the same phase, *e.g.* a dissolved catalyst in a liquid reaction mixture.

### 1.1.1 The difference between homo- and heterogeneous catalysis

Homogenous catalysts offer a number of important advantages, which their heterogeneous counterparts do not have. A homogenous catalyst is highly selective and active, this is usually the result of high accessibility of the catalytic site, good diffusion, because the catalyst is usually a dissolved metal complex. Additionally, it is possible to tune the chemo-, regio- and enantioselectivity. In spite of these advantages, many homogenous catalysts cannot be used in industry. The main disadvantage of homogenous catalyst is the difficulty in the separation process. The problem is that the most conventional separation process – distillation, requires an elevated temperature, and most homogenous catalysts are sensitive to temperature, resulting in catalyst decomposition. Other well known separation methods like chromatography or extraction typically lead to the loss of the catalyst [14]. On the other hand, with heterogeneous catalysis, there are no problems with separation of the catalyst, but an effective concentration of catalyst might be lost, since the reaction occurs only on the exposed active surface.

## 1.2 Nanoparticles

In recent years, there has been a dramatic increase in the interest in nanocatalysis due to new developments in nanomaterial sciences, a statement confirmed by the large number of publications in this field. However, the literature about nanoparticles is unclear about definitions and terminology. Scientists predominantly define a “nanoparticle” as a microscopic particle with at least one dimension less than 100 nm. The word “nano” comes from Greek and means “dwarf”, referring to a size reduction of $10^{-9}$. One nanometer (nm) is one billionth of

a meter and is equivalent to ten Angstroms [15]. The best description of the size of nanoparticles is shown in the picture below, adapted from the article of Gu (Figure 1) [16].

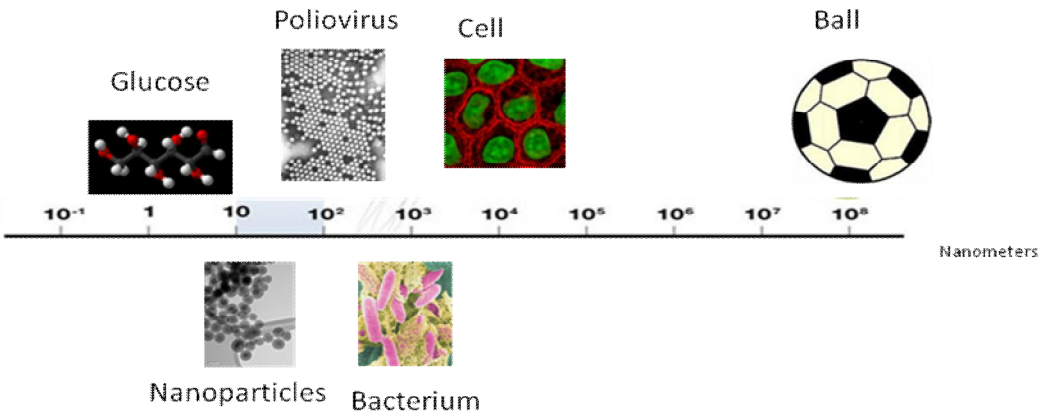


Figure 1. Comparison of the size of atom, nanoparticles and biological entities. Adapted from [16].

Nanoparticles are of great scientific interest as they are effectively a bridge between bulk materials and atomic or molecular structures. They are intently studied because of their novel features. A bulk material should have constant physical properties regardless of its size, but at the nanoscale this is often not the case. Size-dependent properties are observed, such as quantum confinement in semiconductor particles, surface plasmon resonance in some metal particles, and superparamagnetism in magnetic materials. The properties of materials change as their size approaches the nanoscale, and as the percentage of atoms at the surface of a material becomes significant. Nanoparticles exhibit quantum size effects, and have a huge surface area, which has an influence on magnetic properties. Iron oxide nanoparticles exhibit superparamagnetism and quantum tunneling of magnetization. The main reason for this distinctive feature is that each nanoparticle is considered as a single domain. One of the most interesting properties is that in most cases superparamagnetic particles do not retain any magnetization after removal from the magnetic field [17].

### 1.2.1 Iron oxide

Iron oxide is one of the oldest and most popular materials, widespread not only in nature but in laboratories and industry as well. There are sixteen known iron oxides altogether, including hydroxides and oxide hydroxides [18]. The most significant types for chemistry and industry are hematite ($\alpha$-$Fe_2O_3$), maghemite ($\gamma$- $Fe_2O_3$), magnetite ($Fe_3O_4$), goethite ($\alpha$-Fe(O)OH), and ferric hydroxide ($Fe(OH)_3$). Iron oxides have many applications, *e.g.* in the cosmetic industry, magnetic storage, medicine and many others. Magnetite is a common magnetic iron oxide that has a cubic inverse spinel structure with oxygen forming fcc closed packing and Fe cations occupying an interstitial tetrahedral and octahedral sites. The electrons can hop between $Fe^{2+}$ and $Fe^{3+}$ in the octahedral sites at room temperature, rendering $Fe_3O_4$ an important class of half metallic materials [19] .

### 1.2.2 Magnetic properties of iron oxide nanoparticles and colloidal stability

Iron oxide nanoparticles can be classified by their response to an external magnetic field [20]. The magnetic feature depends on the B (magnetic induction) and H (magnetic field). Most of the materials show ferromagnetic behaviours, *e.g.* Co, Fe, Ni. Ferromagnetism is defined as the phenomenon by which materials in an external magnetic field become magnetized and remain magnetized for a period of time. In the case of many materials, the relation between B and H is linear (Eq.1).

$$B = \mu H \qquad (1)$$

$\mu$ - magnetic permeability of the particles [H $m^{-1}$],
for paramagnetics $\mu > 1$, for diamagnetics $\mu < 1$, for vacuum $\mu = 1$.

There is another parameter describing magnetic properties: the magnetic susceptibility, which is also the degree of magnetization of a material in response to an applied magnetic field, defined as follows:

$$\chi = \mu - 1 \quad (2)$$

again for paramagnetics $\chi > 0$, for diamagnetics $\chi < 0$, for vacuum $\chi = 0$.

Superparamagnetism of nanoparticles enables them to have stability and dispersion upon removal of the magnetic field, as no residual magnetic forces exist between particles. In the case of iron oxide nanoparticles smaller than 15 nm, the phenomenon of ferromagnetism is not observed. Below size 15 nm, nanoparticles exhibit very strong paramagentism. Paramagnetism can be understood as permanent atomic magnetic moments, which can be reoriented in an external field. The torque applied by this external magnetic moment will tend to orientate them parallel to the field, reinforcing it. These magnetic domains are disordered in the absence of a magnetic field, but when a field is applied, the magnetic domains align to create a magnetic moment much greater than the sum of the individual unpaired electrons. This does not, however, result in residual magnetization of the particles [21, 22].

A crucial factor, described by Rosensweig [23] of magnetic nanoparticles colloidal solution stability, involves competition between: thermal energy (Eq. 3), magnetic energy (Eq. 4), and gravitational energy (Eq. 5), denoted as $E_t$, $E_m$ and $E_g$ respectively:

$$E_t = k\,T \quad (3)$$

$k = 1.38\,10^{-23}$ [J $K^{-1}$] – The Boltzmann constant,
T [K] – absolute temperature.

$$E_m = \mu_0\,M_d - H\,V \quad (4)$$

$\mu_0 = 4\pi\,10^{-7}$ [H $m^{-1}$] – magnetic permeability of free space,
$M_d$ [A $m^{-1}$] – particles magnetization,
H [A $m^{-1}$] – magnetic field,
V [$m^3$] – magnetic volume of spherical fluid nanoparticle of diameter D.

$$E_g = \Delta\rho \, V \, L \, g \quad (5)$$

$\Delta\rho$ [kg $m^{-3}$] – difference between the powder and the fluid densities,
V [$m^3$] – magnetic volume of spherical fluid nanoparticle of diameter D,
g [N $m^2$ $kg^{-2}$] – gravitational constant,
L [G] – elevation in the gravitional field.

Stability against settling in a magnetic field requires the thermal energy to be large in comparison to the magnetic energy. Another important parameter is the stability against magnetic agglomeration. It is widely accepted that the collision between particles is a common phenomenon. Each particle is permanently magnetized, causing clustering and instability in a magnetic field gradient. The use of an adequate dispersant, however, can prevent these phenomena.

### 1.2.3 Synthesis of iron oxide nanoparticles

Nanostructured particles can be synthesized in two ways: either through “top down” methods such as mechanical grinding of bulk material (for example ball milling), involving the breaking down of large pieces of material to generate the required nanostructures, or by a “bottom up” approach, which involves assembling single atoms or molecules into larger nanostructures [24].

#### 1.2.3.1 Physical methods

Wet grinding is a historical physical method consisting of ball-milling micron-sized particles of ferrite in the presence of a suitable surfactant acting as a grinding aid and a carrier, until the ferrite is in a colloidal state. A surfactant is present to prevent aggregation and the quantity used corresponds approximately to a monolayer coating on the particles. This remains a very time-consuming process (*approx*. 1000 h), and accordingly as a mode of preparation it cannot be applied to a large scale production [25]. For a long time the synthesis of customized size and shape nanoparticles was a scientific challenge. Several authors investigated other

physical methods, *e.g.* gas phase deposition, electron beam lithography or infrared laser pyrolysis [26], all of which suffer from the inability to control the size of nanoparticles.

### 1.2.3.2 Co-precipitation method

"Bottom up" approaches are usually chemical methods, which can produce nanoparticles with narrow size and shape distribution. Synthesis of magnetic nanoparticles can be done through the co-precipitation of an aqueous $Fe^{2+}/Fe^{3+}$ salt solution, by the addition of a base under inert conditions at room temperature. The composition, shape and size of nanoparticles depends on the type of salt used (*e.g.* chlorides, sulphates, nitrates, perchlorates) and other conditions such as: temperature, $Fe^{2+}$ and $Fe^{3+}$ ratio, the pH value and the ionic strength of the media. One conventional method of synthesis entails the addition of a base solution to an aqueous mixture of $Fe^{2+}/Fe^{3+}$ (molar ratio 1:2) (Scheme 1).

$$Fe^{2+} + 2Fe^{3+} + 8OH^{-} \longrightarrow Fe_3O_4 \text{ (black precipitate)} + 4H_2O$$

Scheme 1. The synthesis of $Fe_3O_4$ using co-precipitation method.

According to the results of thermodynamic studies of this process, complete precipitation should be expected between pH = 7.5 to 14, while maintaining a molar ratio of 2:1 under a non-oxidizing environment, otherwise $Fe_3O_4$ can be oxidized to $Fe(OH)_3$, as shown in the reaction below:

$$Fe_3O_4 + 0.25\ O_2 + 4.5\ H_2O \longrightarrow 3Fe(OH)_3$$

Scheme 2. Oxidation of $Fe_3O_4$ under oxidizing conditions.

During the entire synthesis, nitrogen is bubbled through the solution for two reasons, firstly because it protects the critical oxidation of magnetite, and secondly because it produces a smaller particle size compared to other methods where oxygen

is present. The magnetite is then mixed with an aqueous tetramethyl ammonium hydroxide [$(CH_3)_3NOH$] solution or other stabilizing agent to form surfactant coating [21, 27, 28]. One of the most important merits of this method is repeatability, which means that once the synthetic conditions are fixed, the quality of the nanoparticles is fully reproducible [22].

### 1.2.3.3 Thermal decomposition

The thermal decomposition method was used first for the synthesis of high quality semiconductor nanocrystals in the non-aqueous media. A similar procedure was applied for the synthesis of magnetic nanoparticles. Monodispersed magnetic nanocrystals of smaller size can essentially be synthesized through the thermal decomposition of organometalic compounds in high boiling-point organic solvents, containing stabilizing surfactants [22]. Sun *et al.* [19] investigated the synthesis of monodispersed magnetic nanoparticles by a high-temeperature solution-phase decomposition of $Fe(AcAc)_3$ in phenyl ether with alcohol, oleic acid, and oleylamine (Scheme 3).

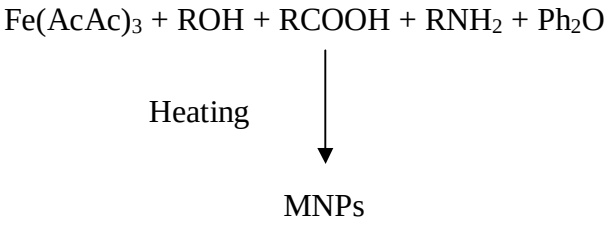


Scheme 3. Thermal decomposition mode of preparation of magnetic nanoparticles. Adapted from [19].

It was mentioned in the paper that the obtained nanoparticles can be easily transformed into either $\gamma$-$Fe_2O_3$ or $\alpha$-$Fe_2O_3$ nanoparticles assemblies by annealing. The investigation proved that particles obtained through this mode of preparation exhibit superparamagnetism. In another article, Sun *et al.* [29] reported a convenient

organic phase process of making monodispersed $MFe_2O_4$ nanoparticles (M = Fe, Mn, Co, Ni, Cr), with a tuneable diameter from 3 to 20 nm, dependent on conditions.

Jana *et al*. [30] proposed a different approach to the synthesis of magnetic nanoprticles, which consists of the pyrolysis of metal fatty acids salts, the most common metal compounds compatible with nonaqueous solutions (Scheme 4). The reaction system is based on: fatty acids (decanoic, lauric, myristic, palmitic, oleic and stearic), a hydrocarbon solvent (octadecan, n-eicosane, tetracosane or a mixture of them), and an activation reagent. The authors showed the possibilities of producing nanocrystals with an adjustable size (3-50 nm) and shape including dots and cubes.

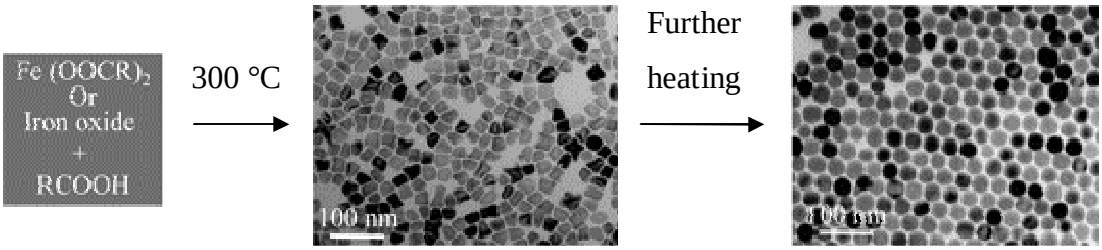


Scheme 4. Formation of $Fe_3O_4$ nanocrystals using pyrolysis method. Adapted from [30].

The control of the size and shape was done by changing the length and concentration of the fatty acids, ligand and precursor. This method was further applied for the growth of oxide nanocrystals of the other magnetic metals ($Cr_2O_3$, MnO, $Co_3O_4$, and NiO nanocrystals). The authors also revealed, that the surface ligands of these magnetic oxide nanocrystals can be readily replaced by dendron ligands, resulting in soluble and extremely stable dendron nanocrystals in a variety of solvents. It was stated that extension of this strategy to a large scale was possible.

A similar method for $Fe_3O_4$ nanoparticles preparation was used by Hyeon *et al.* [31]. The authors put in to use nontoxic and inexpensive iron (III) chloride and sodium oleate for the synthesis of an iron oleate complex, which was decomposed afterward in a temperature range of 240-320 °C. The process is shown in Scheme 5.

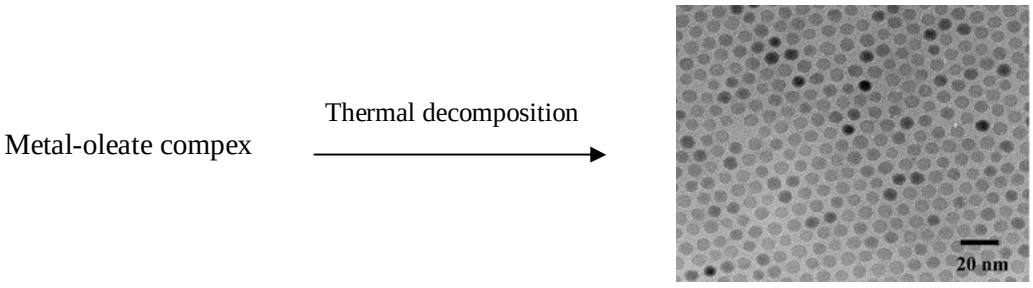


Scheme 5. Thermal decomposition of metal oleate complex. Adapted from [31].

The decomposition temperature and aging period have an influence on particle sizes (5-22 nm). In this synthesis, aging was determined to be a necessary step for the formation of iron oxide nanoparticles. The nanoparticles obtained are dispersible in various organic solvents including hexane and toluene. However, it is unclear whether the particles could also be dispersed in water.

Li *et al*. [32] recently presented a method in which $FeCl_3 \cdot 6H_2O$ was used as a iron source in the preparation of magnetic nanocrystals. Additionally, the mechanism leading to $Fe_3O_4$ in 2-pyrrolidone is discussed and presented below (Scheme 6).

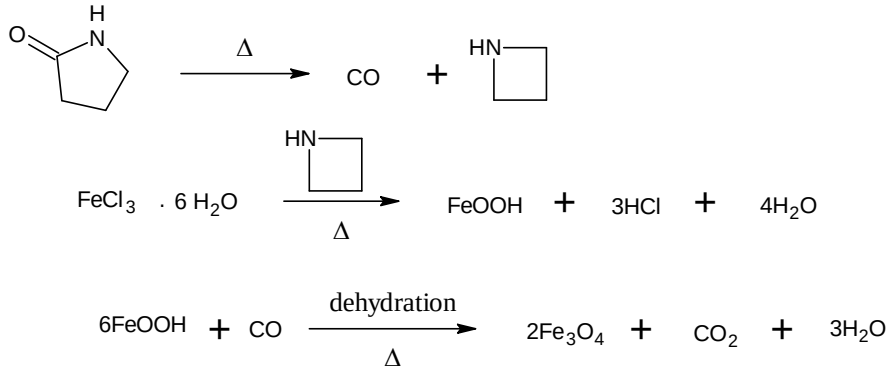


Scheme 6. Mechanism leading to $Fe_3O_4$ in 2-pyrrolidone. Adapted from [32].

They ascertained that the particle size can be controlled at 4, 12, and 60 nm, when the reflux time is 1, 10, and 24 h respectively. With increasing reflux time, the shapes of the particles changed from spherical at an early stage to cubic morphologies for the longer reflux times.

### 1.2.3.4 Hydrothermal synthesis

A broad range of nanomaterials, including iron oxide nanoparticles, can be synthesized under hydrothermal conditions. Wang *et al*. [33] reported a generalized hydrothermal method for synthesizing a variety of different nanocrystals by a liquid-solid-solution reaction. The system consists of metal linoleate (solid), an ethanol-linoleic acid (liquid phase), and a water-ethanol (solution) at different reaction temperatures under hydrothermal conditions. The whole concept of this synthesis is based on a general phase transfer and separation mechanism occurring at the interfaces of the liquid, solid, and solution phases present during the synthesis. A phase transfer process of the metal ions occur spontaneously across the interface of sodium linoleate (solid) and the water–ethanol solution (solution) based on ion exchange, which led to the formation of metal linoleate and the entering of the sodium ions into the aqueous phases. The ethanol in the liquid and solution phases reduced the metal ions at the liquid–solid or solution–solid interfaces, which resulted in production of nanocrystals. Using this mode of preparation, the $Fe_3O_4$ nanoparticles can be synthesized in uniform sizes of approximately 9 and 12 nm.

A similar approach to the process of producing nanoparticles was reported by Deng *et al*. [34]. The synthesis of monodispersed, hydrophilic, single-crystalline ferrite microspheres was done using a hydrothermal reduction. A mixture consisting of $FeCl_3$, ethylene glycol, sodium acetate, and polyethylene glycol was stirred vigorously to form a clear solution, then sealed in a Teflon®-lined stainless steel autoclave, heated to 200 °C, and maintained at this temperature for 8-72 h. Ethylene glycol, which was used in this reaction, is a strong reducing agent with a relatively high boiling point. It has been widely used in the polyol process to provide monodispersed fine metal or metal oxide nanoparticles. However, magnetic spinel ferrite particles have a tendency to agglomerate during their formation in the liquid-phase process. To obtain monodispersed $Fe_3O_4$ particles, a modified synthesis was designed, with the addition of sodium acetate for electrostatic stabilization to prevent particle agglomeration. Importantly, the addition of NaAc assists in the ethylene glycol-mediated reduction of $FeCl_3$ to $Fe_3O_4$. This approach provides a one step, simple, and inexpensive method for the preparation of monodispersed magnetic microspheres with a tuneable diameter range of 200-800 nm.

### 1.2.3.5 The synthesis of nanoparticles in microemulsion

The term microemulsion refers to a single isotropic phase that is a mixture of oil, water and surfactant, or to one that is in equilibrium with coexisting oil and/or aqueous phases, or even to other non-isotropic phases [35]. In water-in-oil microemulsions, the aqueous phase is dispersed as microdroplets (typically 1-50 nm in size) surrounded by a monolayer of surfactant molecules in the continuous hydrocarbon phase [21]. The micro droplets continuously collide, coalesce, and break again, and finally a precipitate forms in the micelles. This is as a result of mixing two identical water-in-oil (w/o) microemulsions containing the desired reactants. The addition of a solvent such as acetone or ethanol to the microemulsions causes precipitation. The extraction of this precipitate can be carried out by filtering or centrifuging the mixture. In this sense a microemulsion can be used as a nanoreactor for the formation of nanoparticles (Figure 2) [22].

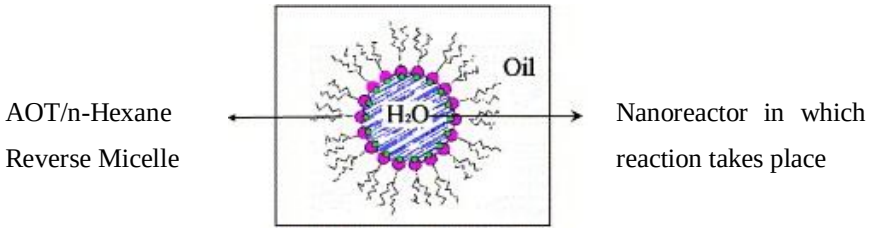


Figure 2. Structure of reverse micelles formed by dissolving AOT, a surfactant in hexane. Adapted from [21].

Gobe *et al*. [36] reported synthesis of superparamagnetic iron oxide nanoparticles with narrow size distribution prepared using an inverse microemulsion. The preparation was carried out by using the aqueous core of aerosol-OT (Dioctyl sodium sulfosuccinate) (AOT)/*n*-hexane reverse micelles (w/o microemulsion). The reverse micelles have an aqueous inner core, which can dissolve hydrophilic compounds. An aqueous solution of $Fe^{3+}$ and $Fe^{2+}$ salts (molar ratio 2:1) was dissolved in the aqueous core of the reverse micelles formed by AOT in *n*-hexane. Chemical precipitation was then achieved by using a deoxygenated solution of sodium hydroxide. The size of the inner aqueous core of reverse micelles is in the nanometer range, so the magnetic nanoparticles prepared inside these nanoreactors

are found to be very small in size, with a narrow size distribution. Several authors have presented slightly modified modes of preparing nanoparticles using microemulsion. Yacob *et al.* [37] presented the results of the production of MNP by precipitation within spontaneously generated micelles from mixtures of single-tailed cationic and anionic surfactants (cetyltrimethylammonium bromide (CTAB) and dodecylbenzenesulphonic acid (DBSA) respectively). Igartua *et al.* [38] described the preparation of colloidal lipid particles containing magnetite from warm emulsions.

Many types of magnetic nanoparticles have been synthesized in a controlled manner using the microemulsion method, the particle size and shapes usually vary over a wide range. Compared to other methods, the yield of nanoparticles synthesis in microemulsion is low. Large amounts of solvent are necessary to synthesize appreciable amounts of material. Due to low efficiency, application of this mode of preparation in a large scale will not be possible [22].

### 1.2.4 Applications of nanoparticles

In the last decade magnetic nanoparticles have proven their outstanding properties repeatedly, which is why research on nanoparticles has been so intensively pursued. This has happened not only for the sake of their fundamental scientific interest, but also for their industrial use. In the next few sections many applications of magnetic nanoparticles will be presented, including catalysis, nanomedicine and cooling systems.

#### 1.2.4.1 Ferrofluids

The nomenclature in the case of magnetic liquids is disorganized. Ferrofluid (lat. ferrum-iron) [39], magnetic nanofluid [40], magnetic fluid [41] and magnetic liquid [42] are all names used to describe the colloidal suspension of nanoscale magnetic monodomain, with reference mainly to magnetite particles in non-conducting liquids. The particles are usually covered by an organic layer as they tend to agglomerate and coagulate. Ferrofluid is defined as a fluid consisting of 1 nm - 1 μm particles and a non-magnetic solvent [23]. The particles are small enough to perform Brownian motion, which is the result of local temperature

differences. Another advantage of Brownian motion is the lack of sedimentation of the nanoparticles in the solution [22].

The first water-based ferrofluid was synthesized by Elmor in 1938, but Papell discovered low viscosity of magnetic fluid in the early sixties, which was patented in 1965 [43]. Ferrofluids are used to form liquid seals (ferrofluidic seals) around the spinning drive shafts in hard disks. Liquid coolant is another common use of ferrofluids. One of the commercial applications is in megaphones and loudspeakers. Ferrofluids have another great feature: they can reduce friction. Due to refractive properties, ferrofluids have several optical applications [39, 44].

### 1.2.4.2 The application of magnetic nanoparticles in catalysis

In this section, emphasis will be put on the application of magnetic nanoparticles in catalysis. Guin *et al.* [45] claimed that the synthesis of surface-modified nanoparticles with appropriate surface modifying agents, and their application to specific catalytic reactions, is one of the major areas of current research in the field of catalysis. The next section will attempt to explain why synthesis of a new class of catalyst, anchored on magnetic nanoparticles, is so significant for modern nanocatalysis.

It is recognized that diffusion and mass transfer coefficients are lower in the liquid phase than in the gas phase. Consequently, interparticle and intraparticle transport limitations are likely to occur in liquid-phase reactions which are catalyzed by solid catalysts. Catalytic liquid phase processes are important in many areas of the fine and specialty chemicals industries, and the use of solid catalysts means easier catalyst separation, recovery and reuse. The activity, selectivity and stability of a solid catalyst suspended in a liquid phase can benefit greatly from the use of small catalyst particles ($< 1$ μm), and were found to be comparable to those of their parent catalysts in solution, or their counterparts immobilized on the solid face. Thus, it is widely accepted that a smaller catalyst particle means a higher activity. It seems that the immobilization of catalysts on the surface of a nanoparticular matrix not only facilitates the isolation and recovery, but also opens a new avenue to regulate the activity and selectivity. The main difficulty is that such small particles are almost

impossible to separate by conventional methods. However, the development of novel materials for immobilizing a catalyst which demonstrate magnetic properties should solve this problem [46, 47]. Additional features like high surface area (calculated as 600 $m^2 cm^{-3}$) [48] combined with a highly dispersed system shows enhanced catalytic behaviour over the current heterogeneous system. The surface of magnetic nanoparticles can be used as a support for noble metals. The separation of transition metals is a difficult chemical process, and the heavy metals contamination in the product is undesirable and must to be limited to ppm.

In summary, using magnetic nanoparticles as a catalyst support, especially when expensive and toxic metals and ligands are employed, offers high activity, selectivity, and minimal loss. It also offers easy separation, recovery and reuse. This catalytic system is of great economic and environmental importance in chemical and pharmaceutical industries reducing costs and providing environmental protection benefits [46].

Nanoparticles have been recognized as a great building material for a new class of catalysts known as nanocatalysts [15]. This part of the report will summarize and review the articles and present developments about magnetic nanoparticle-supported catalysts.

#### 1.2.4.2.1 MNP-based catalysts for C-C coupling reactions

Stevens *et al*. [49] recently reported on synthesis of a Pd-carbene catalyst supported on a composite of iron oxide nanoclusters and polystyrene polymer (Figure 3) for Suzuki C-C coupling reaction.

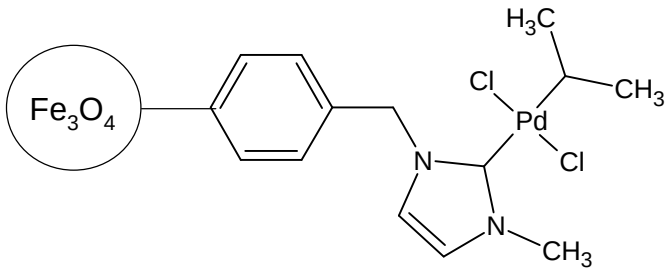


Figure 3. Pd-carbene catalysts supported on iron oxide nanoparticles-polystyrene complexes for Suzuki C-C coupling reaction. Adapted from [47].

Core/shell iron oxide nanoparticles were prepared *via* an emulsion polymerization approach for immobilization of Pd-NHC catalysts. These nanoparticle-supported catalysts are stable and demonstrated high catalytic activity in promoting Suzuki cross-coupling reactions. Magnetically isolated catalysts were recycled without the significant loss of catalytic activity.

The same group [50] examined a similar structure of Pd-carbene catalyst, immobilized on the surface of $Fe_2O_3$ nanoparticles without a polymer layer (Scheme 7).

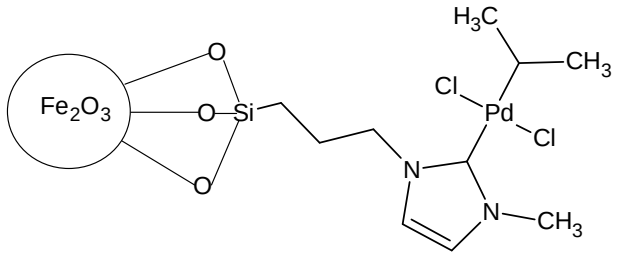


Scheme 7. The Pd-carbene catalyst immobilized on the surface of maghemite nanoparticles. Adapted from [50].

This catalyst was examined in Suzuki, Heck and Sonogashira cross-coupling reactions. The Pd-NHC complex, immobilized on maghemite nanocrystals, demonstrated stability in the organic media at reaction temperatures as high as 110 °C. After several reaction cycles, no significant loss of the catalytic activity of the immobilized catalyst was observed.

Zheng [51] investigated the use of magnetic nanoparticles as an orthogonal matrix to assist solid-phase reactions – a magnetic nanoparticle was able to enter the pores of solid-phase material. A magnetic, nanoparticle-supported, homogeneous Pd catalyst was employed for promoting the Suzuki cross-coupling of aryl halide on resins with an excessive arylboronic acid in the solution. A strong yield dependency on the size of magnetic nanoparticles used was observed. 87 % yield was obtained for 4 nm nanoparticles, 56 % and 32 % for 12 nm and 22 nm respectively. However, more than six days were required to complete the reaction because of the slow diffusion of the particles in and out of the resin pores.

Suzuki cross-coupling reactions catalyzed by Pd coordinated by Simanek-dendron functionalized magnetic nanoparticles were examined by Duanmu *et al.* [52] (Scheme 8).

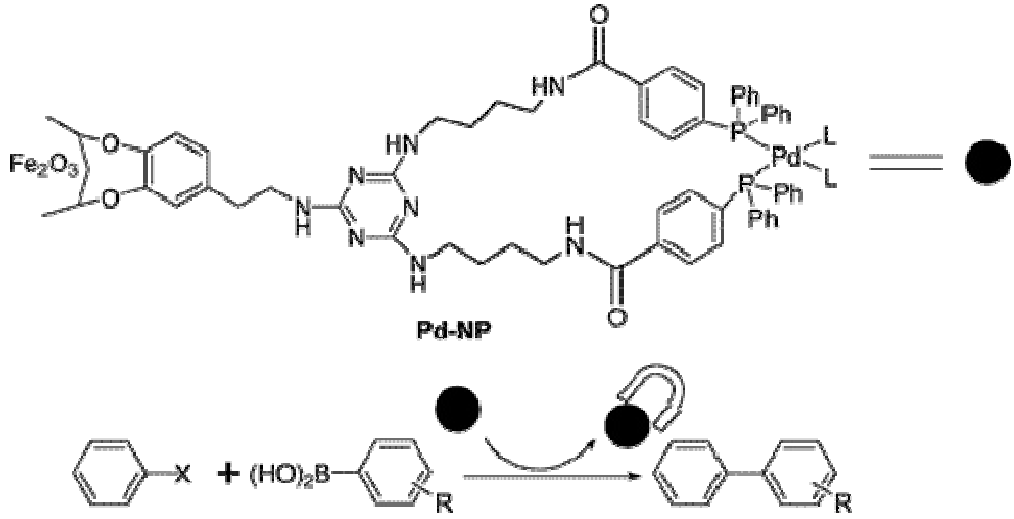


Scheme 8. Iron oxide nanoparticle-supported Pd catalyst for promoting Suzuki cross-coupling reactions. Reprinted with permission from [52]. Copyright (2006) American Chemical Society.

The authors presented a novel strategy for the fabrication of core-shell iron oxide/melamine dendron nanoparticles. Depending on the terminal groups of the dendritic shells, such nanocomposites could be selectively dissolved in water or in various organic media. The activity of the recovered catalyst was found to be maintained at the same level. 80 % yield was achieved for a second-round reaction between iodobenzene and phenylborate, compared with a similar 81 % yield in the first round.

Wang *et al*. [53] investigated the synthesis of palladium coated MNPs with assistance of (3-aminopropyl) trimethoxysilane. The catalytic behaviour of the $Pd/Fe_3O_4$ nanocomposite was investigated for the Heck coupling of acrylic acid with iodobenzene. The product yield decreased from 81 % in the first run to 53 % in the fifth run, then kept constant at 53 % in the subsequent re-use. The aggregation of magnetic catalyst bodies was proposed as the main reason for the decrease in catalytic activity.

Suzuki and Heck reactions have been investigated by Laska *et al*. [54] with a series of Pd catalysts, anchored on $Fe_3O_4$ nanoparticles. Two different types of catalysts were prepared. One used palladium complexes containing phosphine and/or acetate ligands, and the second consisted of $Pd^0$ coated magnetic cores. All the nanocomposite systems were tested for activity in the cross-coupling Heck reaction of styrene with 4-bromonitrobenzene, as well as in a Suzuki coupling between phenylboronic acid and bromobenzene. All of the studied systems were effective in both reactions. The catalysts were separated using an external magnetic field and recycled without the loss of activity seen in the case of nanoparticles coated with palladium acetate complexes and $Pd^0$-NPs. For nanoparticles containing phosphines ligands, there was a marked decrease of activity, observed as 90.8 % for the second run and falling to 12.5 % for the third run.

Zhu *et al*. [55] reported synthesis of 1 nm palladium (0) particles on magnetic nanoparticle support (Scheme 9). These catalysts were active for a Suzuki reaction of bromobenzene and phenylboronic acid with a yield of 83 %. The authors achieved 56 % yield in Heck coupling of bromobenzene and styrene. The catalyst can be easily separated using a magnet, and can be reused at least three times without showing any significant decrease in catalytic performance.

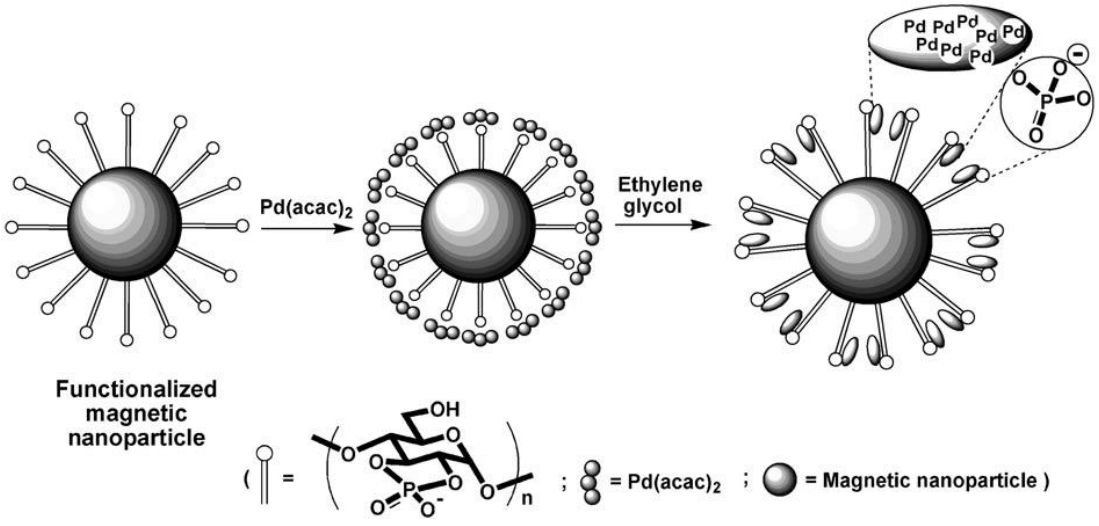


Scheme 9. Synthesis of magnetic nanoparticle-supported palladium nanoparticles Reprinted with permission from [55].

Immobilization of a dipirydylpalldium complex on MNPs using the click chemistry method (Scheme 10) was described by Lv *et al*. [56]. This catalyst exhibited high activity in Suzuki-Miyaura coupling of $PhB(OH)_2$ with bromobenzene. Various aryl halides and aryl boronic acids were used. In most cases, the reactions achieved a conversion of over 80 % in less than 12 h. Reuse of the catalyst was tested using Suzuki coupling of 4-bromoacetophenone and phenylboronic acid as a model reaction. No obvious loss in catalytic activity was observed over five recycling runs.

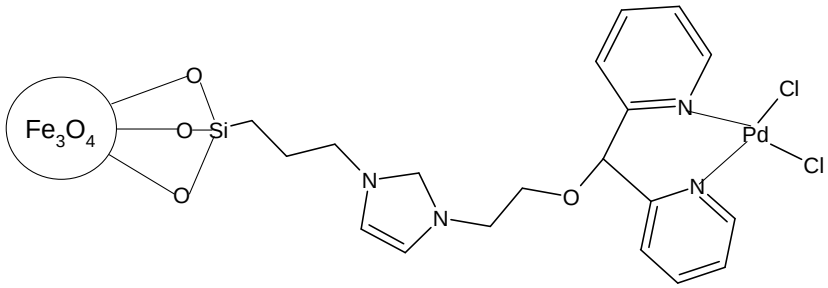


Scheme 10. MNP-supported di(2-pyridyl)methanol-Pd complex. Adapted from [56].

Chouhan *et al*. [57] investigated a $Fe_3O_4$ nanoparticle-supported proline ligand. It was used for a CuI catalyzed Ullmann-type coupling reaction of aryl/heteroaryl bromides with various nitrogen heterocycles. The mode of preparation is shown in Scheme 11. Azide-functionalized magnetite was prepared by treating the nanoparticles with the phosphonic ligand. Immobilization of the proline ligand was carried out by the Cu(I)-catalyzed alkyne-azide [2+3] cycloaddition reaction of $CuSO_4$, sodium ascorbate and triethyl amine to give the proline functionalized magnetic nanoparticles. The application of the CuI catalyst for arylation of the nitrogen nucleophiles was demonstrated. A variety of *N*-heterocycles such as pyrazole, indole and benzimidazole, and a variety of aryl and heteroaryl bromides were tested, providing the corresponding *N*-aryl products in good to excellent yields. The results indicated that both aryl and heteroaryl bromides work well, with the corresponding products having moderate to excellent yields. The recyclability of the magnetic nanoparticle-supported proline ligand was also studied. The nanoparticle-supported proline ligand can be reused for up to four runs without any significant loss of activity.

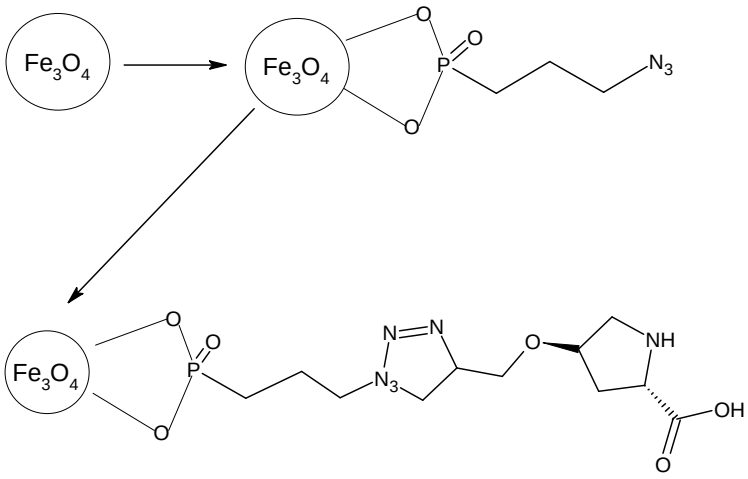


Scheme 11. Synthetic pathway of the production of proline functionalized magnetic nanoparticles. Adapted from [57].

Baruwati *et al*. [58] reported on the development of a highly active catalyst for Suzuki and Heck coupling reactions for aromatic halide derivates. A novel catalytic system was been designed, whereby Pd(0) nanoparticles were anchored on the surface of dopamine-modified $NiFe_2O_4$ nanoparticles. The catalyst system was highly dispersible in various polar solvent systems, namely: water, ethanol and DMF. The synthesized catalyst system was then tested for the Suzuki cross-coupling reaction of aryl halides with phenyl boronic acid, with a slight decrease activity from 93 to 76 % (5th entry) in the case of chloro derivates. For bromo halides, the decrease was from 97 to 74 % (5th entry) and for iodo derivates, it was from 98 to 88 % (4th entry). The same catalyst was then used for the Heck coupling reaction of aryl chlorides with styrene and showed high activity, from 72 to 97 %. It was also mentioned that the presence of dopamine acting as a ligand was beneficial to the catalytic system.

Laska *et al*. [59] reported a mode of preparation for a new, efficient, rhodium catalyst, supported on $Fe_3O_4$ nanoparticles, involving sulfonated triphenylphosphine ligands. An attractive feature of this method is the simplicity of the immobilisation procedure, since it requires no modification of either the NP support or the organometallic species. The catalytic system NP-[Rh(TPPMS)(cod)Cl] – where TPPMS – sodium-3-(diphenylphosphino)benzenesulfonate, cod = 1,5-cyclooctadiene (Scheme 12) was proposed, and showed catalytic activity in coupling reactions of

arylboronic acids to dimethyl itaconate (Scheme 13). 1,4-addition reactions of boronic acids and boronic derivates were tested using NP-[Rh(TPPMS)(cod)Cl] as a catalyst. In each case, excellent conversion was achieved. Moreover, it is notable to mention that the conversion which was given by NP-[Rh(TPPMS)(cod)Cl] is comparable to that given by a homogeneous counterpart under the same conditions.

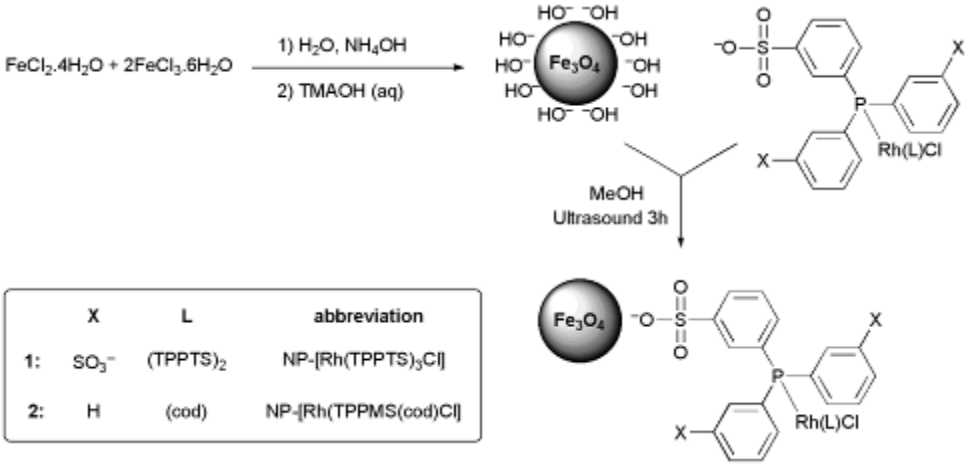


Scheme 12. Preparation of magnetic nanoparticle-supported rhodium catalysts. Reprinted with permission from [59].

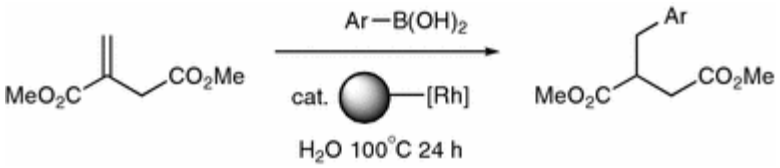


Scheme 13. Addition of arylboronic acids to dimethyl itaconate catalysed by NP-[Rh(TPPMS)(cod)Cl. Reprinted with permission from [59].

Polshettiwar *et al.* [60, 61] reported on the fabrication of nanostructured metal iron oxide under microwave radiation conditions in pure water without using any reducing or capping agent. The iron oxide self-assembled into pine- and snowflake-like three-dimensional morphologies (Figure 4). These nanocomposites were used as a novel support for a Pd catalyst. Nanopine-Pd displayed high catalytic activity for Suzuki, Heck, Sonogashira, and hydrogenation reactions. All of the reactions proceeded efficiently, with good-to-excellent yields, and with unchanged catalytic activity over at least five reaction cycles.

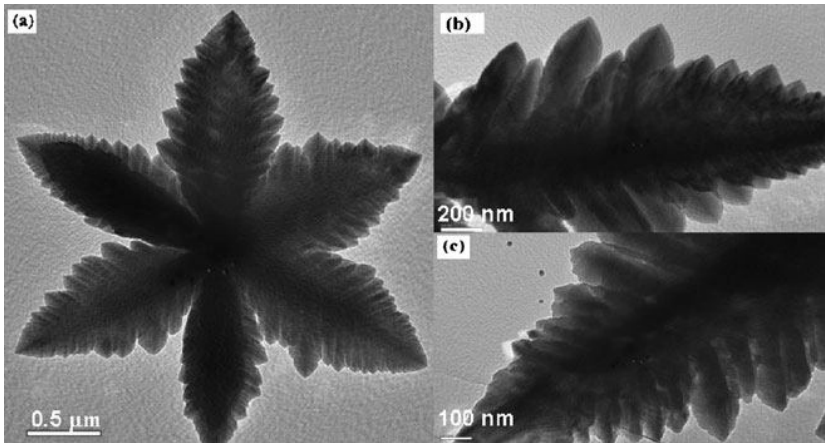


Figure 4. TEM micrographs of dendritic $Fe_2O_3$ at different magnifications. Reprinted with permission from [60]. Copyright (2009) American Chemical Society.

Liu *et al*. [62] tested a $Pd/Fe_3O_4$ catalyst for the carbonylative Sonogashira coupling reaction of aryl iodides, with terminal alkynes and without the use of any phosphine (Scheme 14). For the model reaction (Scheme 14), the best yield was obtained at a CO pressure of 2 MPa, with $Et_3N$ as the base, in toluene, and at a temperature of 130 °C. A series of aryl iodides and terminal alkynes were tested. A yield of more than 70 % was obtained for 15 Sonogashira reaction varieties. After 4 h leaching of palladium was observed, but at the end of the reaction palladium was redeposited onto the support. Recycling was reportedly possible for up to seven cycles without any noteworthy loss in catalytic activity.

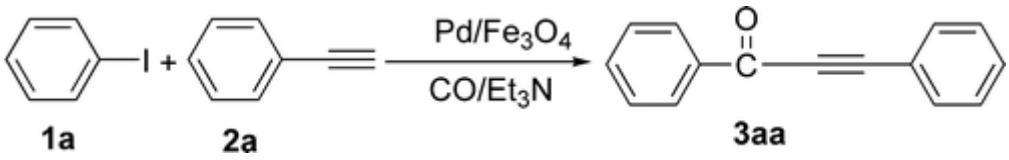


Scheme 14. Carbonylative Sonogashira Coupling Reaction of Iodobenzene. Reprinted with permission from [62]. Copyright (2008) American Chemical Society.

Kim *et al*. [63] described the synthesis of 500 nm silica spheres and functionalised them with amino groups, using a reaction with 3-aminopropyltrimethoxysilane. The amino groups enabled decoration of silica

spheres with $Fe_3O_4$ nanoparticles (Figure 5). Future functionalisation with palladium nanoparticles facilitated synthesis of a $SiO_2$/MNP/Pd catalyst.

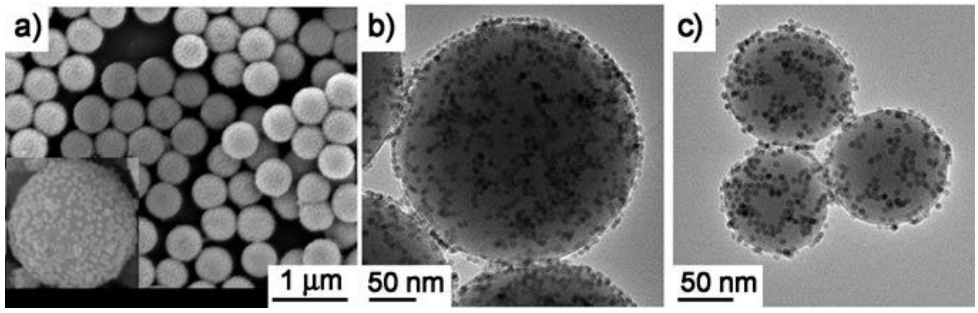


Figure 5. SEM and TEM images of Mag-$SiO_2$. (a) FE-SEM image of 500 nm silica spheres assembled with 14 nm $Fe_3O_4$ nanoparticles (inset: high magnification FE-SEM image), (b) TEM image of 300 nm silica spheres assembled with 7 nm $Fe_3O_4$ nanoparticles, (c) TEM image of 100 nm silica spheres assembled with 7 nm $Fe_3O_4$ nanoparticles. Reprinted with permission from [63].

To investigate the catalytic activity of $SiO_2$/MNP/Pd, a Sonogashira coupling reaction was performed. High catalytic activities (with over 95 % conversion) for the reaction of aryl iodides and aryl bromides were shown. However, recycling tests showed that there was notable catalyst deactivation after four recycles (from 98 to 17 % conversion). The loss of Pd nanoparticles from the silica nanospheres was given as the reason for the decreased catalytic performance.

Luo *et al.* [64] reported on the preparation of MNPs, functionalized with quinuclidine, and on the evaluation of this catalyst in the Morita–Baylis–Hillman (MBH) reaction (Scheme 15). No loss of catalytic activity was observed, even after seven consecutive cycles. The MNP-quinuclidine showed better activity compared with 1,4-diazabicyclo[2.2.2]octane (DABCO) – a standard catalyst for the MBN reaction.

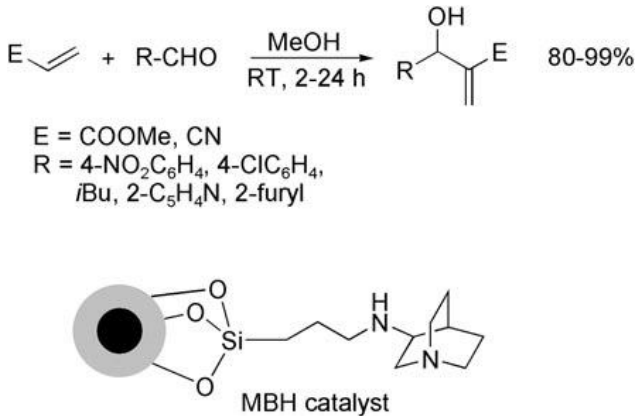


Scheme 15. Morita-Baylis-Hillman reaction with a quinuclidine catalyst supported on MNPs. Reprinted with permission from [65].

### 1.2.4.2.2 MNP-based catalysts for hydrogenation

Hydrogenation is another important chemical transformation. This section will cover the use of magnetic nanoparticle-supported catalysts in hydrogenation of alkynes and alkenes, and transfer hydrogenation of ketones and enantioselective hydrogenation.

Jun *et al.* [66] presented the synthesis of core-shell Co/Pt nanoparticles by a redox transmetalation reaction between $Pt(hfac)_2$ and cobalt nanoparticles. A nanocomposite prepared in this way exhibits superparamagnetic properties. The catalyst was tested for the hydrogenation of various olefins and alkynes (such as styrene, benzaldehyde, nitrobenzene, and 1-decen) under very mild conditions. For the reusability test hydrogenation of 1-decene was chosen, which showed the possibility of 7 reaction cycles without any loss of activity. The authors mentioned that this catalytic system exhibited near-perfect selectivity when reducing the carbonyl group of aldehydes to the corresponding alcohol. TEM data confirmed that the high activity and stability of the Co/Pt catalysts arise from their unchanged composition without aggregation, because of the presence of dodecyl isocyanide.

Guin *et al.* [45] reported on a new route of Pd immobilization on the surface of amine-terminated $Fe_3O_4$ and $NiFe_2O_4$ nanoparticles. The anchoring of dopamine

(DA) molecules on the surface of ferrite nanoparticles was achieved by reflux and sonication. Two catalysts were synthesized: $Fe_3O_4$-DA-Pd and $NiFe_2O_4$-DA-Pd, and were examined for hydrogenation of aromatic nitro and azide compounds and other unsaturated compounds. The results show 100 % conversion in the first run in the case of the 10 compounds presented. The efficiency of the catalysts remained almost unaltered even after 10 cycles. The performance of these catalysts was better in ethanol than in ethylacetate, which was linked to the better dispersion of the catalyst in ethanol.

As mentioned previously, Laska *et al.* [54] investigated the ligand-free NP-$Pd^0$ in the hydrogenation reaction. The NP-$Pd^0$ system promoted complete hydrogenation of benzaldehyde to benzyl alcohol in 4 h under 1 bar of hydrogen pressure, with 100 % selectivity for the C=O group over the aromatic ring. The kinetics of this reaction were also investigated over the range of 40-70 °C, giving an activation energy of 66.1 kJ $mol^{-1}$.

Another report concerning hydrogenation by magnetic nanoparticle-based catalysts is Yi's communication [67], which reported the synthesis of two kinds of nanocomposite made from Pd nanoclusters, supported on silica-coated $Fe_2O_3$ nanoparticles. Monodispersed, silica-coated maghemite nanoparticles were derived in water-in-cyclohexane reverse microemulsion. They were functionalized with mercapto or amine functionalities, which have been known to have a strong affinity for transition metal nanoclusters. Palladium nanoparticles were introduced to the surface-functionalized $SiO_2/Fe_2O_3$ in toluene under microwave radiation using $Pd(OAc)_2$ as a precursor. Pd/$H_2N$-$SiO_2/Fe_2O_3$ and Pd/HS-$SiO_2/Fe_2O_3$ were examined as a catalyst for the hydrogenation of nitrobenzene. They both gave a yield of 99 % over 6 and 5 consecutive runs, respectively. The conversions then decreased gradually in subsequent runs to 87 % and 76 % respectively after 14 runs. The Pd/$NH_2$-$SiO_2$-$Fe_2O_3$ catalyst displayed a higher rate of conversion (0.39 μmol $s^{-1}$) for the hydrogenation of nitrobenzene to aniline than that for the Pd/SH-$SiO_2$-$Fe_2O_3$ or a commercial Pd/C catalyst (0.12 and 0.08 μmol $s^{-1}$, respectively).

Rossi *et al.* [68] reported on the preparation of silica-coated superparamagnetic iron oxide nanoparticles. Nanoparticles prepared in this way were modified with thiol groups in order to immobilize palladium nanoparticles. The catalytic performance was tested in solvent-free hydrogenation of cyclohexene under

mild conditions (p = 6 bar, T = 75 °C). The authors achieved a high TOF = 11500 $h^{-1}$) for this reaction, which was comparable to a standard catalyst Pd/C. The catalyst was recycled up to 20 times without any significant loss in catalytic activity.

The same authors [69] reported a procedure for the preparation of a very similar catalyst. The mode of preparation was different from that used in the previously described paper. A reverse microemulsion process was used for the nanoparticle preparation. Silica-coated nanoparticles were modified with 3-(aminopropyl)-triethoxysilane, which improved the uptake of $Rh^{3+}$ precursor. Pressure of 6 atm of $H_2$ and a temperature of 75 °C were used to reduce precursor onto the surface of magnetic nanoparticles. This catalytic system was tested in hydrogenation of cyclohexene, with a maximum TOF of 40000 $h^{-1}$. It was also tested in benzene hydrogenation with a maximum TOF of 110 $h^{-1}$. For both starting materials the catalyst was reused up to 20 times without significant loss of catalytic activity. The same group [70] reported their results on the hydrogenation of cyclohexane using a ruthenium catalyst, anchored on an identical support. The ruthenium catalyst showed a TOF 420 $h^{-1}$, 18 times lower than the aforementioned rhodium catalyst.

Polshettiwar *et al*. [71] reported synthesis of nickel nanoparticles supported on DA-modified magnetic nanoparticles. The catalyst was examined in the hydrogenation of alkynes. Hydrogenation in methanol was 90 % selective towards alkanes. In dichloromethane, formation of alkenes was preferred (Scheme 16). The catalyst was also tested in the transfer hydrogenation of a series of ketons with good yield and high chemoselectivity. The hydrogenation of phenylacetylene was used to prove the stability of the catalyst. Five recycles were achieved with no loss of catalytic activity.

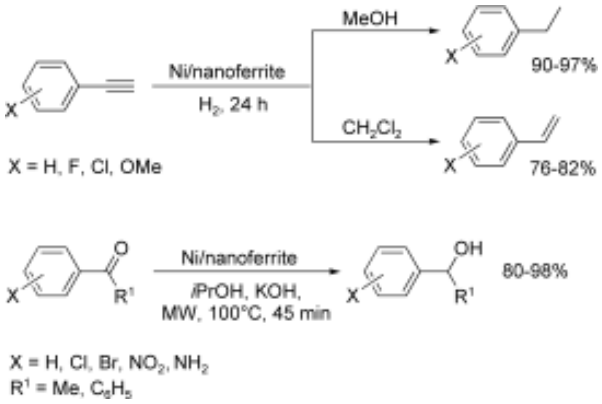


Scheme 16. Hydrogenation and transfer hydrogenation reactions with Ni/nanoferrite catalysts. Reprinted with permission from [65].

Baruwati *et al*. [72] reported on the synthesis of ruthenium catalysts supported on dopamine-functionalized magnetic nanoparticles ($NiFe_2O_4$). The hydrogenation of various alkynes were studied using the ($Ru(OH)_x$/DA-$NiFe_2O_4$). The reactions proceeded at room temperature, and gave the desired products with a yield of over 90 %. The same catalyst was active in the transfer hydrogenation of carbonyl compounds. With a variety of starting materials, all reactions were completed with a yield of 90 % or more, in less than 45 min. The authors used microwave radiation, which provided a great improvement compared to the traditional heating systems. The hydrogenation of acetophenone under microwave radiation was completed in 30 min, compared with the same reaction using a conventional heating system, which needed 4 h to be completed. The high activity and selectivity of the catalyst remained even after five reaction cycles.

The reduction of carbonyl compounds to alcohols, using 2-propanol as a hydrogen donor and catalyzed by $Ru(OH)_x/Fe_3O_4$, was studied by Kotani *et al*. [73]. A variety of aromatic and aliphatic ketones were reduced to the corresponding alcohols in high yields (over 90 %). $Ru(OH)_x/Fe_3O_4$ was tested for a number of different reaction types. The authors only recycled the catalyst once. No significant loss of catalytic activity was observed.

Zhang *et al*. [74] reported on the preparation of a Pt/$\gamma$-$Fe_2O_3$ nanocomposite catalyst. The catalytic activity of Pt/$\gamma$-$Fe_2O_3$ was tested for the selective hydrogenation of *ortho*-chloronitrobenzen. The Pt/$\gamma$-$Fe_2O_3$ catalyst was shown to be very selective towards *ortho*-chloronitrobenzen. Hydrodechlorination of *ortho*-chloroaniline was not observed.

Tsang *et al*. [47] reported on the synthesis of magnetic nanoalloys, encapsulated in quasispherical carbon shells. Sequential spraying, chemical precipitation and controlled pyrolysis were used to prepare this material. Various alloys (FeNi, FeCu, and FeCo) were synthesized and coated with a layer of graphite. Palladium was deposited on the carbon support by impregnation with [$Pd(acac)_2$] (acac = acetylacetonate) in acetone. The FeNi-C-Pd catalyst was tested in hydrogenation of nitrobenzene giving higher initial rates (1.529 $\mu mol\, s^{-1}$) than a commercial Pd/C catalyst (0.835 $\mu mol\, s^{-1}$) from Johnson Matthey. The authors attributed the higher activity observed using the FeNi-C-Pd catalyst to the absence of intraparticle mass transfer limitations, to the smaller size of the catalyst particles and to better Pd dispersion on the support.

The synthesis of platinum nanoparticles immobilized on ionic-liquid-modified MNPs (MNP-IL-Pt) was reported by Abu-Reziq (Scheme 17) [75]. The authors noted that depending on the alkyl group of the linked ionic liquids, the particles were stable and soluble in polar or non-polar organic solvents. MNP-IL-Pt were utilized in catalytic hydrogenation reactions of α, β - unsaturated aldehydes and alkynes. The catalyst was found to be selective for the hydrogenation of the alkynes to the corresponding alkenes. Diphenylacetylene was converted selectively to stilbene, with high (95 %) selectivity for the *cis* isomer; other alkenes were hydrogenated with lower selectivity. The best selectivity was achieved for hydrogenation of α,β-unsaturated aldehydes and 3-phenylprop-2-yn-1-ol (78 % towards *cis* isomer). The recycling experiments were performed using the hydrogenation of diphenylacetylene as a model system for up to four cycles without a significant loss in activity (100 to 97 %) or selectivity (95 to 93 %).

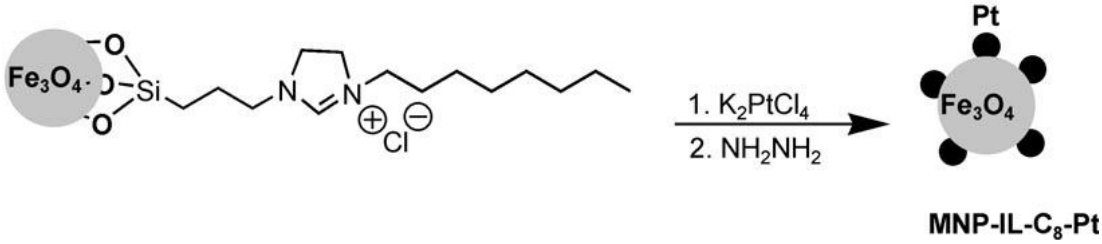


Scheme 17. Preparation of platinum nanoparticles supported on magnetite nanoparticles. Reprinted with permission from [75].

Wang *et al*. [76] described the preparation of Pd nanoparticles in multilayer polyelectrolyte films, fabricated on a magnetic-ferrite core using a layer-by-layer self-assembly technique. A series of unsaturated alcohols were hydrogenated using the nanohybrid catalyst MNP@PAA[PEI–Pd(0)/PAA]$_n$. This resulted in turnover frequency: TOF = 854 $h^{-1}$ for allylic alcohol, TOF = 328 $h^{-1}$ for 3-buten-2-ol , and TOF = 126 $h^{-1}$ for 1-penten-3-ol. These results suggest different steric hindrances. The catalyst was recycled, and showed no significant change in the catalytic activity over 10 recycles.

It is widely accepted that asymmetric catalysis provides a powerful method for the synthesis of optically active molecules, which serve as precursors to pharmaceutically important compounds. Novel heterogenized asymmetric catalyst was synthesized by Hu *et al.* [48] by immobilizing preformed Ru catalyst on magnetite nanoparticles *via* the phosphonate functionality. These nanoparticle-supported chiral catalyst was used for the enantioselective heterogeneous asymmetric hydrogenation of aromatic ketones with total conversion (100 %) and enantiomeric excess (ee) values of up to 98 %. The immobilized catalysts were reused up to 14 times without loss of activity or enantioselectivity. The orthogonal nature of the presented catalyst immobilization approach should allow for the design of other superparamagnetic nanoparticle-supported asymmetric catalysts for a wide range of organic transformations.

Fan *et al*. [46] described in his mini-review an unsuccessful experiment with another ligand BINOL (1,1'-Bi-2-naphthol). The chiral Ti-BINOLate complexes supported on iron oxide/polymer nanoparticles were examined for catalyzing

asymmetric alkylation of benzaldehyde. Moderate reaction yields ranged from 47 to 55 %, with ee values from 15 to 43 %, which were much lower compared to unsupported BINOL.

Panella *et al*. [77] reported on the preparation of cinchonidine modified Pt, which was immobilized on silica MNPs. The magnetic catalyst, modified with cinchonidine, showed activity and enantioselectivity in the asymmetric hydrogenation of various activated ketones. The catalyst showed comparable performance to a well-known commercial Pt/alumina (Engelhard 4759) catalyst. For the recycling tests the hydrogenation of 2 ketopantolactone was used. The catalyst showed a slightly decreased of enantioselectivity over 8 recycles (from 57 to 52 % ee, with conversion being maintained at 100 %).

Li *et al*. [78] immobilized Ru-TsDPEN (TsDPEN=*N*-(*p*-toluenesulfonyl)-1,2-diphenylethylenediamine) on a magnetic siliceous mesocellular foam material. Hydrogenation of dihydroisoquinoline was chosen as the model reaction for the asymmetric reduction of imines. A HCOOH–$Et_3N$ azeotrope was used as a hydrogen donor. It was possible to hydrogenate dihydroisoquinoline with a yield of over 97 % and an ee of over 94 % for different range of pH. Negligible loss of enantioselectivity was noticed, falling from 94 to 90 % over 9 recycles of the catalyst. The authors successfully applied the Ru-TsDPEN/F(M) catalyst in the transfer hydrogenation of a series of aromatic ketones (in aqueous HCOONa) with a 99 % yield and an ee in the range of 88 to 97 %.

#### 1.2.4.2.3 MNP-based catalysts for oxidation

The aforementioned $Ru(OH)_x/Fe_3O_4$ catalyst, synthesised by Kotani *et al*. [73] was successfully applied to aerobic oxidation of alcohols and aerobic oxidation of amines. A wide variety of aliphatic and aromatic alcohols were oxidized to the corresponding aldehydes and ketones with high yields (80-99 %) using molecular oxygen as an oxidative agent. The reaction with amines resulted in the formation of the corresponding nitriles at high yields (53-99 %). Furthermore, $Ru(OH)_x/Fe_3O_4$ was reused for different types of reactions sequentially. The oxidation of 1-phenylethanol was followed by the oxidation of 2,3-dihydroindole, after which the

recovered catalyst was used for the reduction of 3-pentanone. The catalyst could be reused without a significant loss in activity for different reactions.

A very interesting utilization for $Fe_3O_4$ MNPs was proposed by Zhang *et al.* [79]. Bare $Fe_3O_4$ nanoparticles were used for the catalytic removal (oxidation) of phenol and aniline from aqueous solutions. Both phenol and aniline could easily be eliminated from the solution under acidic and neutral conditions in the presence of MNPs and $H_2O_2$. Some intermediates, such as formic acid, acetic acid, fumaric acid and hydroquinone were detected during the reaction. $Fe_3O_4$ MNPs exhibited good stability and reusability. The authors proposed a free radicals mechanism for phenol degradation (Scheme 18).

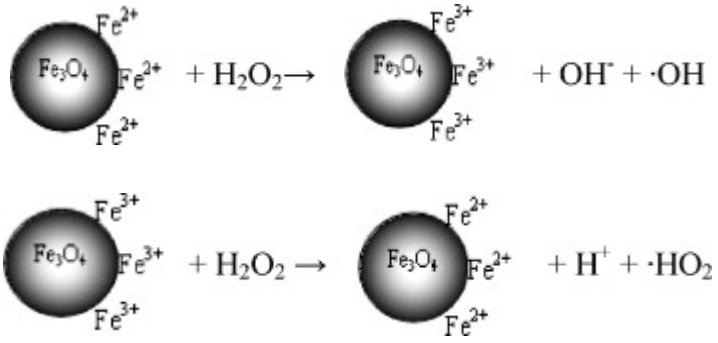


Ph + •OH → organic acid

Organic acid + •OH → $CO_2$ + $H_2O$

Scheme 18. The mechanism of phenol degradation on $Fe_3O_4$ nanoparticles. Adapted from [79].

Rossi *et al.* [70] immobilized Ru onto $NH_2$ modified silica shell coated MNPs. The catalytic activity of the Ru(III) catalyst was investigated in the oxidation of a series of aromatic and aliphatic alcohols, including diols, under 3 atm of molecular oxygen at 100 °C. All alcohols were converted into the corresponding aldehydes and ketones with a high conversion (82-99 %), and great selectivity (over 99 %). No carboxylic acids, which are typically quite common by-products, were observed. Oxidation of 1-phenylethanol was performed to verify the catalyst recyclability. The catalyst could be reused for up to three successive oxidation reactions without a change in substrate conversion after 3 h (>99 % conversion).

The preparation of a hybrid polymer $[[Cu(bpy)(BF_4)_2(H_2O)_2](bpy)]_n$ (bpy = 4,4′-bipyridine) on the surface of amino-functionalized MNPs (size ≈ 200 nm) was reported by Arai *et al.* [80]. A catalyst prepared in this way was utilized for the oxidation of silyl enolates (Scheme 19). A series of silyl enolates were converted to their corresponding α-hydroxy ketones in good yields (75-99 %) under mild conditions. Using a magnetically-supported catalyst resulted in a higher yield when compared with a homogenous Cu-bpy. The authors compared a commercially available support, aminomethylated polystyrene, with a hybrid polymer. The results showed a decrease in catalytic activity when polystyrene was used.

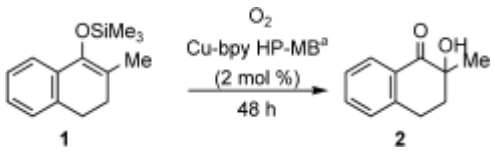


Scheme 19. Synthesis of α-hydroxy ketones by using the Cu(bpy)/HPMB catalyst. Reprinted with permission from [80].

Shi *et al.* [81] utilized bare $Fe_2O_3$ (α or γ, particle size ≥ 100 nm) as a catalyst for oxidation reactions under mild conditions, with hydrogen peroxide used as the oxidizing agent. The authors observed size-dependent activity for oxidation of benzyl alcohol. A conversion of 85 % and a selectivity of 35 % were achieved when nano-γ-$Fe_2O_3$ particles with diameters of 3 to 5 nm were used. For particles in the size range of 20 to 50 nm, the conversion rate decreased to 33 %, with a benzaldehyde selectivity of 97 %. For bulk α- and γ-$Fe_2O_3$ the catalytic activity was low. TON values for nano-$Fe_2O_3$ were similar to those obtained when a homogenous $Fe^{3+}$ catalyst was used. Nano-$Fe_2O_3$ was also an active catalyst for aromatic olefins oxidation. Reusability tests were carried out using oxidation of cyclooctanol. Particles could be recycled even after five times without any deactivation.

More impressive results in benzyl alcohol oxidation (TON = 760 and selectivity >99 %) were obtained by Polshettiwar *et al.* [82]. This high conversion rate was achieved by using palladium nanoparticles supported on dopamine-modified

nanoferrites. A variety of alcohols were successfully oxidized, with a high TON value in a rage of 520 - 800. Furthermore, this catalytic system was also active for the oxidation of olefinic compounds to the corresponding aldehydes (TON = 600-680). The catalyst could be used at least 5 times without any change in activity.

Cyclohexane is one of the starting materials for nylon 6 and nylon 66 production. Tong *et al*. [83] reported on an effective, novel $CoFe_2O_4$ catalyst for aerobic oxidation of cyclohexane. The sol-gel auto-combustion method was used for the preparation of a cobalt-ferrite complex. Kinetic studies showed that the optimum activity was 16 %, with 92 % selectivity towards cyclohexanone and cyclohexanol at 16 atm of oxygen and a temperature of 145 °C over 6 h. A $CoFe_2O_4$ catalyst was also tested for oxidation of linear alkanes, and was less effective (3-9 % of conversion). After six runs for cyclohexane oxidation no changes were observed for selectivity, but the conversion of cyclohexane dropped from 15.5 to 12.7 %.

Aschwanden *et al*. [84] prepared maghemite and magnetite nanoparticles, which were embedded in a ceria matrix in cerium and iron at an atomic ratio 5:3. $Au(OAc)_3$ was used as a precursor for gold nanoparticles, which were precipitated insitu on to the ceria matrix. An $Au/CeO_2/FeOx$ catalyst was tested in dibenzylamine oxidation. A conversion of 50 % and a selectivity of 90 % were achieved after 5 h of reaction. A series of other amines, including benzylamine, *N-tert*-butylbenzylamine, and indoline were oxidized to the corresponding imines, with good conversions (49-100 %) and excellent selectivities (87-100 %). The reusability of the $Au/CeO_2/FeO_x$ was tested using the oxidation of dibenzylamine. The activity of the catalyst decreased after three cycles, with an average loss of 5 % activity after each reaction.

Mori *et al.* [85] reported the synthesis of MNPs encapsulated in a hydroxyapatite matrix by the consecutive precipitation of precursors under basic conditions. Calcium on the surface of the prepared nanocomposite was exchanged with ruthenium, leading to a new catalyst. The catalytic performance of this new material (RuHAP-$\gamma$-$Fe_2O_3$) was tested for oxidation of alcohols. Molecular oxygen

was used as oxidative agent for oxidation of different benzylic, allylic, aliphatic, and heterocyclic alcohols at room temperature and under atmospheric pressure. The results are summarized in Scheme 20.

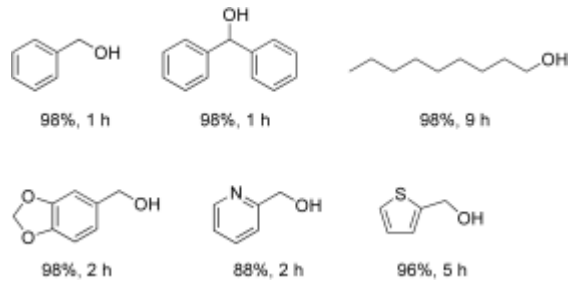


Scheme 20. Substrate scope for the aerobic oxidation of alcohols with the Ru/HAP-γ-$Fe_2O_3$ catalyst. Reprinted with permission from [65].

The RuHAP-γ-$Fe_2O_3$ catalyst was also active in the oxidation of sterically bulky alcohols; 3,5-dibenzyloxybenzyl alcohol and cholestanol. No metal leaching was detected. There was no requirement for a co-catalyst, and the catalyst was recycled with no significant loss of catalytic activity.

Schatz *et al*. [86] reported on the synthesis of TEMPO (2,2,6,6-tetramethylpiperidine-1-oxyl) modified, graphene-coated cobalt nanoparticles. The click-chemistry protocol was used for grafting TEMPO on the surface of the nanoparticles. The catalytic tests showed CoNP–TEMPO as an active catalyst for the chemoselective oxidation of benzylic and aliphatic alcohols. Sodium hypochlorite was used as a primary oxidant. No carboxylic acid by-products were observed, and the catalyst could be recycled by magnetic separation six times without any loss of activity.

#### 1.2.4.2.4 MNP-based catalysts for epoxidation

Epoxidation is another important reaction for the chemical industry. Some research was done using a magnetic nanocatlyst for this reaction. The first study, describing the application of magnetically separable catalysts, was done by Hyeon *et al.* [87]. Hematite (α-$Fe_2O_3$) particles with an average diameter of 400 nm were

synthesized using a hydrothermal procedure and stabilized by PVP (poly (vinylpyrrolidone)). Then, a dense silica layer of the desired thickness (50 nm) was deposited on the surface. This nanocomposite was impregnated with ammonium molybdate, which was then reduced. The activity of the Mag-Mo-Nano catalyst was tested for the epoxidation of *cis*-cyclooctene, and other alkenes. High yields of epoxides (>80 %) were found for substrates such as cyclododecene, cycloheptene, cyclohexene, and indene. Magnetic separation and recycling of the Mag-Mo-Nano catalyst was investigated. This catalyst was successfully recycled and reused six times in the epoxidation of *cis*-cyclooctene with no major loss of activity.

Tang *et al*. [88] reported on the functionalisation of $SiO_2$-FePt MNPs with titanium, using a layer-by-layer, bottom-up approach. This resulted in Ti−O−Si species on the surface of the nanocomposite. Different amounts of tetrabutyl orthotitanate (TBOT) were used to cover the shell of silica-coated FePt nanoparticles. The authors postulated a substitution of Si sites by Ti, since TBOT diffuses into the silica layer. Epoxidation of *trans*-stilbene in the presence of *tert*-butyl hydroperoxide was used for the evaluation of the catalyst. The best results (15 % conversion, >90 % selectivity) gave a sample with 18.9 wt % $TiO_2$. A further increase in the titanium concentration decreased the catalytic activity, which was related to the formation of unreactive Ti-O-Ti units instead of catalytically active Ti-O-Si active sites.

Shylesh *et al*. [89] reported on the synthesis of silica-coated MNPs with $[(L\text{-}L)MoO(O_2)_2]$ (L-L = (3-triethoxysilylpropyl) [3-(2-pyridyl)-1-pyrazolyl] acetamide) grafted onto the surface (Scheme 21). The catalytic activity of this hybrid complex was evaluated for epoxidation of a series of alkenes (cyclooctene, cycloheptene, cyclohexene, styrene, 1-octene), with a different yield of epoxides (96-77 %). For this catalyst, the best combination of solvent and oxidant was $CHCl_3$ and t-BuOOH. The authors compared MCM-41 and silica-nanosphere-supported Mo catalysts of similar loading, which gave poorer results.

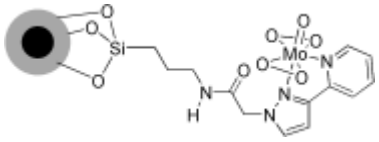

Scheme 21. Heterogenized molybdenumperoxo catalyst for olefin epoxidation on silica-coated MNPs. Reprinted with permission from [65].

Zhang *et al*. [90] presented a Ag/MNP catalyst, synthesized in a one-pot procedure using PVP as a stabilizer and a coupling link between Ag and $Fe_3O_4$ nanoparticles. This nanocomposite turned out to be a very efficient catalyst for the epoxidation of styrene, using TBHP (tertbutyl hydroperoxide) as an oxidant in toluene. Styrene oxide was formed with a yield of 84 % after 13 h, with a TOF value of 1473 $h^{-1}$. No deactivation was observed after five cycles of reaction. The higher catalytic activity of this system compared with either bare-Ag nanoparticles or a mixture of Ag and $Fe_3O_4$ nanoparticles was explicated by a synergetic interaction between nanoparticles.

Mori *et al*. [91] reported on the synthesis of FePt@Ti-$SiO_2$ using FePt nanoparticles stabilized by oleic acid and oleylamine by a two-step coating method *via* a ligand exchange and a sol−gel process route, using tetraethyl orthosilicate and tetrapropylorthotitanate. The catalyst was tested in epoxidation of cyclooctene giving consistent activity (TON = 48) for four cycles. Hydrogen peroxide was used as an oxidant.

#### 1.2.4.2.5 MNP-based catalysts for hydroformylation

There has been considerable interest recently in employing nanoparticle magnetic catalysts to hydroformylation reaction. The use of magnetic nanoparticles for the immobilization of Rh-based catalyst was reported by Yoon *et al.* [92]. The surface of magnetic ferrite nanoparticles ($CoFe_2O_4$) was coated with a Rh-based cationic complex, [Rh(cod)($\eta^6$-benzoic acid)]$BF_4$. The nanomagnet-supported catalyst showed excellent catalytic activity, with a good regio-selectivity toward the hydroformylation reaction of 4-vinylanisole (Scheme 22), which is comparable to that of its homogeneous counterpart. Besides great reaction yield (>99 %), the recovered catalyst exhibited no loss of catalytic activity for four more rounds of the reaction.

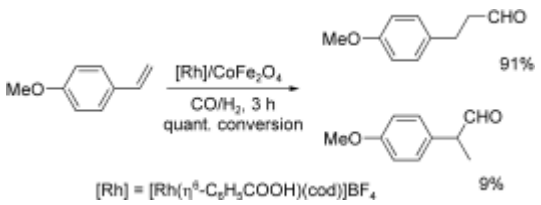


Scheme 22. Hydroformylation catalyzed by rhodium supported on MNPs. Reprinted with permission from [65].

Abu-Reziq *et al.* [93] proposed as a new method, based on combining the features of magnetic nanoparticles and dendrimers. Polyaminoamido (PAMAM) dendron were grown on nanomagnetite ($Fe_3O_4$, coated with a silica shell). The dendrons on silica-coated nanomagnetite were phosphonated by the reaction of the terminal amino groups with diphenylphosphinomethanol, prepared *in situ* from diphenylphosphine with paraformaldehyde. Covered by silica and phosphonated dendrons, iron oxide nanoparticles were complexed with $[Rh(cod)Cl]_2$, and applied in catalytic hydroformylation of different olefin substrates at 50 °C, $p(CO)$ = 34.5 bar, $p(H_2)$ = 34.5 bar.

These new catalysts showed high selectivity and reactivity. The reaction was highly regio-selective for the branched aldehyde. This catalytic system was used for up to five runs without any significant loss in activity or selectivity.

### 1.2.4.2.6 MNP-based catalysts for other reactions

Shi *et al.* [94] reported on the preparation of MNPs coated with $PW_{12}O_{40}^{3-}$(POM) anions *via* a layer of silver nanoparticles. The photocatalytic activity of the resulting material was investigated using degradation of rhodamine B as a standard reaction. It was found that compared to pure POM, the decolourization fraction of rhodamine B in a 2 h operation was 2.8 to 3.4 times higher by using the POM-based nanocomposite.

Asymmetric acylation, using chiral 4-*N*,*N*′-dimethylaminopyridine (DMAP) derivatives supported on MNPs, were discussed by Gleeson *et al.* [95]. The catalyst was prepared according to the procedure shown in Scheme 23. The catalysts allowed

alcohol (presented in Scheme 24) to be resolved, with 99 % ee and 72 % conversion. A series of sec alcohols were promoted for kinetic resolution, giving 62-89 % conversion and 70-99 % ee The recyclability tests demonstrated that the catalyst retained excellent activity and selectivity over 32 iterative cycles.

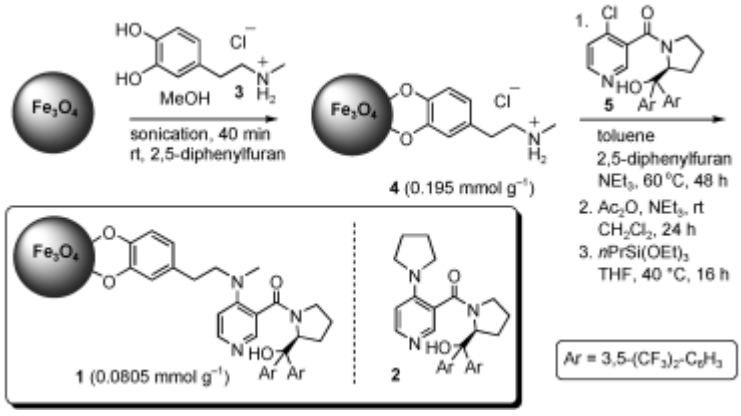


Scheme 23. Synthesis of DMAP $Fe_3O_4$ based catalyst. Reprinted with permission from [95].

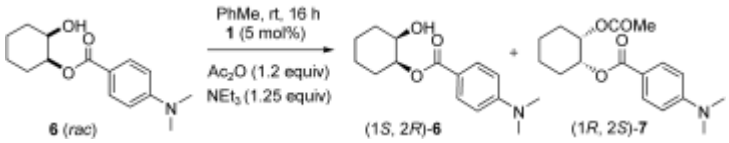


Scheme 24. Asymmetric acylation. Reprinted with permission from [95].

Another example of using MNPs as support for an acylation catalyst was reported by Dalaigh *et al*. [96]. The catalyst was prepared by grafting DMAP on to MNPs coated with a silica layer. The performance and recyclability of the catalyst was investigated for the acetylation of 1-phenylethanol (Scheme 25). It was possible to carry out this reaction with a good yield (>94 %), at room temperature, and at very low catalyst loadings. The catalyst was recycled for 30 times without any discernable loss in catalytic activity.

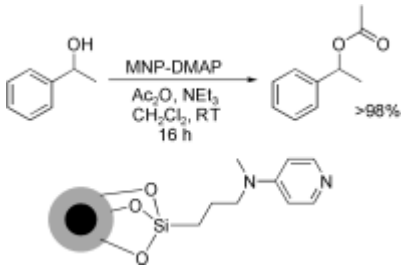


Scheme 25. Acetylation of 1-phenylethanol with a DMAP derivative supported on MNPs. Reprinted with permission from [65].

A series of reactions were investigated with high yield (over 90 %) using a DMAP-MNP catalyst, including peracetylation of D-glucose, protection of indole with *tert*-butoxycarbonyl (Boc) and rearrangement of a quaternary *O*-acyl enolate.

Lee *et al*. [97] reported on the synthesis of a mesoporous silica, with MNPs grafted onto the pore surface and functionalized with chiral ligands for catalytic asymmetric dihydroxylation. MNPs were synthesised inside of the pores by thermal decomposition of iron propionate. The silica support was then functionalized with cinchona alkaloid inside the pore channels. The catalyst was used for dihydroxylation of a series of olefins, and exhibited high ee (93-99 %), comparable to a homogeneous ligand. The catalysts could be recycled eight times.

The hydration of nitriles is one of the most imperative technologies for the large-scale synthesis of amides. Polshettiwar *et al*. [98] reported on the synthesis of ruthenium hydroxide ($Ru(OH)_x$) supported on MNP in water. The nanomaterial synthesized using the above procedure was evaluated in hydration of nitriles. The reaction proceeded in water without using any organic solvents, not even during the workup stage. High yields (61-88 %) were obtained for a variety of nitriles, including benzonitrile derivatives, aliphatic and heterocyclic nitriles.

A very promising and interesting concept for using bare MNPs for catalysis purposes was investigated by Martinez *et al*. [99]. Magnetite is an excellent Lewis acid catalyst, and was used for the four-component Aza-Sakurai reaction (Scheme 26). Unmodified commercial magnetite was used in these experiments. The best yield was obtained using toluene as a solvent with a temperature of 110 °C. The reaction performed even without mixing. A series of compounds were tested, with

good yields in most cases. The process could be repeated up to 15 times without losing effectiveness.

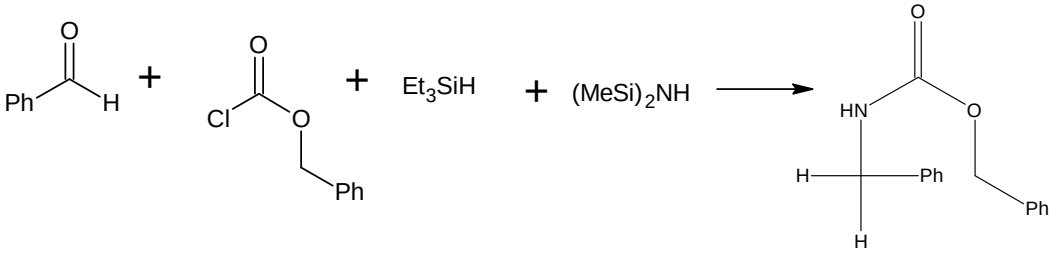


Scheme 26. Aza Sakurai reaction. Adapted from [99].

Phan *et al.* [100] investigated the synthesis of cobalt MNPs using a microemulsion procedure. To create basic sites, nanoparticles were functionalized with *N*-[3-(trimethoxysilyl)propyl]ethylenediamine *via* silane chemistry. A Knoevenagel condensation of benzaldehyde with malononitrile was chosen for the catalyst evaluation (Scheme 27). Complete conversion was achieved in benzene, under reflux, after 5 min of reaction. The catalyst could be reused several times without a significant degradation in activity. Several aromatic and heteraromatic aldehydes were reacted with malononitrile under mild conditions, with a good conversion.

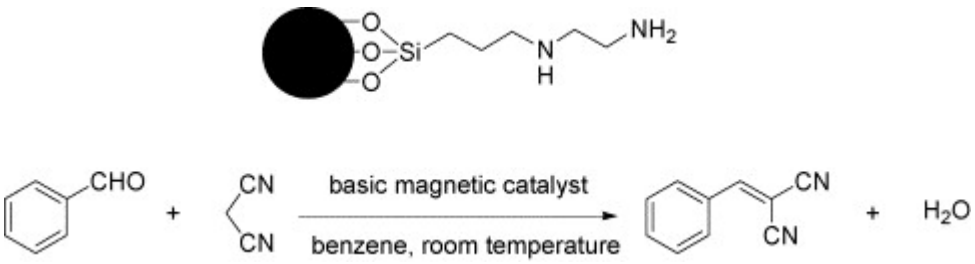


Scheme 27. Knoevenagel reaction of benzaldehyde with malononitrile using MNP catalyst. Reprinted with permission from [100].

A magnetic nanoparticle-supported catalyst for atom-transfer radical polimeryzation (ATRP) was recently investigated by Ding *et al.* [101]. The magnetite (20-30 nm) was used to support the catalyst for ATRP. $Fe_3O_4$ magnetic

nanoparticles were refluxed with 3-aminopropyltrimethoxysilane in dry toluene, to anchor amine groups onto their surface using silane chemistry. Acryloxyl groups were introduced using the reaction of the amine groups with acryloyl chloride. The Michael reaction of the acryloxyl groups with tetraethyldiethylenetriamine (TEDETA) attached the ligand onto the support, and the synthesized product was complexed with CuBr. The iron oxide nanoparticle-supported ATRP catalyst was employed for the polymerization of methyl methacrylate. The activity of the recycled catalyst was regenerated by copper metal or *in situ* regeneration using reducing agents such as alkylamine or tin (II) compounds.

A report published by Hara *et al*. [102] covered one important reaction, particularly from an environmental point of view: catalytic dechlorination with molecular hydrogen. The authors applied a Pd nanocluster catalyst supported on magnetically separable hydroxyapatite (Pd/HAP-γ-$Fe_2O_3$). A variety of aromatic chlorides and bromides could be dehalogenated to their corresponding arenes in high yields (>99 %). The dechlorination of chlorobenzene produced benzene with an excellent TOF of 2500$h^{-1}$ under only 1 bar of $H_2$ pressure. Catalyst screening studies further revealed that the most promising results were obtained with 2-propanol as the solvent and NaOH as the base. The catalytic activity of Pd/HAP-γ-$Fe_2O_3$ was found to be significantly higher than that of HAP-Pd and Pd/γ-$Fe_2O_3$ because of the presence of very small Pd nanoclusters on the surface of the HAP-γ-$Fe_2O_3$ support. Additionally magnetic nanoparticles were tested as a supporting material for enzymes and biomimetics. Jiang *et al*. [103] reported on lipase supported on MNPs and its application in estrification. A similar concept was examined with good results by Gardimalla *et al*. [104]. The authors used MNP-supported lispase for catalyzing chiral resolution of racemic carboxylates. Aspartic acid (Asp) and Histidine (His) residues supported on a 12 nm maghemite nanoparticle, were investigated by Zheng *et al*. [105] as a biomimetic nanocatalyst for hydrolyzing paraoxon (phosphoester) and 4-nitrophenyl acetate (carboxylic ester).

In summary, the immobilization of homogeneous catalysts on various support materials (such as organic polymers and inorganic silica and other metal oxides) has been investigated for many years. The aim has been to better recover and recycle catalysts, especially when expensive and/or toxic heavy-metal complexes are

employed. However, immobilization of homogeneous catalysts usually decreases the catalytic activity (or efficiency), due to the problem of diffusion of the reactants to the surface-anchored catalysts. In order to increase the active surface area, porous support materials such as zeolite and porous silica have been employed and have shown some promising results.

Another way to increase the surface area is to utilize smaller-sized support materials with the same total volume. When the size of the support materials is decreased to the nanometer scale, the surface area will increase dramatically, and the nanometer-sized supports will even be dispersible in a solution, forming an emulsion. However, in this extreme case of immobilized systems, the same problems of isolation and recycling of homogeneous catalysts will still be encountered. Many approaches were attempted to overcome these drawbacks, including using biphasic systems, and supporting the active species on membranes, polymers or dendrimers. These solutions have found some applications in industry, but there is still a huge need to work out new supports with a bigger surface area and easier separation methods. Laska *et al*. [59] claimed that one of the most promising nanoparticulate supports for the development of high-performance catalyst supports is superparamagnetic iron oxide. It is widely accepted that superparamagnetic nanoparticles are a new and powerful tool for the synthesis of drugs and chemical intermediates and hence, they open a new horizon for large-scale catalytic reactions in the chemical and pharmaceutical industries. The simplicity of the presented catalyst immobilisation approach, the remarkably high catalytic activity, and the easy separation procedure are promising directions for designing other efficient, nanomagnet-based systems for a range of catalytic reactions.

#### 1.2.4.3 Biomedical application of iron oxide nanoparticles

It was mentioned earlier that nanoparticles can be used in biomedical applications. They have become very attractive for biological and medical applications because of the progressions in methods for the synthesis, coatings and analysis of naoparticles [106]. There are various fields within the biosciences where nanoparticles can be very useful, such as tissue engineering; drug, radionuclide and gene delivery, magnetic resonance imaging contrast enhancement; hyperthermia;

detoxification of biological fluids, cell separation, tissue repair and magnetofection [107-109].

The major disadvantage of most medical treatments is that they are non-specific. The damaging side effects of therapeutic remedies are caused by their administration: they are not targeted specifically, but employ general distribution systems. This makes direct drug delivery the most promising application of magnetic nanoparticles. Nanoparticles are capable of carrying pharmaceuticals on their surface, and by applying an external magnetic field the drugs could be directed to the target organ for accurate release [110]. Berry and Curtis [109] proposed that nanoparticles could be delivered intravenously and transported using blood circulation to the area which required treatment. In other cases the particles could be injected directly to the afflicted region. This localized dosage could therefore be limited to the biologically active minimum. The required properties for use in a human body are that it must be chemically passive. Magnetic nanoparticles are physiologically well tolerated *in vivo*; Babincova *et al.* [111] reported that, for example, a dextran - magnetite $LD_{50}$ had no measurable effect, and thus can be assumed to lack toxicity. The most difficult tasks for a scientist to fulfil working on the medical application of nanoparticles are, according to Neuberger [106], avoiding discovery by the reticulendothelial system, providing functional groups to coat the surface, and stabilization of the nanoparticles in a biological suspension with a pH of around 7.4 and a high salt concentration. In the next paragraphs, three of most promising applications of nanoparticles to bioscience will be discussed.

MRI is a non-invasive method using nuclear magnetic resonance to render images of the inside of an object. The most common application of MRI is to provide clear imaging showing physiological and pathological changes in living tissue. Using MRI is possible because of the different relaxation times of hydrogen atoms in water molecules [106, 107]. The protons in a variety of tissues respond differently, which gives an opportunity to picture anatomical structures. Recent research makes it possible to image *in vivo* at near-microscopic resolution. Magnetic nanoparticles have been recognized as facilitating exceptional MRI contrast to enable better differentiation between healthy and pathological tissue. They have been discovered to increase specificity and selectivity due to modifications of the relaxation time of the protons. One of the most common contrast reagents in standard MRIs are gadolinium chelates, which travel through the bloodstream and are non-specific,

enabling rapid accumulation in the liver. This does mean, unfortunately, that they have a short imaging window. The present and future applications using the particles are to enable imaging of the gastrointestinal tract, spleen, liver and lymph node [109]. However nanoparticles were also used experimentally in the cardiovascular system and in the cerebral area with increased permeability of the blood-brain barrier [110].

Another very promising application of MNPs is a drug targeting system. Achieving precise drug delivery to a specific location, where it will then remain for a specified amount of time, is one of the most challenging problem of modern pharmacotherapy. The concept of administrating remedies attached to the surface of a nanoparticle thus enables enormous potential to prevent the drugs from accumulating in and damaging healthy tissue.

In most cases the surface of nanoparticles is covered with dextran, PVA or polyglycols, which reduces the uptake of nanoparticles into macrophage cells, therefore preventing the body's innate immune system from attacking the drug carriers. This increases biocompatibility, resists protein absorption and increases circulation time. With the use of an external magnetic field and gradient, it is possible to confine the particles to a designated tissue area [112].

One method for the delivery of cytotoxic drugs, as an example, would be to use MNPs, which definitely has an advantage over non-targeted methods. The area which has received the greatest amount of research attention within the magnetic drug delivery topic is the targeting of chemotherapeutic drugs. Lübbe *et al.* [114] reported on the first clinical trials in humans, using magnetic nanoparticles with epirubicin bounded on the surface. Epirubcin is an anthracycline drug used for chemotherapy against breast, ovarian, gastric and lung cancer, and lymphomas. Bonadonna *et al.* [115] reported that epirubicin is also very effective in solid tumour treatment. Further research by Lübbe *et al.* [111] showed that treatment using ferrofluids is safe in the case of cancer tumors, but that there is still more to do to improve this method of treatment.

Hyperthermia can be induced in tumours to break the termoregulation system and facilitate localized treatment. This method applies electromagnetic radiation or ultrasound to enable a heat source. Magnetic nanoparticles are very useful for magnetic induction hyperthermia (one of the therapies for cancer treatment),

whereby the cancerous tissues are exposed to an alternating magnetic field [20]. MNPs can be injected directly into the tumour or in to the artery supplying the tumour [109]. Through the oscillation of the magnetic moment inside the particles, the magnetic field's energy is liberated in the form of heat and then conducted to the location of the tissue, destroying the tumour cells. This will facilitate tumour necrosis without causing cellular necrosis of the surrounding healthy tissues [113]. The temperature in the tumour can easily be controlled as per the Marie Curie temperature of the specific chosen material and by manipulating the parameters of the magnetic field. Cancer cells are destroyed at temperature lower than 43 °C, whereas normal cells can survive at higher temperatures.

There are two different types of hyperthermia method, one called 'magnetic hyperthermia', characterized by temperatures of up to 47 °C. This method, combined with radiotherapy and chemotherapy, is an effective tumour treatment. Hilger *et al.* [116] investigated another hyperthermia method, called 'thermoablation', in which the temperatures used are above 55 °C. This promotes coagulation or even carbonation of both the cancer tissues and normal tissues. For this reason, thermoablation only has a limited value for clinical applications. As a summary, the application of magnetic nanoparticles for hyperthermia is a promising tool in the fight against tumours.

In summary, the use of magnetic nanoparticles in the area of medicine opens up new ways for more efficient, selective drug delivery to local tissue, avoiding many side effects. Their use in MRI is still under consideration, however, thanks to new method of particle synthesis, functionalization, coatings and analysis, MNPs are even more attractive for all kinds of medical applications in the future.

In summary, the immobilization of homogeneous catalysts on various support materials (such as organic polymers and inorganic silica and other metal oxides) has been investigated for many years. The aim has been to better recover and recycle catalysts, especially when expensive and/or toxic, heavy-metal complexes are employed. However, immobilization of homogeneous catalysts usually decreases the catalytic activity (or efficiency), due to the problem of diffusion of the reactants to the surface-anchored catalysts. In order to increase the active surface area, porous support materials such as zeolite and porous silica have been employed and have shown some promising results.

Another way to increase the surface area is to utilize smaller-sized support materials with the same total volume. When the size of the support materials is decreased to the nanometer scale, the surface area will increase dramatically, and the nanometer-sized supports will even be dispersible in a solution forming an emulsion. However, in this extreme case of immobilized systems, the same problems of isolation and recycling of homogeneous catalysts will still be encountered. Many approaches were attempted to overcome these drawbacks, including using biphasic systems and supporting the active species on membranes, polymers or dendrimers. These solutions have found some applications in industry, but there is still a huge need to work out new supports with a bigger surface area and easier separation methods. Laska *et al*. [59] claimed that one of the most promising nanoparticulate supports for the development of high performance catalyst supports is superparamagnetic iron oxide. It is widely accepted that superparamagnetic nanoparticles are a new and powerful tool for the synthesis of drugs and chemical intermediates, and hence they open a new horizon for large-scale catalytic reactions in the chemical and pharmaceutical industries. The simplicity of the presented catalyst immobilisation approach, the remarkably high catalytic activity, and the easy separation procedure are promising directions for designing other efficient, nanomagnet-based systems for a range of catalytic reactions.

### 1.3 Challenges

- To synthesise stable MNPs (magnetic nanoparticles)
- To find a method of preventing MNPs from aggregation
- To evaluate surface chemistry methods to immobilize catalysts on the surface of MNPs
- To evaluate catalytic activity of different catalysts based on MNPs for various reactions
- To improve catalyst recovery and recycling
- To apply active catalysts in flow mode and asses the influence of different micro and capillary reactors on process intensification

# CHAPTER 2

## Catalysts supported on magnetic nanoparticles - batch experiments

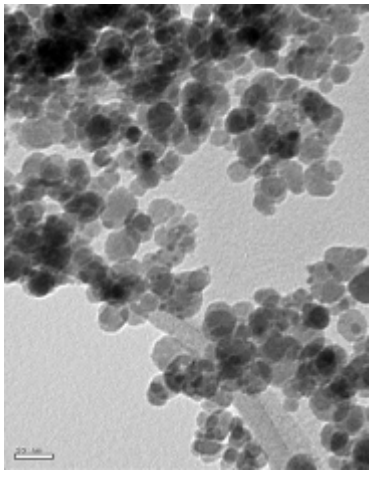

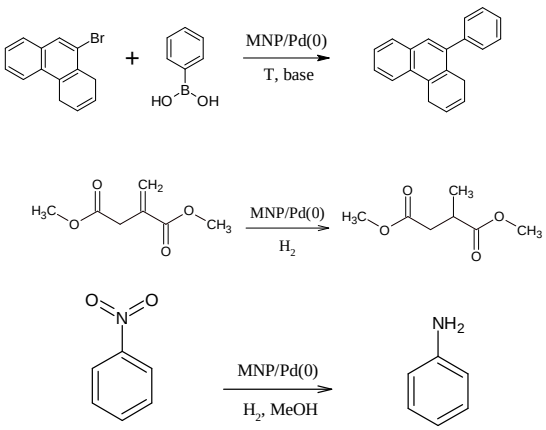

## 2 Introduction

This chapter describes different methodologies for the preparation of magnetically separable catalyst supports and initial trials of different batch catalytic reactions, including asymmetric reactions, utilizing a range of magnetic nanoparticle catalysts. The other subject of this chapter will be the evaluation of different nanoparticle coatings to prevent them from aggregation.

### 2.1 Synthesis of magnetic nanoparticles

Magnetic nanoparticles were synthesized using the methodology described below. This method was applied because of its simplicity as well as because the starting materials were readily accessible at low prices. Iron oxide nanoparticles were prepared by a slight modification of the known co-precipitation method [117], in which co-precipitation of ferric and ferrous salts in a basic medium is followed by stabilization using $OH^-$ ions. In a typical synthesis, $FeCl_3 \cdot 6H_2O$ and $FeCl_2 \cdot 4H_2O$ were dissolved under $N_2$ in an acidic solution, such that the $Fe^{3+}$ to $Fe^{2+}$ molar ratio was 2. The as-prepared solution was added dropwise to a deoxygenated $NH_4OH$, with vigorous stirring. The black precipitate was isolated from the solvent *via* magnetic decantation. The washing–decantation procedure was repeated three times, followed by washing twice with a TMAOH (Tetramethylammonium hydroxide) solution. Finally, the suspension was precipitated with acetone and methanol. Magnetic nanoparticles prepared using this procedure were very easy to separate using a standard permanent magnet (surface magnetization 0.3 T, MMG MagDev, UK) (Figure 6). TEM micrographs confirmed that the average particle size was *ca.* 10 nm, although there was a relatively narrow size distribution (Figure 7). For synthetic details, see Appendix 2 sec. 3.1.

Figure 6. Quick separation using permanent magnet.

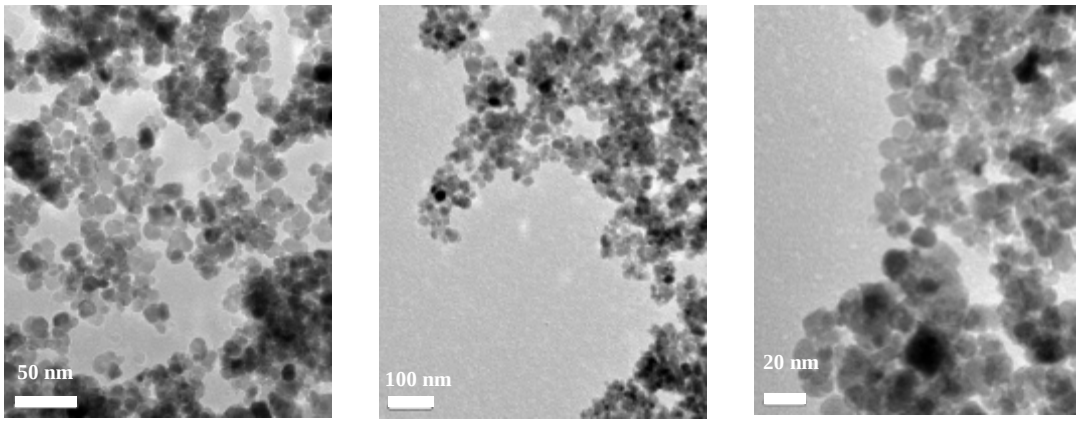


(a) (b) (c)

Figure 7. TEM micrographs of $Fe_3O_4$ nanoparticles at different magnification: scalebar (a) 50 nm, (b) 100 nm, (c) 20 nm.

A magnetically separable support, prepared using the above-mentioned method, was used to synthesize various asymmetric catalysts. The modes of preparation, and catalysts testing, are described in the next paragraphs.

### 2.1.1 Synthesis of MNP/[R-BINAS-Rh(cod)$Cl_2$] and its application in the asymmetric hydrogenation of DMIT

Sulfonation of R-BINAP ((*R*-(+))-(1,1′-Binaphthalene-2,2′-diyl)bis (diphenylphosphine)) (Scheme 28) was carried out. The sulfonated groups were incorporated in order to anchor the catalyst on the surface of the nanoparticles. The sulfonation of R-BINAP requires specific reaction conditions in order to eliminate

the formation of phosphine. The sulfonation of R-BINAP was accomplished using the procedure proposed by Wan and Davis [118], which consisted of dissolving R-BINAP in concentrated sulfuric acid. Then, 20 % $SO_3$ in concentrated sulfuric acid was dropped into the solution under argon. Afterwards, methanol was added to precipitate any sodium sulfate present. Sulfonated R-BINAP (R-BINAS) was recovered as a solid by vacuum drying the filtered methanolic solution. A yellow solid was created and analysed using a NMR technique. The spectra showed a mixture of sulfonated R-BINAP, mainly in two positions of the naphthalene ring. Different results were shown by elementary analysis and according to these results the R-BINAP were sulfonated in six positions. For this experiment, it was not considered important to show how many sulfonate groups the R-BINAP consist of. The main purpose was to introduce polar groups to the R-BINAP molecule. For synthetic details, see Appendix 2 sec. 3.2.

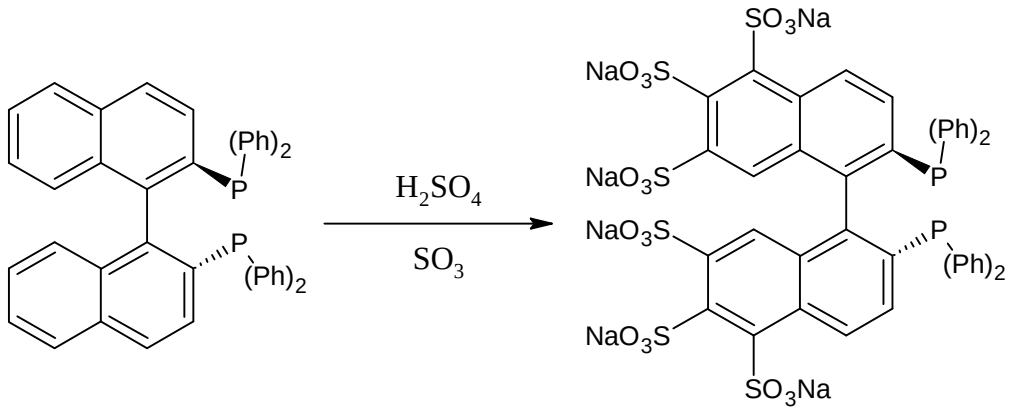


Scheme 28. Sulfonation of R-BINAP.

The next step in this mode of preparation was complexing $[Rh(cod)Cl_2]_2$, cod = cycloocta-1,5-diene) with R-BINAS. The procedure described by Noyori [119], was used. Two equiv. of R-BINAS were treated with one equiv. of $[Rh(cod)Cl_2]_2$ in pure THF at room temperature, under argon (Scheme 29).

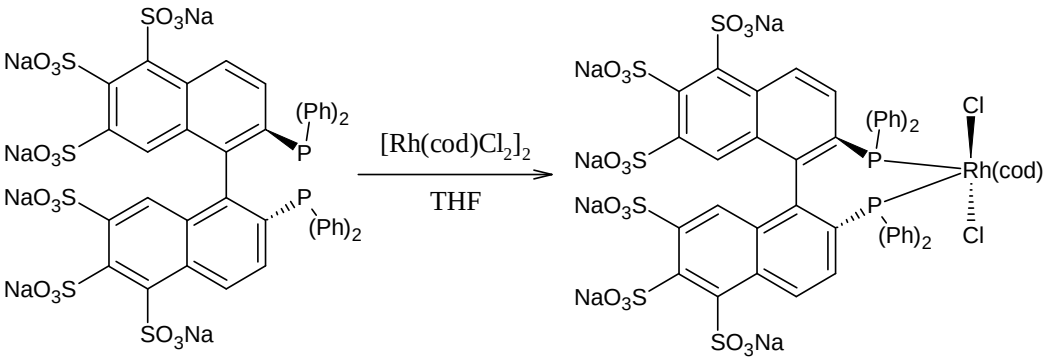


Scheme 29. Complexation of R-BINAS with $[Rh(cod)Cl_2]_2$.

The immobilization of R-BINAS-Rh complex on $Fe_3O_4$ nanoparticles MNP/[R-BINAS-Rh(cod)$Cl_2$] was carried out in pure methanol in an ultrasonic bath. The catalyst was dried under vacuum for 3 days. The supernatant was analyzed using AAS using Rh standard. Results showed that over 99 % of the complex was absorbed on the surface of the nanoparticles (Scheme 30). For synthetic details, see Appendix 2 sec. 3.2.

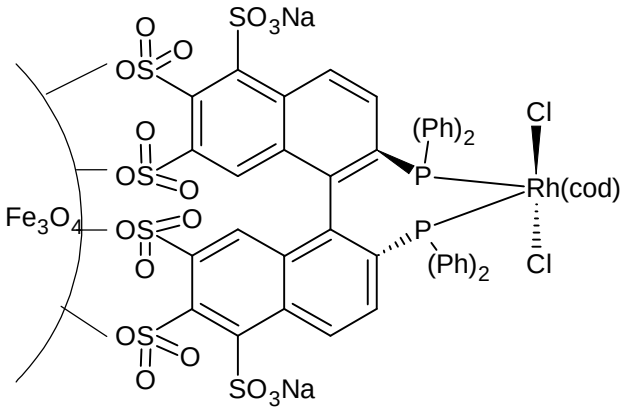


Scheme 30. Immobilized R-BINAP derivates on the surface of MNPs.

The synthesized catalyst was tested in the hydrogenation of DMIT (dimethyl itaconate) (Scheme 31). The hydrogenation was carried out in a 50 $cm^3$ high pressure stainless steel reactor (Figure 8), under 3.5 bar $H_2$ pressure and at 50 °C. The molar ratio was S/C = 100 (S - substrate, C - catalyst). After 4 h of reaction, the catalyst was separated by magnetic decantation.

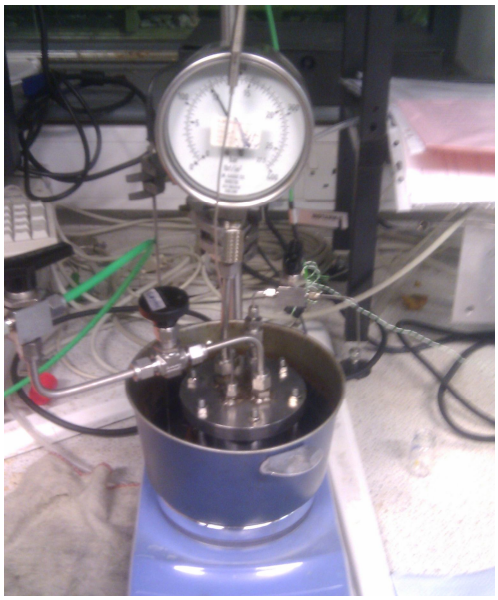

Figure 8. Picture of the high pressure stainless steel reactor.

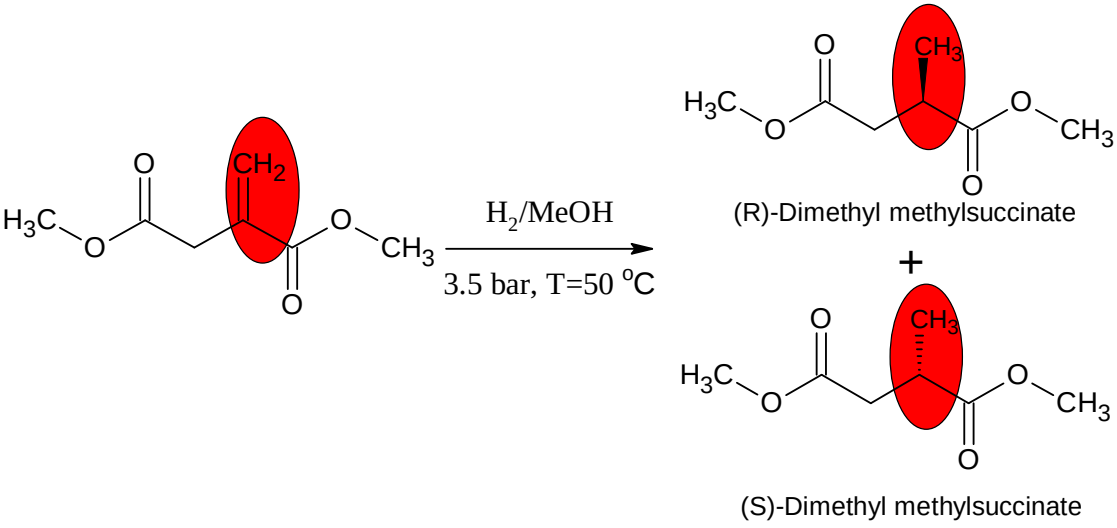


Scheme 31. Asymmetric hydrogenation of DMIT using R-BINAP-modified nanoparticles.

The product of the hydrogenation was analyzed using $^{1}$H NMR, GC and HPLC. The NMR showed that the product was pure dimethyl methylsuccinate. GC showed that there was 100 % conversion, and the HPLC showed that there was 97 % ee (% ee $= \frac{[R]-[S]}{[R]+[S]} 100\%$ , % ee - enantiomeric excess). From two possible products R and S-enatiomer, the R-enantiomer (Scheme 31) was produced in excess. The reaction was repeated 10 times. The catalyst still gave 100 %

conversion after 10 uses, but starting from the second cycle and thereafter, the ee fell to nearly 0 %. It was decided to repeat the whole synthesis procedure for R-BINAP, and also for S-BINAP. Unfortunately, the results were disappointing. 100 % conversion was achieved, but once more, the % ee was nearly zero). For synthetic details, see Appendix 2 sec. 3.3. Additionally, a blank control test was carried out. Bare nanoparticles were used for hydrogenation of DMIT in the same conditions. No product was observed. TEM studies indicated slight aggregation after coating with catalysts and after hydrogenation (Figure 9). The significantly darker dots on TEM micrographs might be caused by agglomeration of particles during sample preparation.

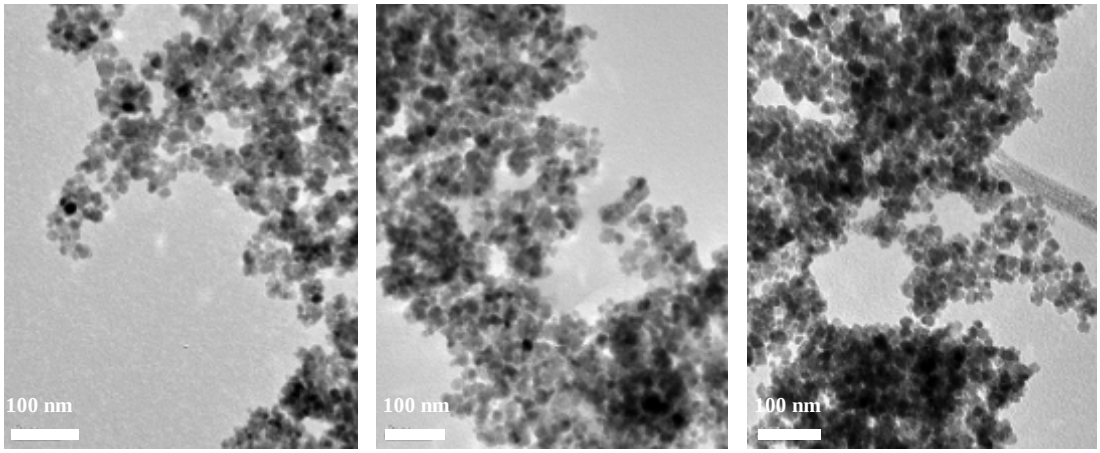


(a) (b) (c)

Figure 9. TEM micrographs: (a) bare nanoparticles, (b) nanoparticles coated with R-BINAP based catalyst, (c) nanoparticles coated with R-BINAP based catalyst after hydrogenation of DMIT.

### 2.1.2 Synthesis of MNP/[R-P-Phos-Rh(cod)$Cl_2$]

In this experiment no pretretment of R-P-Phos ((R)-(+)-2,2',6,6'-Tetramethoxy-4,4'-bis(diphenylphosphino)-3,3'-bipyridine)) was necessary. This ligand includes polar groups, which can be immobilized on the surface of nanoparticles. Noyoris' procedure [119] for complexing Rh with R-P-Phos ligand was applied. Two equiv. of R-P-Phos were treated with one equiv. of $[Rh(cod)Cl_2]_2$ in pure THF at room temperature and stirred for 1.5 h under argon (Scheme 32). The

immobilization of a R-P-Phos-Rh complex on $Fe_3O_4$ nanoparticles MNP/[R-P-Phos-Rh(cod)$Cl_2$] was carried out in pure methanol for 3 h in an ultrasonic bath. AAS analysis results showed that over 99 % of the complex was absorbed on the surface of the MNPs (Rh standard was used). For synthetic details, see Appendix 2 sec. 3.4.

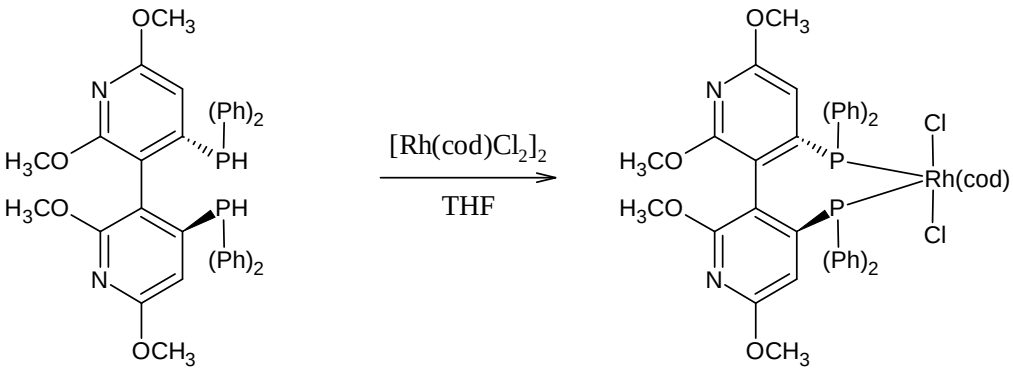


Scheme 32. Complexation of R-P-Phos with Rh(cod)$Cl_2$.

The hydrogenation of dimethyl itaconate (Scheme 31) was carried out in a 50 $cm^3$ high pressure stainless steel reactor under 3.5 bar $H_2$ pressure and at 50 °C. The molar ratio was equal to S/C = 100 (S - substrate, C - catalyst). After 4 h of reaction, the catalyst was separated by magnetic decantation. The product was analyzed using $^1$H NMR, GC and HPLC. The NMR showed a mixture of substrate and product. The GC showed that there was 50 % conversion. Separation of the substrate and product was carried out using CC (column chromatography). Unfortunately, the ee was around 0 %.

### 2.1.3 Synthesis of MNP/[R-P-Xyl-Phos-Rh(cod)$Cl_2$]

A structurally similar ligand, R-P-Phos(R-(+)-P-Xyl-Phos-((R)-(+)-2,2',6,6'-Tetramethoxy-4,4'-bis(di(3,5-xylyl)phosphino)3,3'bi-pyridine), was used for the preparation of the next catalyst. Noyoris' procedure [119] for complexing Rh with R-P-Phos ligand was applied. Two equiv. of R-P-Phos ligand were treated with one equiv. of [Rh(cod)$Cl_2$]$_2$ in pure THF at room temperature under argon (Scheme 33).

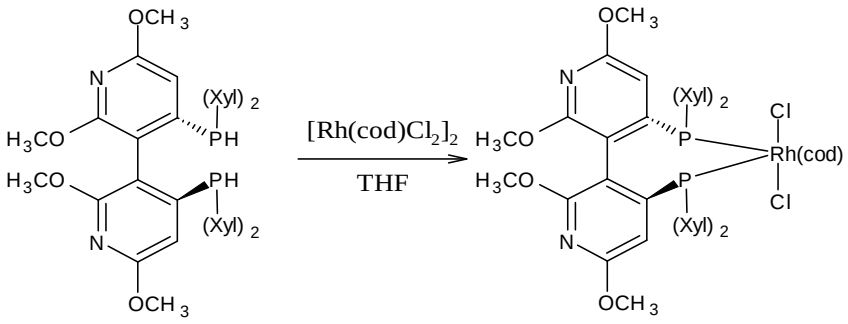


Scheme 33. Complexation of R-P-Phos with $[Rh(cod)Cl_2]_2$.

The immobilization of a R-P-Xyl-Phos–Rh complex on $Fe_3O_4$ nanoparticles was done in pure methanol in an ultrasonic bath. The supernatant was analyzed using AAS, using Rh as a standard. The results showed that over 99 % of the complex was absorbed on the surface of the nanoparticles. For synthetic details, see Appendix 2 sec. 3.5.

The hydrogenation of dimethyl itaconate (Scheme 31) was carried out using the same conditions used in the experiment in section 2.1.2. The product of the hydrogenation was analyzed using $^1$H NMR, GC and HPLC. The NMR showed a clean product. The GC showed 100 % conversion. Unfortunately, the ee was around 0 %. The procedure was carried out under the same conditions one more time, with high conversion, but without any results in terms of enantioselectivity.

### 2.1.4 Synthesis of MNP/Au(0) and its application in oxidation reactions

Discouraged by the results in asymmetric catalysis, it was decided to avoid using very expensive asymmetric ligands, and instead to develop non-chiral catalysts based on MNPs. There has been considerable recent interest in employing gold catalysts to oxidation reactions. Williams' group [117] recently synthesized water-soluble, Au-coated magnetic iron oxide nanoparticles by the reduction of $Au^{3+}$ onto their surfaces. Such nanoparticles were tested in the oxidation of 2–butanol and benzyl alcohol using a solvent free method proposed by Zhang *et al*. [120]. Using a similar procedure, gold-coated MNPs were prepared. The MNPs were dispersed in an aqueous solution of TMAOH and stirred with sodium citrate. Ammonium hydroxide ($NH_4OH$) and 1 % gold(III) chloride hydrate ($HAuCl_4$) were added incrementally and alternately. The supernatant was analyzed for Au content using the

AAS analysis. Over 99 % of the gold was immobilized on the surface of the nanoparticles. For synthetic details, see Appendix 2 sec. 3.6. The catalyst was tested in the oxidation of *tert*-butanol and benzyl alcohol, using $H_2O_2$ as the oxidation agent. The reactions were carried out at 90 °C. Different molar ratios between the catalyst and the substrate were tested (100, 300, 600). The progress of each reaction was analyzed using TLC. In each case, no products of oxidation were observed. After 24 h the catalyst was separated using magnetic decantation and the oxidation agent was evaporated. The reaction mixture was analyzed using GC and NMR. Again, no oxidation product was observed. For synthetic details, see Appendix 2 sec. 3.7.

Different methods of oxidation by molecular oxygen were applied, as described by Mori and Nishimura [85, 121]. Benzyl alcohol, MNP/Au(0) (molar ratio = 200) and toluene were placed into a reaction vessel with a reflux condenser. The resulting mixture was stirred at 90 °C under $O_2$ flow. The result of the reaction was monitored by GC, NMR analysis. After 24 h, no product of oxidation was observed. It was possible due to lack of the control of gold particles size. For synthetic details, see Appendix 2 sec. 3.8. Discouraged by these results of oxidation on MNP/Au(0), it was decided to test another important catalyst – ruthenium.

### 2.1.5 Synthesis of MNP/Ru(0) and its application in dihydroxylation reaction

It is well known that the dihydroxylation reaction and its asymmetric variants represent an important milestone in modern organic synthesis. This technology has been widely applied to the synthesis of pharmaceuticals and fine chemicals. Osmium is the most common catalyst used in the dihydroxylation process, but ruthenium has recently been demonstrated [97] to catalyze *cis*-dihydroxylation of alkenes. Herein, the dihydroxylation of different alkenes using MNP/Ru(0) and different dihydroxylation agents ($NaIO_4$, $H_2O_2$, $O_2$) will be presented. For the immobilization of ruthenium onto the surface of nanoparticles, Kurihara's [122] polyol method was applied. $RuCl_3 \cdot nH_2O$ was dissolved under $N_2$ in ethylene glycol, and MNPs were added. The mixture was refluxed for 3 h. The AAS analysis showed no presence of ruthenium in the supernatant, which proved the total immobilization of Ru on catalyst support. For synthetic details, see Appendix 2 sec. 3.9.

The first dihydroxylation method was carried out on the basis of Ho's work [123]. A diluted sulphuric acid solution with $NaIO_4$ was used as an oxidant in this reaction and placed in tubes of Carousel 12 Reaction Station, Radleys Discovery Technologies, UK. MNP/Ru(0) was added in to test tubest, followed by mixture of EtOAc - MeCN (1:1). Appropriate amounts of alkene (styrene, dimethyl fumarte, dimethyl maleate) were added. The reaction mixtures were stirred for 24 h at room temperature. The products were analyzed using GC analysis. The results after 24 h of this experiment are summarized in Table 1. All of the reactions ran according to the (Scheme 51-54). For synthetic details, see Appendix 2 sec. 3.10.

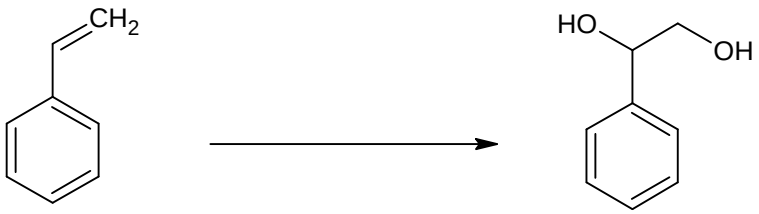


Scheme 34. Dihydroxylation of styrene using MNP/Ru(0).

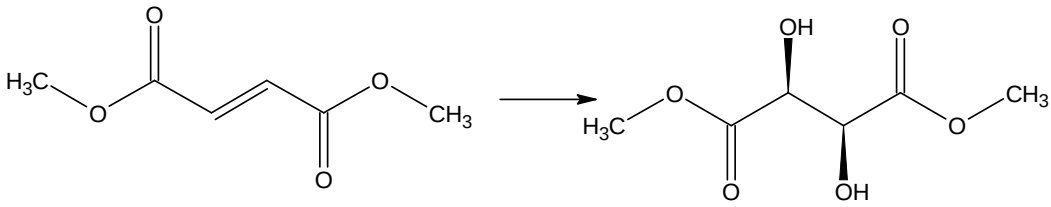


Scheme 35. Dihydroxylation of dimethyl fumarte using MNP/Ru(0).

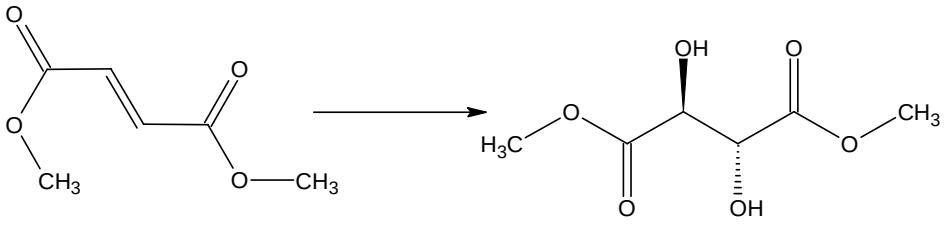


Scheme 36. Dihydroxylation of dimethyl maleate using MNP/Ru(0).


Scheme 37. Dihydroxylation of 1-decene using MNP/Ru(0).

Table 1. Conversion of alkenes catalysed by MNP/Ru(0).

| Substrate | Conversion [%] |
|---|---|
| Styrene | 88 |
| dimethyl fumarte | 92 |
| dimethyl maleate | 85 |

Encouraged by these results, the catalyst was used to dihydroxylate the same alkenes using the method reported by Dobler *et al*. [124], in which molecular oxygen was used as the dihydroxylation agent. Appropriate amounts of alkene (styrene, dimethyl fumarte, dimethyl maleate, 1-decene) were diluted in *tert*-butanol and an aqueous buffer solution (pH = 10). The catalyst (S/C = 100) (S - substrate, C - catalyst) was then added. The mixture was stirred at 50 °C under $O_2$ flow for 24 h. Conversion was measured using GC. The starting material totally disappeared. The structure was analyzed using the NMR technique. Unfortunately, the information gathered from NMR was repeatedly unclear and satisfying results could not be obtained. For synthetic details, see Appendix 2 sec. 3.11.

Hydrogen peroxide was the last oxidising agent used for dihydroxylation of alkenes, according to the procedure presented by Jonsson [125]. Olefins (styrene, dimethyl fumarte, 1-decene) were dissolved in a mixture of water and acetone in tubes of Carousel 12 Reaction Station, (Radleys Discovery Technologies, UK). The MNP/Ru(0) and $H_2O_2$ were added. The reaction was stirred for 24 h at room temperature. After 24 h of the reaction, the mixture was analyzed using GC. No products of dihydroxylation were observed. In summary, $NaIO_4$ is the only oxidising agent which was successfully applied for the dihydroxylation of olefins on MNP/Ru(0). For synthetic details, see Appendix 2 sec. 3.12.

### 2.1.6 Synthesis of MNP/Pd(0) and its application in DMIT hydrogenation

The modified procedure described in Lyon *et al.* [117] was used for the preparation of MNP/Pd(0). MNPs were dispersed in water and sonicated for 30 min. $H_2PdCl_4$ was used as the metal source and $NaBH_4$ as the reducing agent. The Pd loading on the MNP was 3 % w/w. MNP/Pd(0) was fully characterized because of its various application in this work. The average particle size of the MNPs was *ca.* 10 nm, with 2-3 nm particles of palladium on their surface, as confirmed by TEM

analysis (Figure 10). The SQUID-VSM analysis confirmed the superparamagnetic behaviour of the catalyst (Figure 11), and powder X-ray diffraction (XRD) proved the presence of palladium (Figure 12). SQUID-VSM analysis was carried out by Professor Quentin Pankhurst's group at University College London. For synthetic details, see Appendix 2 sec. 3.13.

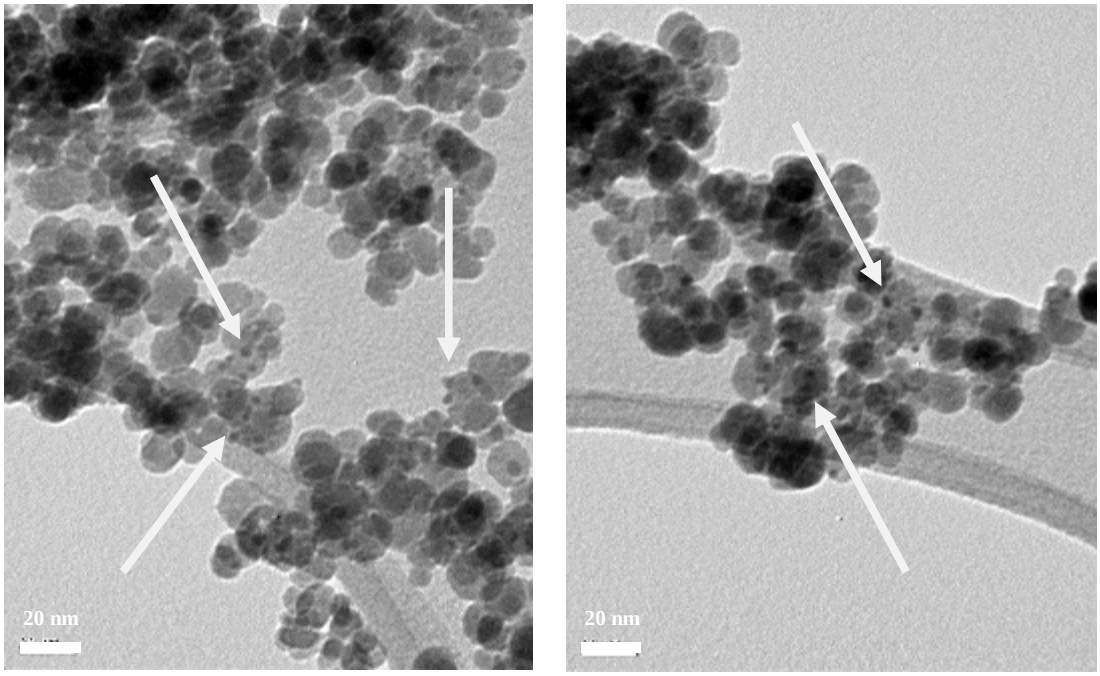


(a) (b)

Figure 10. TEM micrographs of MNP/Pd(0). White arrows indicate Pd(0).

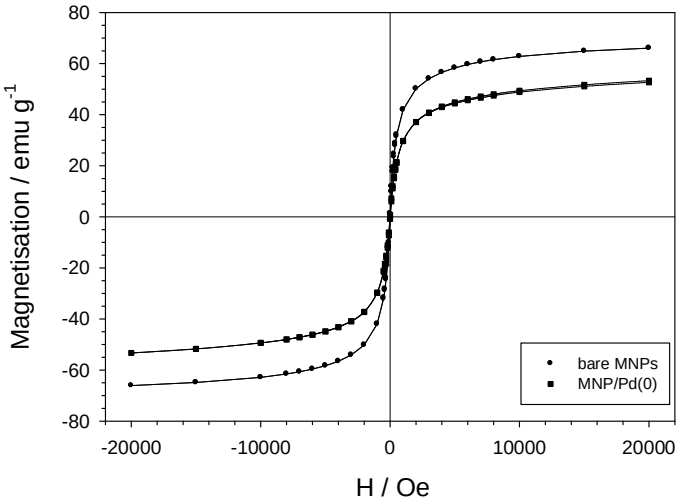


Figure 11. SQUID-VSM magnetization curves of bare and Pd(0)-bearing MNPs. Pd contents was 3 wt % .

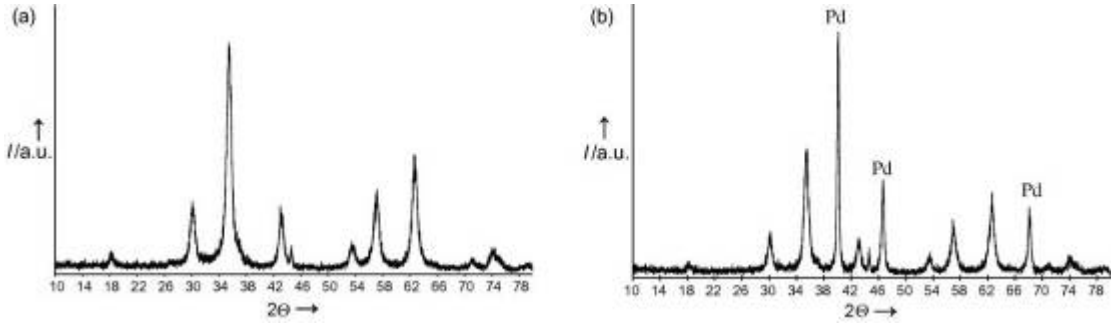


Figure 12. XRD patterns for MNP-based Pd catalysts: (a) bare MNPs, (b) MNP/Pd(0).

The MNP/Pd(0) catalyst was shown to be very effective in catalysing the hydrogenation of double bonds. The MNP/Pd(0) system was used for hydrogenation of olefinic C=C in dimethyl itaconate (Scheme 38). The hydrogenation was carried out in a 50 $cm^3$ high pressure stainless steel reactor under 3.5 bar $H_2$ pressure and at 50 °C, where S/C = 100 (S - substrate, C - catalyst). After 4 h of reaction, the catalyst was separated by magnetic decantation. For synthetic details, see Appendix 2 sec. 3.14.

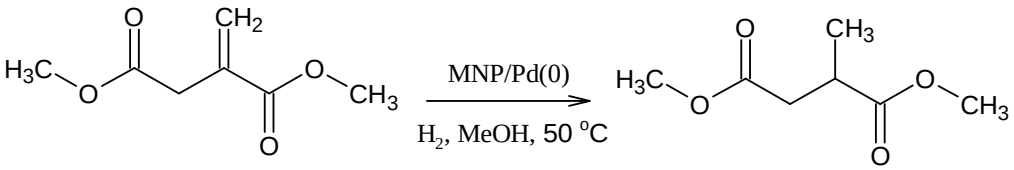


Scheme 38. Hydrogention of DMIT using MNP/Pd(0).

The product was analyzed using $^1H$ NMR and GC. The NMR showed a clean product. GC showed 100 % conversion. It was possible to hydrogenate the DMIT quantitatively for four cycles using the same catalyst, which suggests that the catalyst activity was sustained at the same level. This catalytic system was chosen for further studies on its application in a capillary reactor, described in Chapter 3.

### 2.1.7 Application of MNP/Pd(0) in nitrobenzene hydrogenation

The MNP/Pd(0) catalyst was also tested in hydrogenation of NB (nitrobenzene) (Scheme 39), and appeared to be a very effective catalyst. The hydrogenation of NB was carried out in similar conditions to the hydrogenation of DMIT. The reaction mixture was stirred at 50 °C for 4 h under 3.5 bar $H_2$ pressure. It was possible to hydrogenate NB quantitatively using catalyst, with S/C = 100 (S - substrate, C - catalyst). The catalyst was recycled, and three more cycles were repeated with 100 % conversion to aniline. For synthetic details, see Appendix 2 sec. 3.15. Kinetic studies were carried out in the microreactor using this system as a model reaction. The results of these studies are described in Chapter 4.

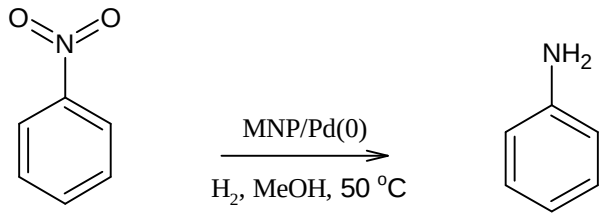


Scheme 39. Hydrogenation of NB using MNP/Pd(0).

### 2.1.8 Application of MNP/Pd(0) in tandem Knoevenagel - hydrogenation

In this section attention has been focused on the utilization of MNP/Pd(0) in a tandem Knoevenagel condensation - hydrogenation (Scheme 40). All experiments were carried out with collaboration with Dr. Urszula Laska. Knoevenagel reactions are some of the most important C–C bond forming organic transformations, creating electrophilic olefins from active methylene groups and carbonyl compounds [126]. Iron oxide nanoparticles are shown to promote Knoevenagel condensations at excellent yields. Their functionalization with palladium offers an efficient catalyst for C-C double bond hydrogenation.

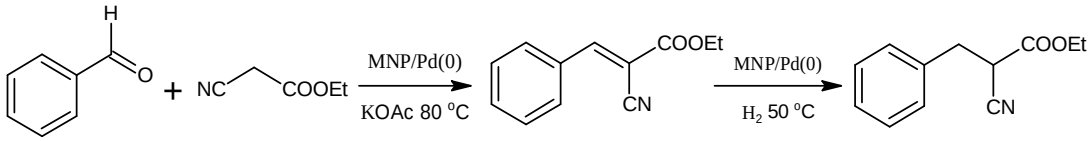


Scheme 40. Tandem Knoevenagel condensation - hydrogenation reaction**.**

Initial experiments were carried out for the Knoevenagel condensation of ethyl cyanoacetate and benzaldehyde at 80 °C. The reactions were performed in both the presence and in the absence of a base, until the disappearance of the substrates (as monitored by GC). Initially the toluene and insoluble inorganic base (potassium acetate) were used. The presence of an insoluble base may facilitate the separation of products from the reaction mixture. However, as it can be seen in the next section, potassium acetate caused severe catalyst deactivation during the hydrogenation step of the tandem reactions (Knoevenagel/hydrogenation). Therefore, the organic-soluble base (ethylene triamine) was also used in the tandem reactions. As can be seen in Figure 13, both systems (MNP and MNP/Pd(0)) can catalyse Knoevenagel condensation in the presence of a base, with bare MNPs resulting in faster kinetics. The presence of organic-soluble $Et_3N$ provided faster kinetics, which were almost the same as for MNP/Pd(0) with KOAc (Figure 13). For synthetic details, see Appendix 2 sec. 3.16 and 3.17.

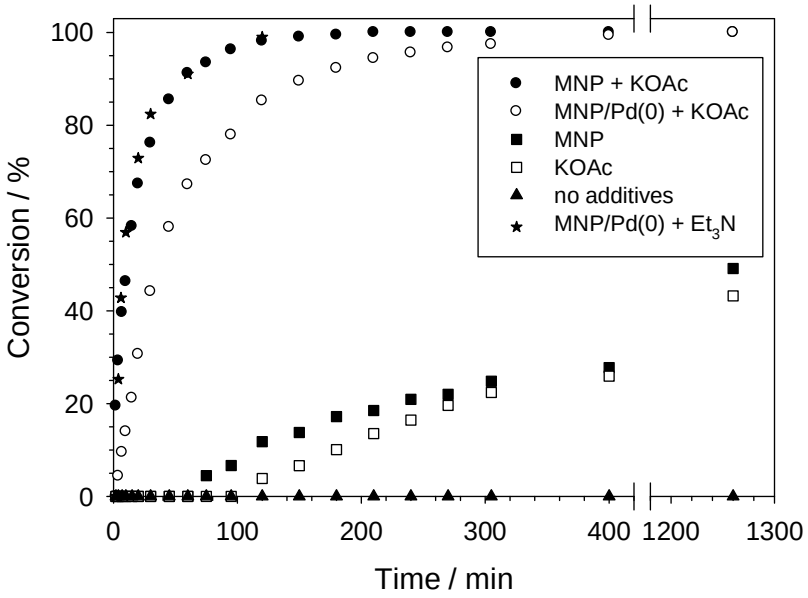


Figure 13. The catalytic role of magnetite on the Knoevenagel condensation.

Iron oxide alone can also promote condensation, but at a rate far slower than in the presence of a base, leading to 65 % conversion after 20 h. When potassium acetate (KOAc) was used as the only catalyst, the process was even less successful. At this point, it was interesting that a cooperative effect between MNPs and the base was observed, when applied together. Control experiments

confirmed that no reaction was observed when simply mixing ethyl cyanoacetate and benzaldehyde The activity of MNPs in the aldol-type reaction arises from Brönsted basicity of iron oxide nanoparticles stabilized with $OH^-$ anions. The efficiency of MNP-based catalysts was affected by the solvent polarity and the nature of the base that was employed. The rate of reaction was much faster in methanol than in toluene; however, a number of undesired by-products were detected, lowering the overall reaction conversion. The main by-product was identified as a product of transesterification of ethyl cyanoacetate into methyl cyanoacetate, which can occur in the presence of a base. The catalytic activity of the MNP/Pd(0) in aldol condensation is lower than that observed for bare MNPs (Figure 13), presumably due to the presence of palladium nanoparticles, reducing access to the iron oxide/$OH^-$ sites. Moreover, the Pd(0) impregnation procedure lowered the number of $OH^-$ anions, stabilizing the MNP's surface. The palladium functionality is, however, necessary to test the MNP/Pd(0) system as a potential bifunctional catalyst in the tandem reaction. From previous experiments, it is known that the MNP/Pd(0) has been found to be very effective for the hydrogenation of the C=C bond (DMIT hydrogenation). Having this in mind, it was decided to extend the process by the additional step of reducing the ethyl *trans*-α-cyanocinnamate olefinic bond. The reaction proceeded under bubbling hydrogen at 50 °C and lead to the completion within 2 h. Ethyl α-cyanohydrocinnamate was formed as the only product of hydrogenation.

#### 2.1.8.1 MNP/Pd(0) catalyst recovery and reusability: kinetics studies

The reaction of benzaldehyde with ethyl cyanoacetate in the presence of a base was chosen as a model reaction for catalyst reuse studies. To test the stability and recyclability of the iron oxide-based catalysts, the nanoparticles were recovered magnetically, washed, and reused in subsequent runs under the same reaction conditions. The initial tests on MNP/Pd(0) in Knoevenagel reaction showed that the catalyst was stable, giving stable initial rate of reaction around $1.5 \times 10^{-6}$ mol $g^{-1}_{cat}$ $s^{-1}$ in all four tandem cycles (Figure 14). However, after the tandem reaction, the initial rates of hydrogenation decreased significantly for the

reused catalyst, going from $3.77 \times 10^{-4}$ mol $g^{-1}_{cat}$ $s^{-1}$ in the first run to $1.87 \times 10^{-5}$ mol $g^{-1}_{cat}$ $s^{-1}$ in the second (Figure 15).

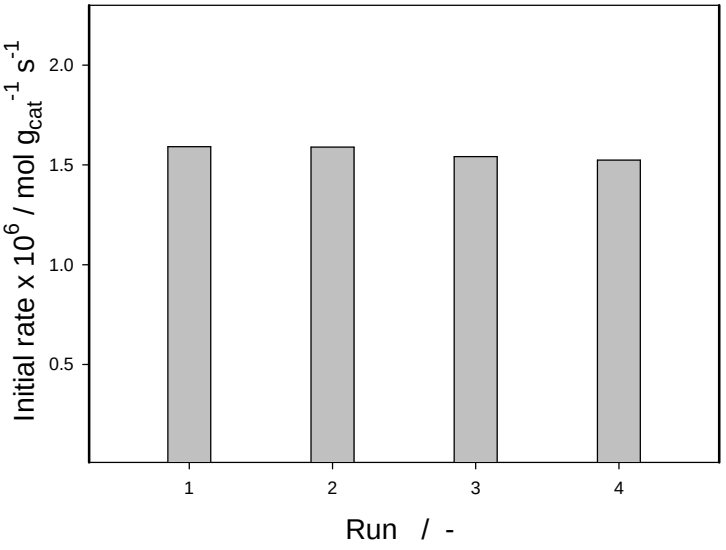


Figure 14. Recycling efficiency of the MNP/Pd(0) catalyst for a Knoevenagel reaction in a tandem Knoevenagel - hydrogenation process with KOAc.

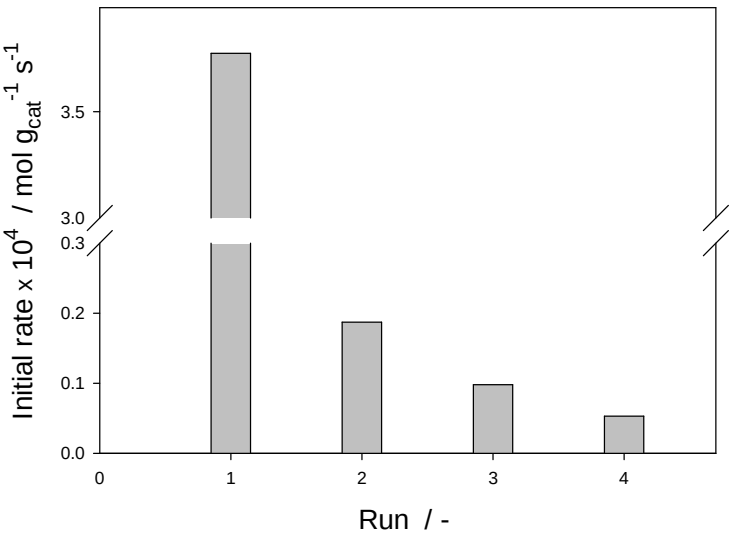


Figure 15. Recycling efficiency of the MNP/Pd(0) catalyst for hydroegenation in tandem Knoevenagel - hydrogenation process with KOAc hydrogenation.

Since the amount of soluble palladium detected by AAS analysis in a reaction mixture was less than 0.8 % of the initial Pd amount, it is clear that such a big decrease in initial reaction rate is not primarily caused by the active metal leaching.

Thus, two other possibilities of catalyst deactivation have to be taken into account: (*i*) aggregation of magnetic nanoparticles leading to the lower availability of active sites (Pd(0)), or (*ii*) coordination of palladium by KOAc leading to catalyst poisoning. That is why it was decided to use $Et_3N$ as a base source. The use of organic, soluble $Et_3N$ as a base resulted in a stable catalyst. The applied catalyst, MNP/Pd(0), was active for both reactions: Knoevenagel condensation (Figure 16) and hydrogenation (Figure 17) in four consecutive runs of the tandem process. This shows the potential of magnetic based nanocatalysts for tandem processes.

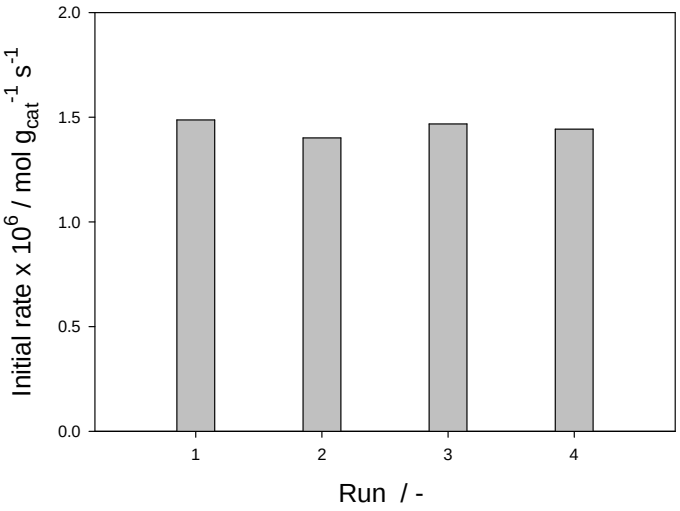


Figure 16. Recycling efficiency of the MNP/Pd(0) catalyst for Knoevenagel condensation in a tandem Knoevenagel - hydrogenation process with $Et_3N$.

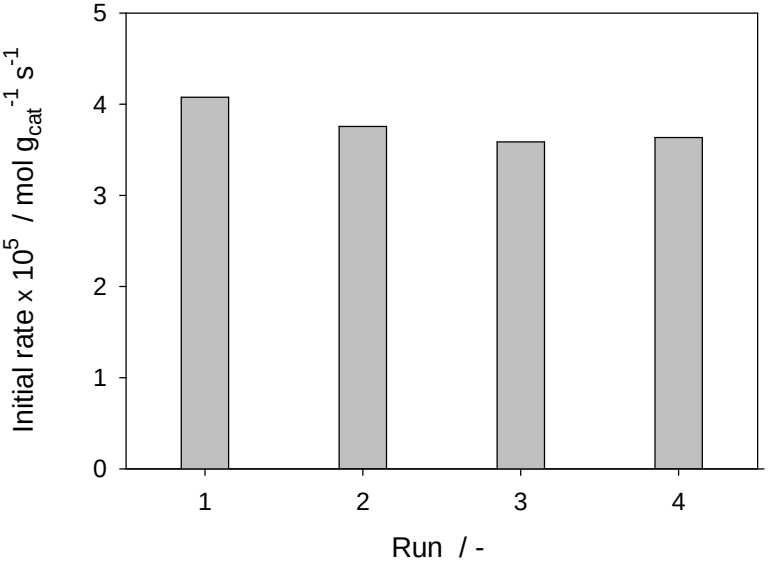


Figure 17. Recycling efficiency of the MNP/Pd(0) catalyst for hydrogenation in a tandem Knoevenagel - hydrogenation process with $Et_3N$.

### 2.1.8.2 MNP/Pd(0) catalyst stability

All XPS measurements were performed and interpreted by Dr. Karen Wilson form the School of Chemistry, Cardiff University. The origin of the differences in catalyst activity and stability when $Et_3N$ or KOAc is used as the base were subsequently investigated by XPS. Table 2 shows the surface compositions for fresh and spent catalysts. While there is a decrease in the atomic Fe:Pd ratio, the magnitude of this change is the same when both $Et_3N$ or KOAc are used as the base, thus this cannot account for differences in NP performance by differential Pd loss. Following the reaction, an increase in K and N content can be observed, suggesting that KOAc does bind to the surface of the catalyst. The N 1s signal was observed at 399.5 eV and could be attributed to $NEt_3$ or C≡N groups from ethylcyanoacetate, so binding of $NEt_3$ cannot be unequivocally determined.

Table 2. XPS compositions of MNP/Pd(0) nanoparticles following tandem Knoevenagel condensation and hydrogenation.

| | **Weight / %** | | | | | | | |
|---|---|---|---|---|---|---|---|---|
| Sample | Fe 2p | O 1s | N 1s | Pd 3d | C 1s | K 2p | Atomic Fe:Pd | Pd(II):Pd(0) |
| Fresh | 59.4 | 28.1 | | 0.6 | 11.9 | | 0.004 | 80:20 |
| Spent using $Et_3N$ base | 47.1 | 28.2 | 0.8 | 0.2 | 23.7 | | 0.002 | 0:100 |
| Spent using KOAc base | 57.8 | 27.2 | | 0.2 | 14.1 | 0.7 | 0.002 | 29:71 |

Closer inspection of the high resolution Pd 3d spectra reveal that there are significant differences in the two spent catalysts following tandem Knoevenagel and hydrogenation reactions. The spin orbit $Pd_{7/2}$ and $Pd_{5/2}$ of the fresh catalyst are split into two poorly resolved doublets at 337.7, 342.9 and 335.9, 341.1 eV corresponding to the binding energy of Pd(II) and Pd(0) respectively. Deconvolution of these components reveals that the fresh catalyst is comprised of *ca.* 80 % surface Pd(II). In the presence of $Et_3N$, complete reduction of Pd(II) is observed with only Pd(0)

visible in the spent catalyst. However, when the reaction is performed in the presence of KOAc, the catalyst remains largely oxidic, which suggests that adsorbed K inhibits $H_2$ dissociation and reduction of Pd clusters. Thus, in the absence of poisoning from adsorbed K, the activity of Pd-MNP catalysts in tandem Knoevenagel - hydrogenation reactions can be maintained. Experiments on the flow Knoevenagel - hydrogenation tandem reaction were carried out in the microreactor and were described in Chapter 4.

## 2.2 Initial experiments in microreactors and aggregation of nanoparticles

While evaluation was carried out of different catalysts supported on magnetic nanoparticles for various reactions, initial experiments on the applications of successful batch reaction were carried out in the microreactors. Two different microreactors were employed for these experiments: a Standard Slit Interdigital Micro Mixer, SSIMM-Ni25T11 form Institut für Mikrotechnik Mainz GmbH, (Figure 18a), and Mikroreaktor: XXL-ST-04, form LTF GmbH Ilmenau (Figure 18b). Further details of the microreactors can be found in Chapter 4.

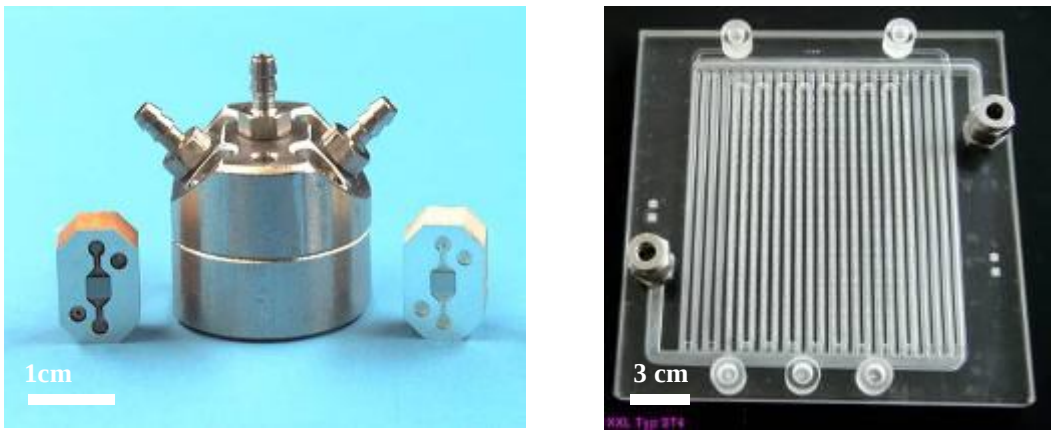


(a) (b)

Figure 18. Pictures of microreactors: (a) SMSIMM, (b) XXL-ST-04.

Unfortunately, due to the aggregation of catalysts, it was impossible to proceed with the experiments. The SSIMM reactor became blocked immediately, while in the XXL-ST-04 reactor MNP catalysts slowly sedimented with the flow of the reagent and finally caused blockage. Lu [127] claimed that, as a result of

anisotropic dipolar attraction, nanoparticles of iron oxides tend to aggregate into large clusters, and thus lose the specific properties associated with single-domain, magnetic nanostructures. The solution to this problem was to more efficiently prevent the magnetic nanoparticles from aggregation, by coating them with a layer of non-magnetic material. In the next few paragraphs, the efforts to eliminate aggregation will be presented.

### 2.2.1 Alumina coated magnetic nanoparticles

In the first instance, it was decided to coat the MNPs with an alumina layer. In order to do this, a procedure proposed by Wan [128] was used. For the synthesis of a mesoporous alumina shell, triblock copolymer Pluronic F-127 or P-123 were used as the structure-directing agent, and aluminium chloride as an inorganic precursor. $NH_3$ was added to hydrolyze the alumina precursor. The procedure required a calcination step at 1000 °C for 2 h, which probably caused sintering of the MNPs. For synthetic details, see Appendix 2 sec. 3.18. After this procedure aiming to coat the MNPs with an alumina layer, it was not possible to redisperse the MNPs in any solvent. In conclusion, the presented procedure did not solve the problem with particle aggregation.

### 2.2.2 Carbon coated magnetic nanoparticles

Lu *et al.* [22] suggested that coating with a carbon layer might prevent the aggregation of nanoparticles. A slightly modified method, proposed by Lu *et al.* [129], was used to coat MNPs with a carbon layer. The synthesis is described as follows: MNP were freshly prepared using a standard method, and suspended in dry toluene. Afterwards, the MNPs were mixed with an excess amount of Pluronic surfactant P-123, which has two functions: it prevents the agglomeration of nanoparticles, and acts as the carbon source for surface coating of the MNP. After drying, the solid was thermally treated at 850 °C for 2 h under a flow of nitrogen to achieve carbon-protected nanoparticles. For synthetic details, see Appendix 2 sec. 3.19 The second method, described by Almeida [130], was carried out simultaneously. In this procedure, furfuryl alcohol (FA) was used as a precursor of carbon. For this process, MNPs were mixed with furfuryl alcohol in the presence of

oxalic acid as the polymerization catalyst. The polymerization was carried out at 90 °C for 8 h. After the analogous thermal treatment (850 °C for 2 h under a flow of nitrogen) as in the above experiment, a shiny black powder was obtained. For synthetic details, see Appendix 2 sec. 3.20. As was the case when coating with an alumina layer, coating with carbon requires a calcination step, which probably caused sintering of the MNPs. It was not possible to redisperse the MNPs in any solvent after calcination.

### 2.2.3 Silica coated nanoparticles

Disappointed with the results of coating nanoparticles with a carbon or alumina protecting layer, attention was focused on the method presented by Lu [127]. According to this publication, it was possible to coat the MNP with amorphous silica, produced *via* the hydrolysis of a sol-gel precursor tetraethyl orthosilicate (TEOS). Since the iron oxide surface has a strong affinity toward silica, no pre-treatment was required to promote the deposition and adhesion of silica. In a typical procedure, a water solution of MNPs was sonicated with 2-propanol. Under continuous mechanical stirring, an ammonia solution and various amounts of TEOS were added consecutively to the reaction mixture. The reaction was allowed to proceed at room temperature for 3 h under continuous stirring. For synthetic details, see Appendix 2 sec. 3.21. The growth of silica shells on the iron oxide nanoparticles involved the base-catalyzed hydrolysis of TEOS, and the subsequent condensation of silica onto the surfaces of iron oxide cores. The core-shell nanoparticles could be separated from the reaction *via* magnetic decantation. Due to the presence of negative charges on the surfaces of silica shells, nanoparticles could form very stable dispersions in water and other polar solvents without adding other surfactants. To confirm the presence of silica on iron oxide, IR analysis was carried out. Two sample: the first with pure nanoparticles and the second with coated nanoparticles, were tested. The plots shown below (Figure 19) were generated, and the presence of $SiO_2$ groups was clearly visible. Vibration from the symmetric stretching Si-O of silica can be observed at around 1100 $cm^{-1}$. The lower frequencies of around 820 $cm^{-1}$ correspond to asymmetric Si-O stretching. Those signals were not visible in the pure $Fe_3O_4$ spectra.

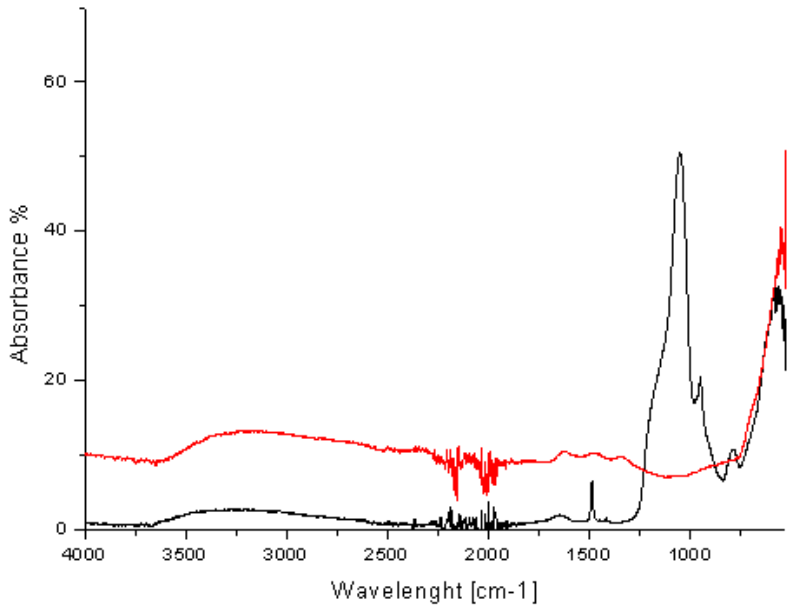


Figure 19. IR spectrum: $Fe_3O_4$ - red plot, $Fe_3O_4/SiO_2$ - black plot.

Different anti-aggregating agents (PVP - polivinylopyrolidon, TMAOH - tetramethylamonium hydroxide, CA - citric acid) were used during preparation of the MNPs/$SiO_2$. The TEM micrographs, shown in Figure 20 proved that the best dispersion was achieved for the method utilizing TMAOH as a surfactant.

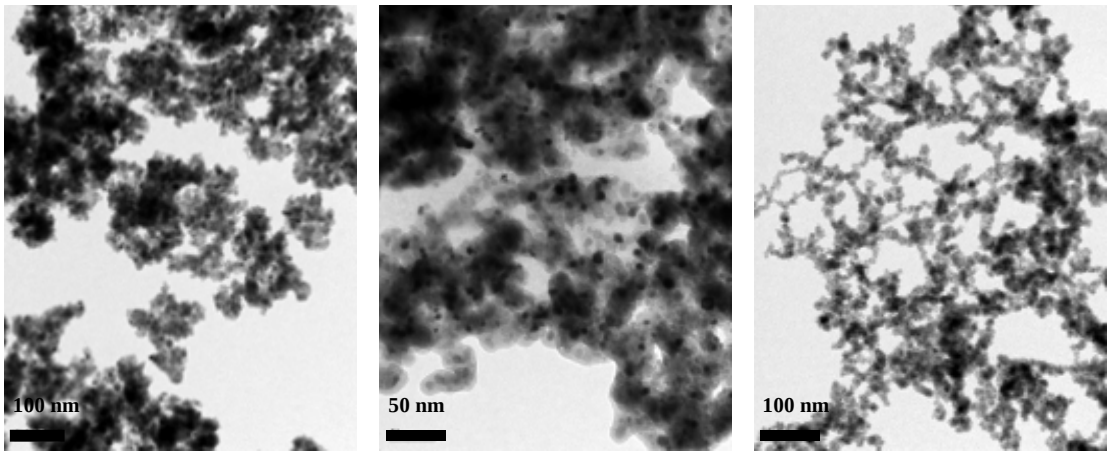


(a) (b) (c)

Figure 20. TEM micrograph of MNP/$SiO_2$ with: (a) PVP, (b) citric acid, (c) TMAOH used in synthesis.

The particles synthesized using this method were slightly aggregated, but were easily redispersed in a polar solution after drying. At the same time it was very easy to separate them using a permanent magnet. Magnetisation curves (Figure 21)

obtained by SQUID-VSM showed the typical characteristics of superparamagnetic behaviour for all MNP samples; zero coercivity and no remanence on hysteresis. Three times smaller magnetization was observed for MNP/$SiO_2$ compared with pure MNPs. SQUID-VSM analysis was carried out by Professor Quentin Pankhurst's group, at University College London.

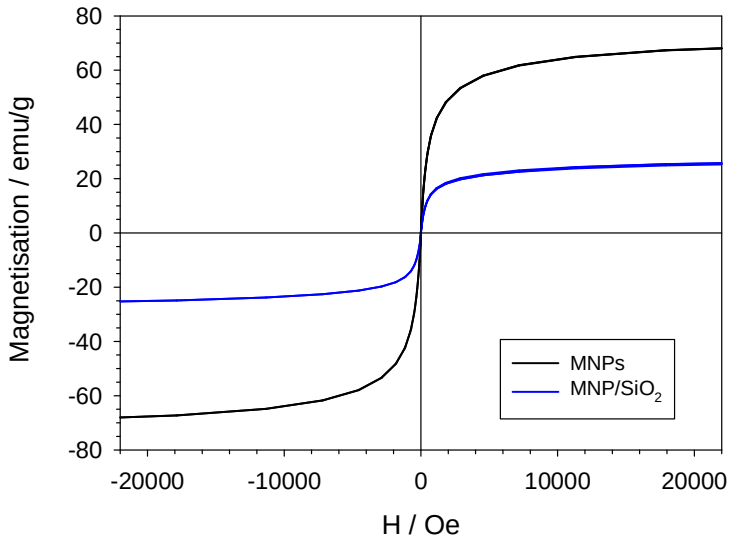


Figure 21. Magnetization curves of MNP (black line) and MNP coated with a silica layer (blue line).

To improve the size distribution, the other method of preparation, involving microemulsions was used, which is described in the next paragraph.

### 2.2.4 Silica-coated nanoparticles in microemulsions

Due to the aggregation of silica-coated nanoparticles, it was decided that a more sophisticated method of coating should be used. Jacinto [69] described and showed very good quality pictures of silica coated MNPs using a water-in-oil (W/O) microemulsion method. This method of preparation has been widely used to synthesize uniform sized nanoparticles of various kinds. Microemulsions are isotropic and thermo-dynamically stable, single-phase systems that consists of three components: water, oil, and an amphiphilic surfactant. The surfactant lowers the interfacial tension between water and oil, resulting in the formation of a transparent

solution. The water nanodroplets present in the bulk oil phase serve as a nanoreactor for the synthesis of the silica layer. In a typical procedure, polyoxyethylene(5)isooctylphenyl ether was dispersed in cyclohexane. Then $Fe_3O_4$, dispersed in cyclohexane, was added. After this step, ammonium hydroxide was added to form a reverse microemulsion. Tetraethylorthosilicate (TEOS) was used as a precursor of silica. For synthetic details, see Appendix 2 sec. 3.22 and 3.23. The particles were excellently dispersed, but it was not possible to fully separate them from the reaction media, especially from polar solvents. Jacinto [70] in his publications only used non-polar solvents and thus, because of the charged surface, it was easy to separate the aggregated MNPs *via* magnetic decantation from non-polar solvents.

Due to disappointing results in the separation of MNPs synthesised in microemulsions, it was decided to tune the silica shell thickness. It was suspected that decreasing thickness of shell would improve the magnetic properties of nanoparticles and solve the problem of incomplete separation. It was possible to tune the silica layer thickness, changing the initial amount of TEOS. The experiment was carried out with a different concentration of precursor in cyclohexane (1.1 %, 0.5 %, 0.14 %, and 0.07 %). The results are shown in Figure 22. For the 1.1 % TEOS concentration, the size of MNP/$SiO_2$ was around 50 nm (Figure 22a) for 0.5 % it was 30 nm (Figure 22b), and for 0.14 % it was 20 nm (Figure 22c). For the TEOS concentration of 0.07 % it was impossible to detect any silica layer, and it was impossible to disperse the MNP/$SiO_2$ after synthesis (Figure 22d). For smaller particles (with a thinner silica layer), it was possible to observe faster magnetic separation. However, it was impossible to fully separate the MNP/$SiO_2$ using a standard permanent magnet used in our laboratory. This is why it was decided that MNP/$SiO_2$ should be used as a support for different catalysts synthesised using the method described in Section 2.2.3. The dispersion, according to the TEM measurements, was not satisfying, however the particles were easy to disperse in polar solvents from a dry powder, and were very easy to separate (up to 5 min) using a standard permanent magnet.

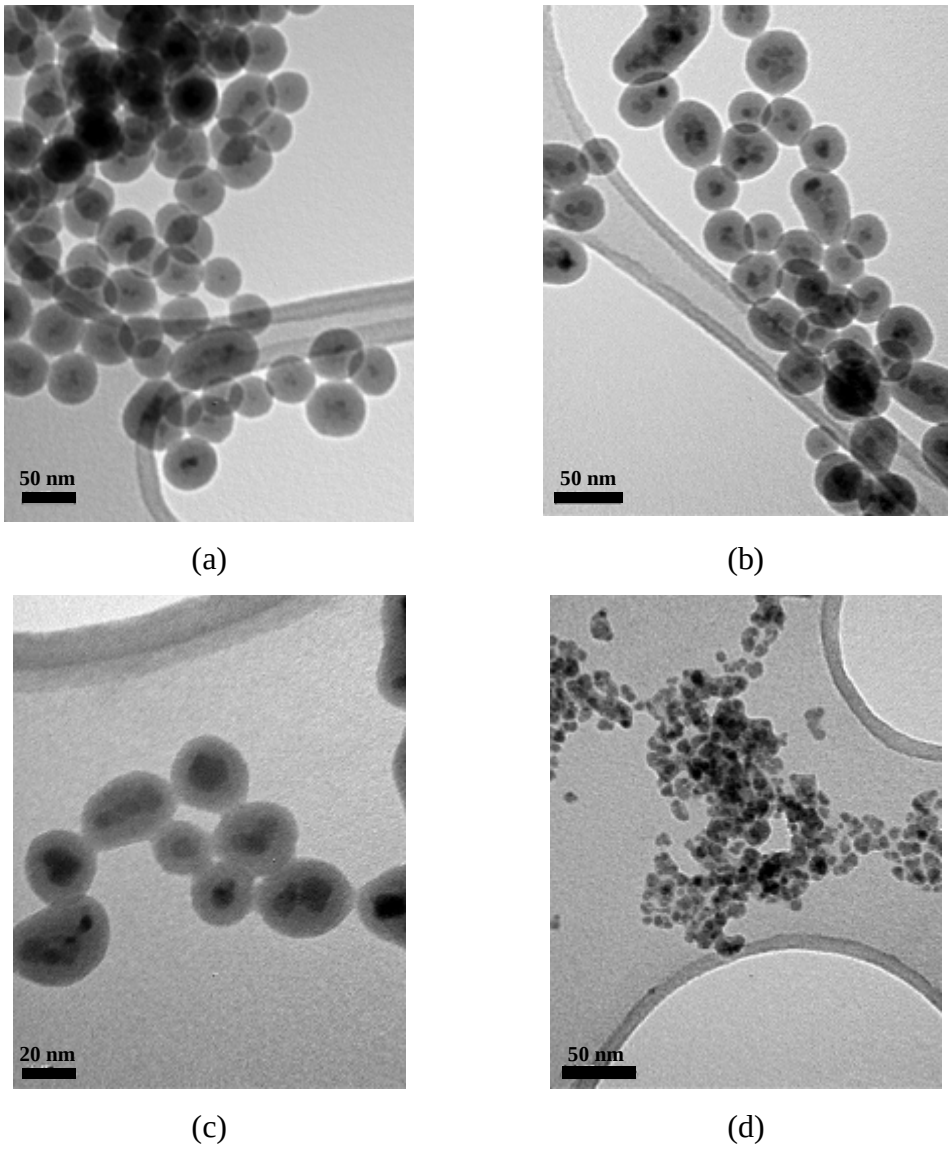


(a) (b)

(c) (d)

Figure 22. TEM micrograph of MNP/$SiO_2$ with different precursor concentrations: (a) 1.1 %, (b) 0.5 %, (c) 0.14 % and (d) 0.07 %.

### 2.3 Preparation of metal nanoparticulate catalysts supported on MNP/$SiO_2$

All catalysts presented below were prepared using a modified method proposed by Nakao *et al*. [131]. Metal precursors ($RuCl_3$, $RhCl_3$, $PdCl_2$, $AgNO_3$, $HAuCl_4 \cdot 3H_2O$) were dissolved in water. In the case of $PdCl_2$, a HCl solution was added. The solution was heated until the metal salt was completely dissolved. MNP/$SiO_2$ (silica coated magnetic nanoparticles) was added to the solution, followed by an aqueous solution of sodium dodecyl sulfate. The metal particles were

precipitated with $NaBH_4$ used as a reducing agent. Catalysts prepared in this way were then washed separated and dried. For synthetic details, see Appendix 2 sec. 3.24. The next few paragraphs will discuss these catalysts, which were applied in different chemical reactions to select a good chemical model for kinetic studies in flow systems.

### 2.3.1 Characterization of MNP/$SiO_2$/Au(0) and its application in benzyl alcohol and cyclohexane oxidation

Gold-doped MNP/$SiO_2$ (MNP/$SiO_2$/Au) was synthesised using the aforementioned method [131] and was characterized by TEM (Figure 23a) and Energy-dispersive X-ray spectroscopy (EDX), (Figure 23b). This proved the presence of gold nanoparticles.

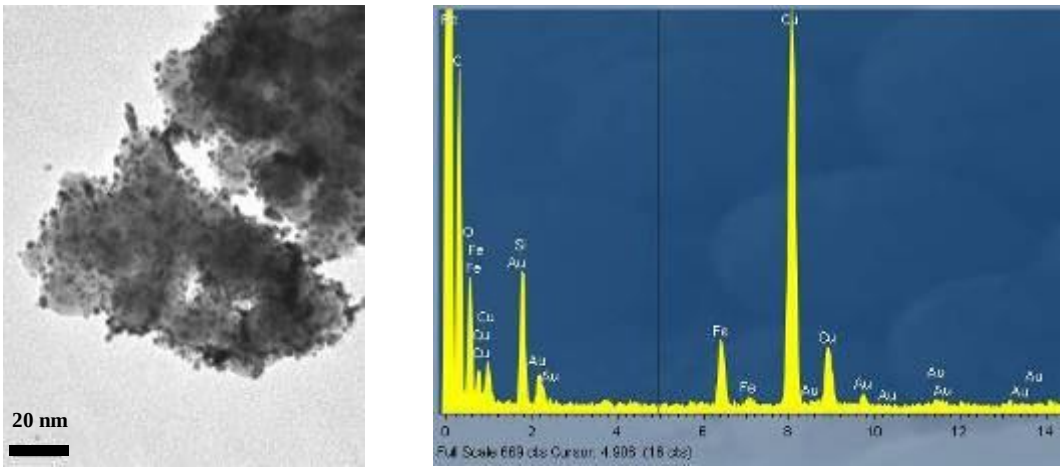


(a) (b)

Figure 23. (a) TEM micrograph of MNP/$SiO_2$/Au, (b) EDX spectrum of MNP/$SiO_2$/Au.

MNP/$SiO_2$/Au catalyst was tested using the oxidation of benzyl alcohol. The method described by Mori and Nishimura [85, 121], which uses molecular oxygen was applied. The reaction vessel, equipped with reflux, was charged with benzyl alcohol in toluene and MNP/$SiO_2$/Au. The resulting mixture was stirred at 90 °C under $O_2$ flow. The result of the reaction was monitored by GC and NMR analysis. After 24 h

of reaction, no product of oxydation was observed. For synthetic details, see Appendix 2 sec. 3.25

MNP/$SiO_2$/Au was also tested for oxidation of cyclohexane, using the method described by Zhu *et al*. [132]. The aerobic catalytic oxidation of cyclohexane was carried out with no solvent. Cyclohexane and a MNP/$SiO_2$/Au catalyst mixture was stirred at 80 °C under flow of oxygen for 6 h. The reaction mixture was directly analyzed by gas chromatography analysis, and no product was observed. For synthetic details, see Appendix 2 sec. 3.25.

### 2.3.2 Characterization of MNP/$SiO_2$/Ag(0) and its application in styrene epoxidation and benzyl alcohol dehydrogenation

Silver-doped MNP/$SiO_2$ (MNP/$SiO_2$/Ag) was synthesised using the aforementioned method [131] and was characterized by TEM (Figure 24a), and Energy-dispersive X-ray spectroscopy (EDX), (Figure 24b). This proved the presence of silver nanoparticles.

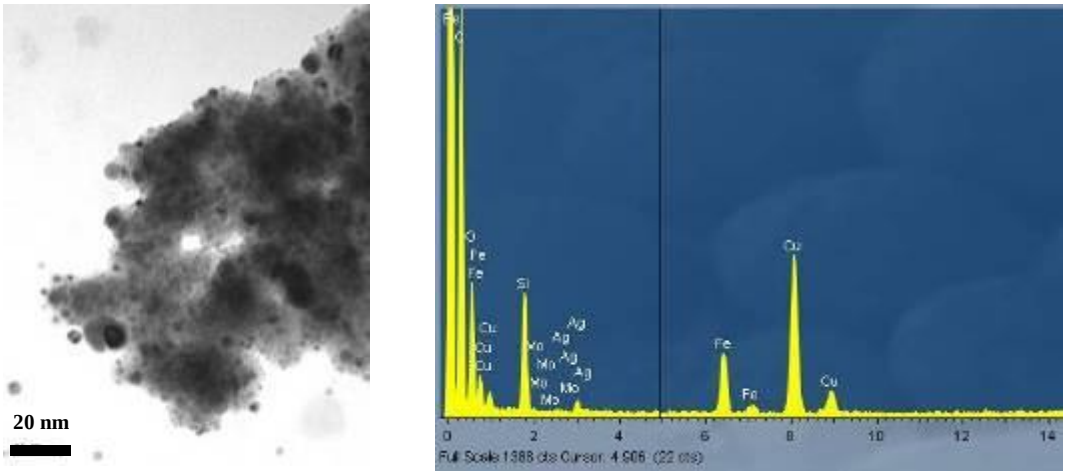


(a) (b)

Figure 24. (a) TEM micrograph of MNP/$SiO_2$/Ag, (b) EDX spectrum of MNP/$SiO_2$/Ag.

MNP/$SiO_2$/Ag was tested using the epoxidation of styrene, following a method described by Zhang *et al*. [90]. Styrene in toluene was mixed with MNP/$SiO_2$/Ag,

and tertbutyl hydroperoxide (TBHP) was used as an oxidant. After 12 h of reaction, no styrene oxide was observed. The only products observed were by-products (mainly benzyl alcohol, acetophenone, and some other unidentified products). For synthetic details, see Appendix 2 sec. 3.26.

For a second catalytic test, the dehydrogenation of benzyl alcohol was chosen. The conditions described by Mitsudome [133] were applied to this experiment. Benzyl alcohol was dissolved in *p*-xylene, and the catalyst was added. The reaction mixture was heated up to 130 °C with continuous stirring under an Ar atmosphere. The progress of the reaction was followed using GC analysis. After 12 h no product was observed. For synthetic details, see Appendix 2 sec. 3.27.

### 2.3.3 Characterization of MNP/$SiO_2$/Rh(0), MNP/$SiO_2$/Ru(0), MNP/$SiO_2$/Pd(0) and its application in DMIT hydrogenation

MNP/$SiO_2$/Rh(0), MNP/$SiO_2$/Ru(0), MNP/$SiO_2$/Pd(0) were synthesised using the aforementioned method [131], and characterized by TEM (Figure 25a, Figure 26a, Figure 27a) and Energy-dispersive X-ray spectroscopy (EDX), (Figure 25b, Figure 26b, Figure 27b respectively). This proved the presence of rhodium, ruthenium and palladium nanoparticles.

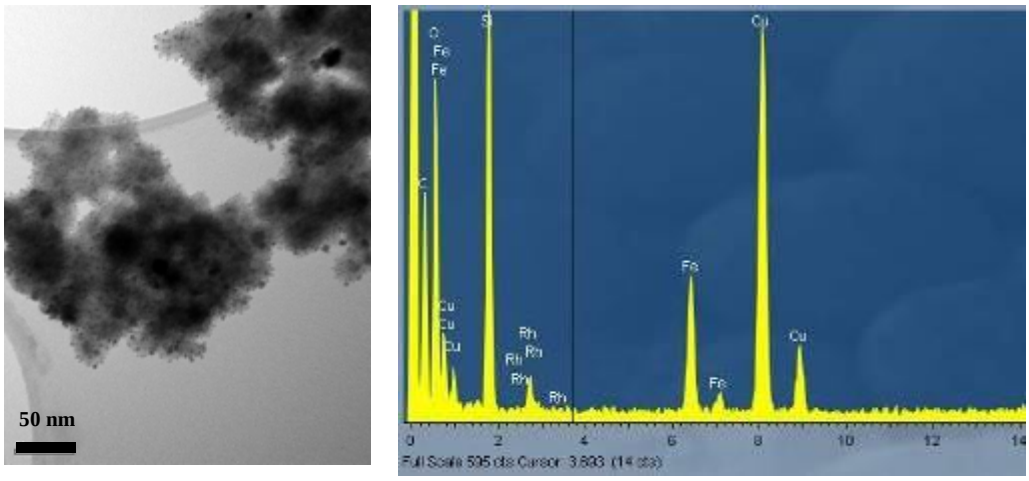


(a) (b)

Figure 25. (a) TEM micrograph of MNP/$SiO_2$/Rh(0), (b) EDX spectrum of MNP/$SiO_2$/Rh(0).

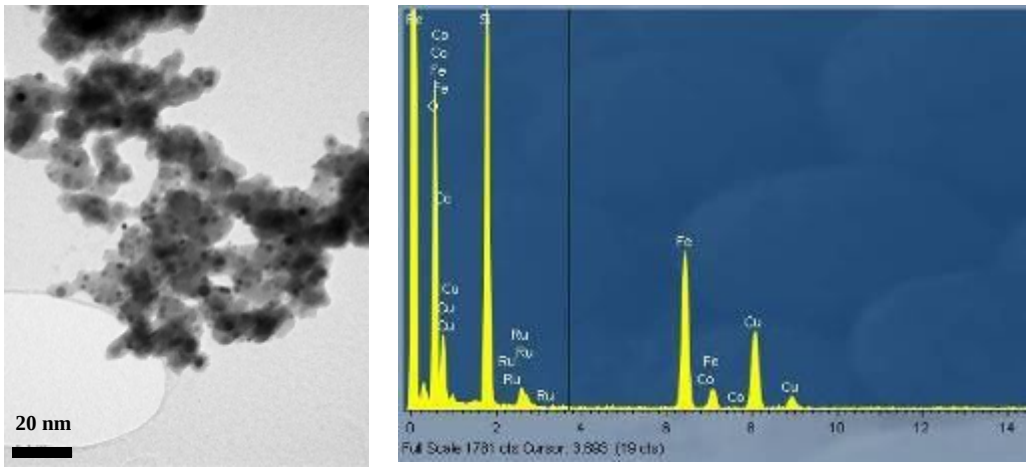


(a) (b)

Figure 26. (a) TEM micrograph of MNP/$SiO_2$/Ru(0), (b) EDX spectrum of MNP/$SiO_2$/Ru(0).

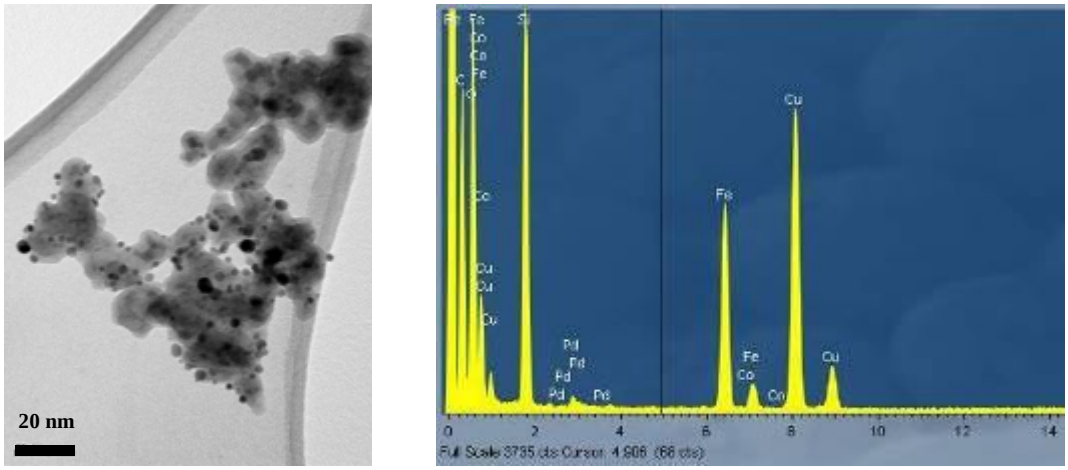


(a) (b)

Figure 27. (a) TEM micrograph of MNP/$SiO_2$/Pd(0), (b) EDX spectrum of MNP/$SiO_2$/Pd(0).

MNP/$SiO_2$/Pd(0) catalyst was also characterized using SQUID-VSM, which confirmed the superparamagnetic behaviour of the catalyst (Figure 28). Higher magnetization was observed for bare nanoparticles MNP, comparing with MNP/$SiO_2$ MNP/$SiO_2$/Pd(0). SQUID-VSM analysis was carried out by Professor Quentin Pankhurst's group, at University College London.

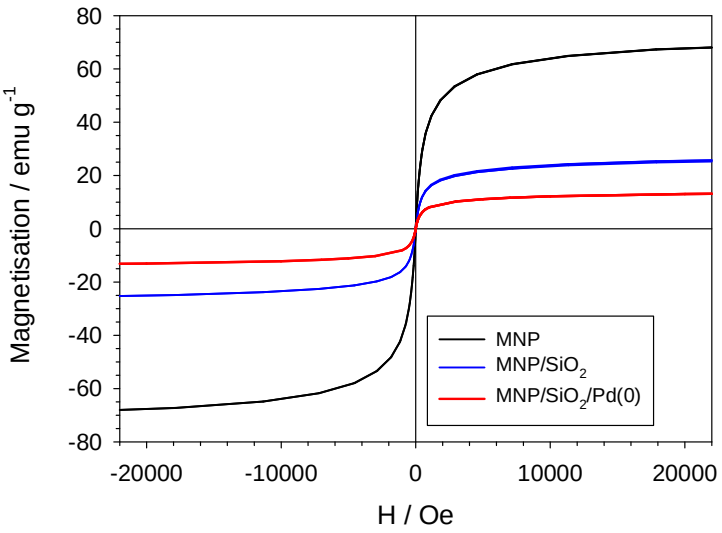


Figure 28. SQUID-VSM magnetization curves of MNP, MNP/$SiO_2$ and MNP/$SiO_2$/Pd(0).

The aim of this experiment was to test the activity of three different catalysts in the same exemplary reaction, and under the same conditions. Hydrogenation of dimethyl itaconate (Scheme 38) was carried out in the reactor under the 3.5 bar pressure of $H_2$ and at 50 °C. Methanol was used as a solvent. After a reaction, samples were analyzed using $^1$H NMR and GC. For synthetic details, see Appendix 2 sec. 3.28. The results of these experiments are summarized in Table 3.

Table 3. The results of hydrogenation applying magnetic nanocatalyst. S/C is a molar ratio substrate to active metal attached to nanoparticles.

| Catalyst | S/C | Run | Time | Conversion |
|---|---|---|---|---|
| MNP/$SiO_2$/Pd | 100 | 1 | 1h | 100 % |
| | | 2 | 1h | 100 % |
| MNP/$SiO_2$/Rh | 100 | 1 | 1h | 100 % |
| | | 2 | 1h | 95 % |
| MNP/$SiO_2$/Ru | 100 | 1 | 1h | 100 % |
| | | 2 | 1h | 97 % |

Conditions: p = 3.5bar, T = 50 °C, reaction time 1 hour, solvent: methanol.

All three catalysts showed high activity in this reaction, giving a conversion of 100 % after 1 h in the first run. The catalysts were recycled and the reactions were repeated for a second time. The catalyst containing Pd(0) still showed conversion of 100 %, after the same reaction time. The reactions with applied MNP/$SiO_2$/Rh(0), MNP/$SiO_2$/Ru(0) resulted with 95 % and 97 % conversion respectively. Additionally, a blank control test was carried out, where nanoparticles coated with silica (with no metal particles) were used for the hydrogenation of DMIT under the same conditions. No product was observed.

## 2.4 Conclusions

- Novel methods for the preparation of magnetically separable catalysts were presented.
- 100 % conversion was achieved in the case of hydrogenation of DMIT catalysed by MNP/[R-P-Xyl-Phos-Rh(cod)$Cl_2$] and MNP/[R-BINAS-Rh(cod)$Cl_2$]. Conversion of 50 % was achieved in the case of MNP/[R-P-R-Phos-Rh(cod)$Cl_2$]. The % ee was equal to zero.
- It was demonstrated that MNP/Ru(0) is a very promising catalyst for the dihydroxylation reaction of styrene, dimethyl fumarte and dimethyl maleate. $NaIO_4$ was proven to be the most effective oxidation agent.
- The MNP/Pd(0) catalyst was shown to be very effective in catalysing the hydrogenation of DMIT. No loss of catalytic activity was observed over 4 cycles. This catalytic system was chosen for further studies on its application in a capillary reactor, described in Chapter 3.
- The MNP/Pd(0) catalyst was also tested in the hydrogenation of nitrobenzene, and was shown to be very effective. The catalyst was recycled and three more cycles were repeated with 100 % conversion to aniline. Kinetic studies were carried out in a microreactor using this catalytic system as a model reaction. The results of these studies are described in Chapter 4.
- The application of iron oxide nanoparticles for accelerating the Knoevenagel condensation was demonstrated. Moreover, impregnation of the MNPs with Pd(0) resulted in a system exhibiting excellent catalytic performance in tandem aldol condensation-hydrogenation processes, under mild conditions.

- Many attempts were made to find an appropriate coating which could prevent aggregation of the MNPs, including carbon, alumina and silica. Silica was chosen to be the best protecting material. MNP/$SiO_2$ was easy to disperse in polar solvents from a dry powder, and was very easy to separate (up to 5 min) using a standard permanent magnet. All of these advantages suggested that this material is suitable as a magnetically separable support for different catalysts.
- A variety of catalysts were prepared using MNP/$SiO_2$ as a support, including Ru, Rh, Pd, Ag, and Au nanoparticles.
- MNP/$SiO_2$/Rh(0), MNP/$SiO_2$/Ru(0), and MNP/$SiO_2$/Pd(0) were very effective catalysts for DMIT hydrogenation. MNP/$SiO_2$/Pd(0) was chosen for further kinetic studies in a microreactor. The results are presented in Chapter 4.
- In all cases, the catalysts could be easily isolated from the reaction system by decantation in a magnetic field, and the catalysts could be recycled for subsequent runs.

# CHAPTER 3

## A flow reactor with magnetically entrapped and manipulated nanoparticle catalysts for continuous hydrogenation and Suzuki reaction

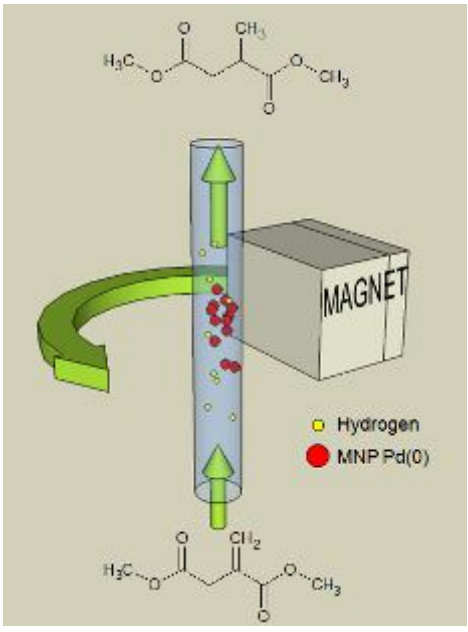

## 3 Introduction

One of the most exciting and significant developments in organic synthesis involved the innovative incorporation of flow processes into laboratory-based synthesis platforms [134]. Alternative flow methods, which utilize packed-bed reactors, microreactors or reaction chips, are replacing established methods of batch synthesis. The small size of these platforms allows better control and variation of experimental conditions such as temperature and pressure, leading to their superiority over existing batch techniques [135]. Additionally, flow approaches can provide improved reactivity as well as better selectivity and stability [136]. Until recently, all reported studies of catalytic MNPs were performed in batch mode. In 2010, Schatz *et al*. [136] described the use of MNP-supported catalysts for the kinetic resolution of racemic 1,2-diphenylethane-1,2-diol *via* asymmetric monobenzoylation in both batch and flow modes (Figure 29).

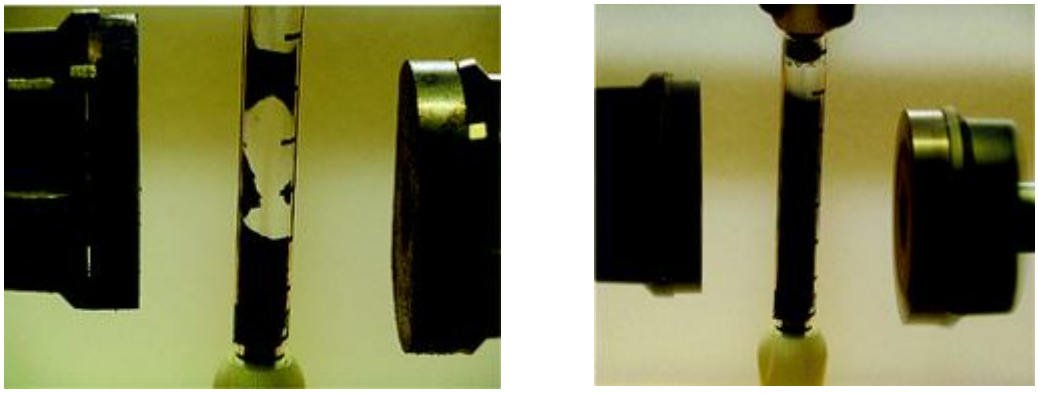

(a) (b)

Figure 29. Co/C-supported catalyst in a glass column (a) entrapped by an external magnetic field, (b) agitated in the rotating magnetic field while $CH_2Cl_2$ was passed through the reactor. Reprinted with permission from [136]. Copyright (2010) American Chemical Society.

This demonstrated the feasibility of using an external magnetic field to trap and manipulate a catalyst in an open capillary. However this technique needs to be extended to multi-phase systems, and there is a need to consider reactor engineering aspects, if these systems are to find wider application in manufacturing. This article

was published on-line on 28 December 2009 and presented below initial experiments on hydrogenation of DMIT were finished at the same time. This work was done independently of the results described by Schatz *et al*. [136].

This chapter reports on the investigations carried out to design and construct a capillary reactor with magnetically entrapped and manipulated nanoparticle catalysts for continuous hydrogenation and C-C coupling reactions.

## 3.1 Flow reactor with magnetically entrapped and manipulated nanoparticle catalysts using an electromagnet

The initial experiments on magnetic entrapment of MNP catalysts were carried out using an electromagnet (Figure 30) designed and manufactured by Professor Quentin Pankhurst's group, at University College London. The main idea was to use alternating magnetic field created by four electromagnetic bars in order to entrap and rotate the MNP based catalyst inside the capillary reactor. Unfortunately, using this magnet it was not possible to entrap the MNP catalyst, even though the highest possible strength of magnetic field for this magnet was used. That is why it was decided to build a reactor based on a standard permanent magnet (MMG MagDev, UK**)** used in our laboratory, which will be described in the next section.

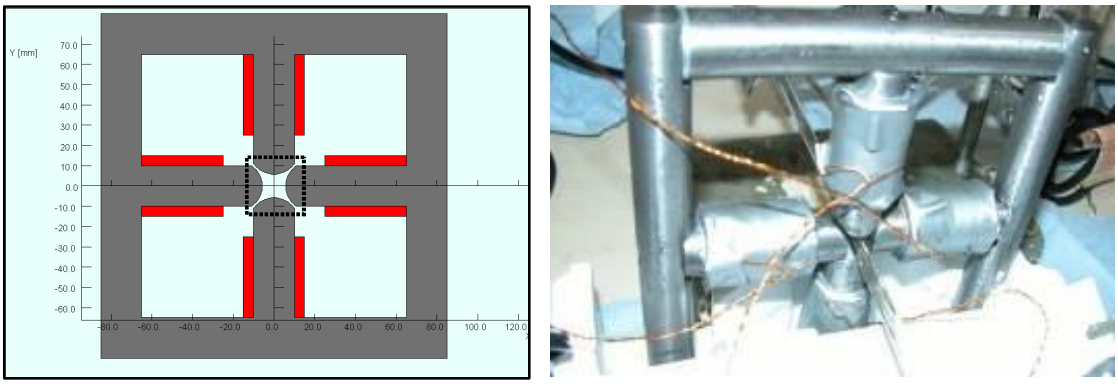


(a) (b)

Figure 30. Flow reactor: (a) cross section of an exemplar reactor; red represents the coils, (b) capillary reactor with an electromagnet for magnetic nanocatalyst entrapment and manipulation.

### 3.2 Flow reactor with magnetically entrapped and manipulated nanoparticle catalysts using a permanent magnet

A novel flow reactor with magnetically-entrapped and manipulated nanoparticle-supported catalysts has been developed. The reactor combined a capillary tube (mounted vertically, ID 6 mm) and an integrated tube-and-shell heat exchanger with a permanent magnet (surface magnetization 0.3 T, MMG MagDev, UK) which could rotate around the capillary at up to 220 rpm. An old motor from a rotary evaporator was used to move the magnet around the capillary. The capillary reactor was equipped with a HPLC frit, through which gases could be injected (Scheme 41).

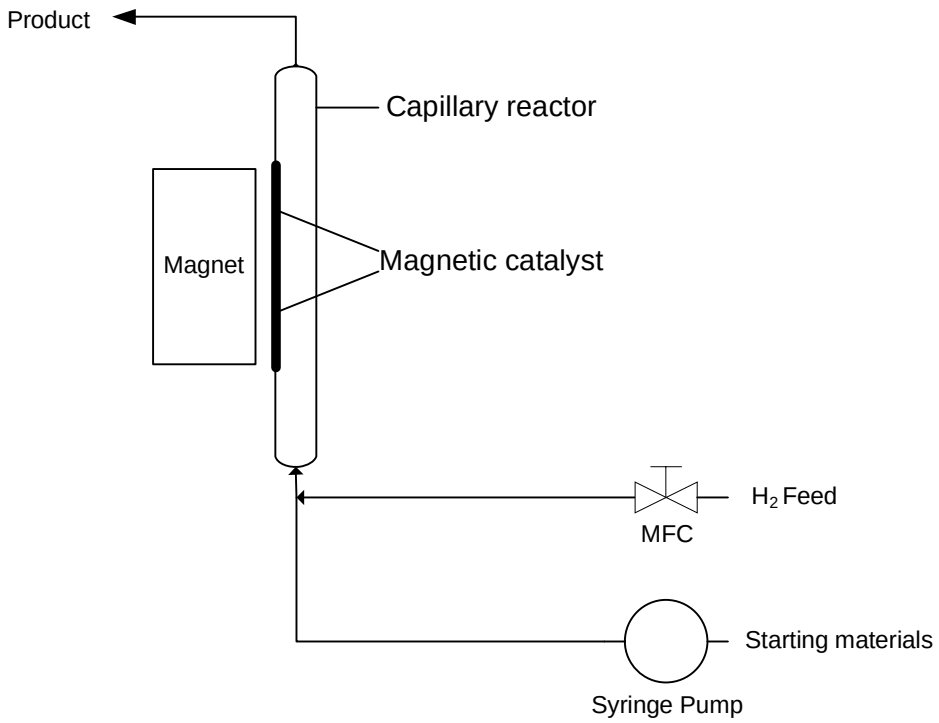


Scheme 41. Scheme of a capillary reactor with magnetically-entrapped and manipulated nanoparticle-supported catalysts.

The initial trials were carried out for silica-coated MNPs, but the magnetic field was not strong enough to retain particles in the field defined by the magnet. Some of them were carried by the flow of the liquid, others fell under the influence of gravitational forces. Bare MNPs were used in the next tests. They exhibited higher magnetization in comparison to MNP/$SiO_2$ (Figure 21). For bare MNPs it was

possible to trap them in the capillary using the magnet. In a usual procedure, suspensions containing MNPs were injected using a needle. When the catalyst agglomerated in the magnetic field (Figure 31a) the rotation of the magnet was started (Figure 31b). The performance of the reactor was characterised using the two-phase hydrogenation of dimethyl itaconate (DMIT) and the Suzuki reaction. The results of these experiments will be described in next two sections.

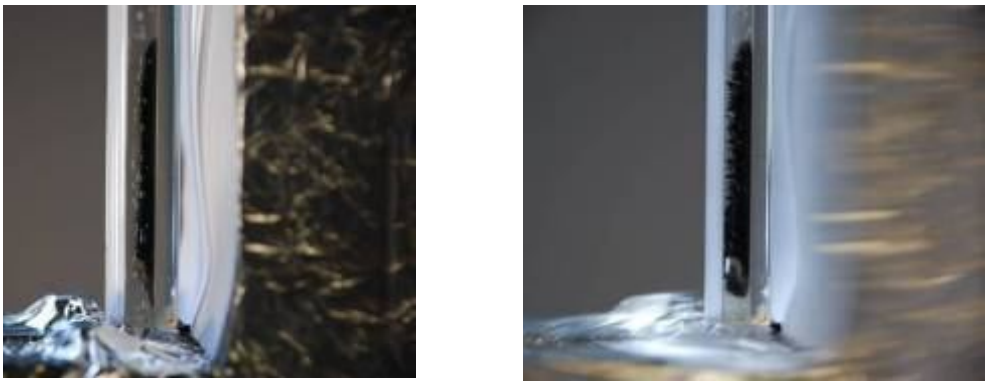

(a) (b)

Figure 31. Glass capillary reactor with a magnetically entrapped catalyst for hydrogenation: (a) with resting external magnet, (b) with rotating external magnet.

### 3.2.1 Continuous hydrogenation of DMIT in a flow reactor with magnetically entrapped and manipulated MNP/Pd(0)

For this work an MNP/Pd(0) catalyst was used. The method of preparation and characterization of this catalyst was described in Chapter 2. The hydrogenation of DMIT (Scheme 38) was used to characterise the reactor by investigating the effect on the reaction rate of different temperatures, and different liquid and gas flow rates, reactant concentrations and rotation rates of the magnet. For synthetic details, see Appendix 2 sec. 3.29. In all experiments in this chapter gas flow rate was messured at NTP (Normal Temperature and Pressure).

Figure 32 shows the steady-state single-pass conversions obtained for various DMIT concentrations and liquid flow rates. Quantitative hydrogenation of DMIT was obtained for a residence time of 35 s. ( $\tau = \frac{\beta \upsilon}{\dot{\upsilon}}$, where $\beta = \frac{\upsilon_L}{\upsilon_L + \upsilon_G}$),

β - saturation. Increasing the liquid flow rate or the initial concentration of DMIT resulted in a lower conversion.

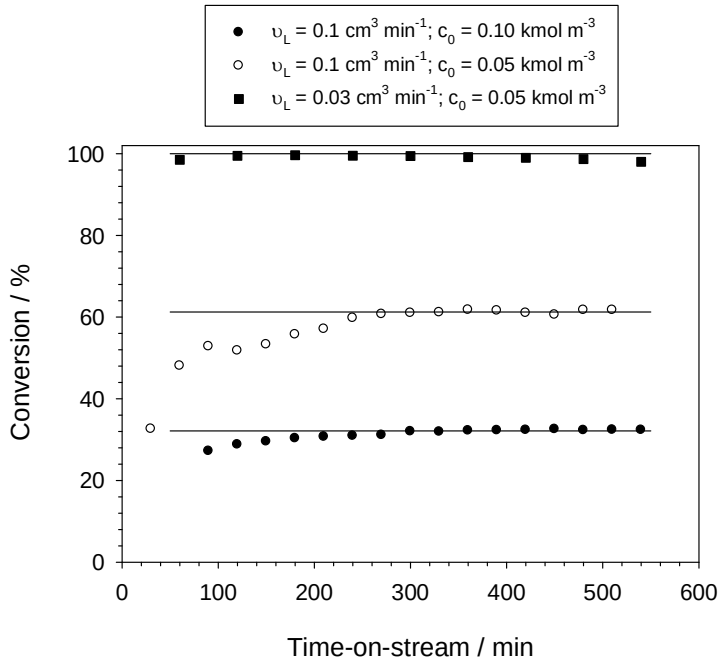


Figure 32. The evaluation of steady-state conversion in the reactor with magnetically entrapped catalyst for various reaction conditions (T = 303 K, p = atmospheric, $\upsilon_G$ = 1 $cm^3$ $min^{-1}$, n = 160 $min^{-1}$).

The relatively long time to reach steady-state conversion (90-240 min depending on the experimental conditions) may have resulted from the slow reorganization of the nanoparticle 'bed' in the rotating magnetic field. An important observation from these initial experiments was that the rotating magnet always retained the catalyst nanoparticles in the space defined by the external magnetic field, even during two-phase bubble flow. AAS analysis of the product solution over the course of 8 - 10 h of reaction showed that the loss of catalyst was between 0 and 0.35 % (average 0.15 %) of the initial amount. It was mainly due to the catalyst removal from the magnetic field. During the batch process, no palladium leaching was observed. The catalytic bed of MNPs was stable without loss of material as long as the Reynolds number, *Re* (Eq. 6) was below *ca*. 100 when using methanol as the reaction medium. Increasing the Reynolds number (by increasing the superficial velocity) resulted in the gradual loss of nanoparticles thus, a stronger magnetic field would be necessary to use this technology at higher flow rates.

$$\mathrm{Re} = \frac{u_s \rho d}{\eta} \tag{6}$$

$d$ – capillary diameter [m],

$Re$ – Reynolds number [-],

$u_s$ – superficial velocity [$m^3\ m^{-2}\ s^{-1}$],

$\eta$ – dynamic viscosity [N s $m^{-2}$],

$\rho$ – density [kg $m^{-3}$].

The influence of the rotation rate of the magnet on the steady-state conversion and overall rate of reaction ($r_A$, Eq. 7) is shown in Figure 33. It is worth noting that the overall rate of reaction, calculated in this work, depends on both: rate of chemical reaction itself and the rates of mass transfer of hydrogen and DMIT.

$$\left(-r_A\right) = \frac{\upsilon c_0 X}{m_{cat}} \tag{7}$$

$(-r_A)$ – overall rate of reaction [mol $g_{cat}^{-1}\ s^{-1}$],

$m_{cat}$ – mass of catalyst [g],

$\upsilon$ – volumetric flow rate [$m^3\ s^{-1}$],

$c_0$ – initial concentration [kmol $m^{-3}$],

X – conversion [-].

For an initial DMIT concentration of 0.1 kmol $m^{-3}$ and liquid flow rate of 0.1 $cm^3\ min^{-1}$ at 303 K, 22 % conversion ($1.14 \times 10^{-5}$ mol $g_{cat}^{-1}\ s^{-1}$) was obtained with the magnet at rest compared with a 32 % conversion ($1.67 \times 10^{-5}$ mol $g_{cat}^{-1}\ s^{-1}$) obtained for the rotating catalytic bed. This could be explained by the more efficient mass transfer of hydrogen in the presence of moving nanoparticles [137] and better catalyst accessibility. Varying the rotation rate over the range 120-200 rpm did not have a pronounced influence on the rate of hydrogenation.

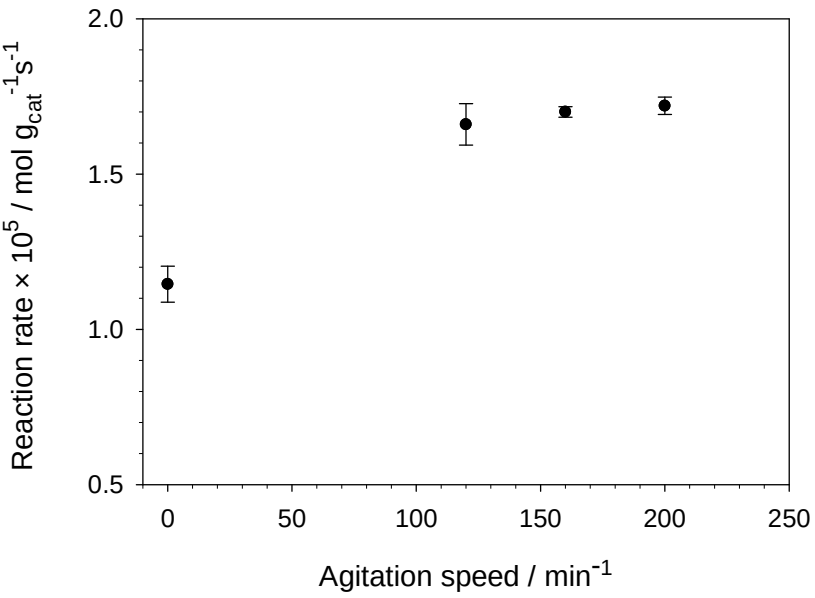


Figure 33. The influence of the agitation speed of the permanent magnet on the overall reaction rate (T = 303 K, p = atmospheric, $\upsilon_L$ = 0.1 $cm^3$ $min^{-1}$, $\upsilon_G$ = 1 $cm^3$ $min^{-1}$, $c_0$ = 0.1 kmol $m^{-3}$).

Increasing the reaction temperature decreased the conversion of DMIT and the rate of the reaction (Figure 34) due to the decreased solubility of hydrogen gas and a decrease of hydrogen partial pressure in the gas bubbles due to methanol vaporization. The solubility of hydrogen in the methanol was calculated based on the values of the Henry constant published by d'Angelo and Francesconi [138] and the Antoine equation for methanol from Lange's Handbook of Chemistry [139]. For details, see Appendix 2 sec. 2.3. The increase of the solubility of hydrogen in the liquid phase increased the rate of the reaction, however a fuller explanation of the temperature influence would require rigorous mathematical modelling of the process.

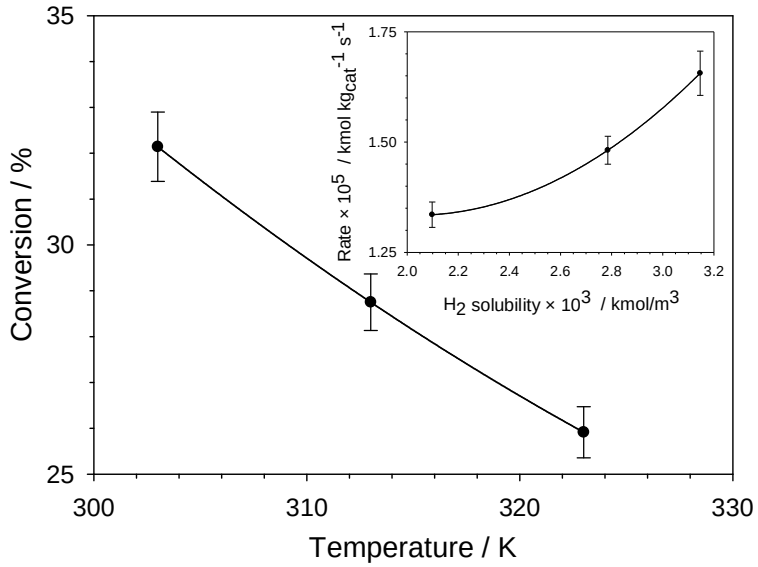


Figure 34. The influence of temperature on the conversion of DMIT. Insert: The influence of hydrogen solubility in the organic phase on the reaction rate (p = atmospheric, $\upsilon_L$ = 0.1 $cm^3$ $min^{-1}$, $\upsilon_G$ = 1 $cm^3$ $min^{-1}$, $c_0$ = 0.1 kmol $m^{-3}$, n = 160 $min^{-1}$).

The influence of the initial DMIT concentration on the overall rate of reaction is shown in. Figure 35. A saturation-like isotherm was observed, suggesting a heterogeneous mechanism for the hydrogenation reaction using magnetic nanocatalyst.

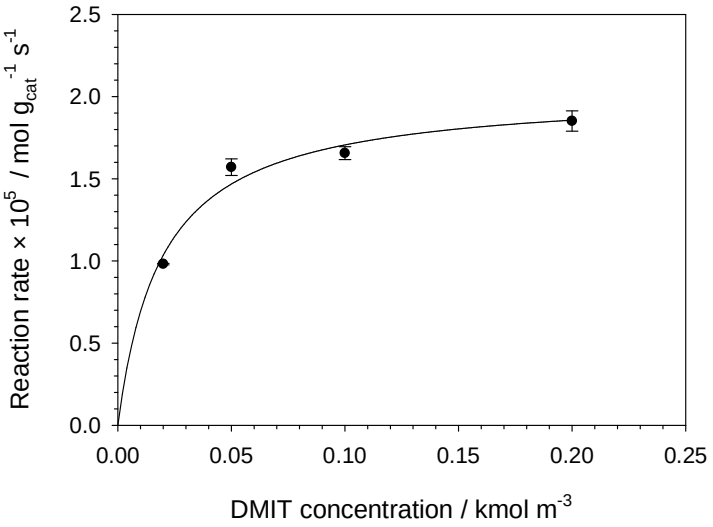


Figure 35. The influence of DMIT concentration on the average rate of reaction (T = 303 K, p = atmospheric, $\upsilon_L$ = 0.1 $cm^3$ $min^{-1}$, $\upsilon_G$ = 1 $cm^3$ $min^{-1}$, n = 160 $min^{-1}$).

Increasing the liquid phase flow rates, hence decreasing the residence time of reactants in the bed of nanoparticles, decreased the conversion as shown in Figure 36; however, the overall rate of the process was constant. The effect of the gas flow is more complicated; the initial increase of conversion at higher flow rates is due to the enhanced availability of hydrogen in the solution, but at the highest flow rate used, the conversion fell. This can be explained by the observation of large gas bubbles (Figure 36a) leading to a smaller mass transfer area and therefore a lower overall rate of reaction. A more efficient gas distribution system should be designed for the next generation reactor. Gas flow rate was messured at NTP (Normal Temperature and Pressure).

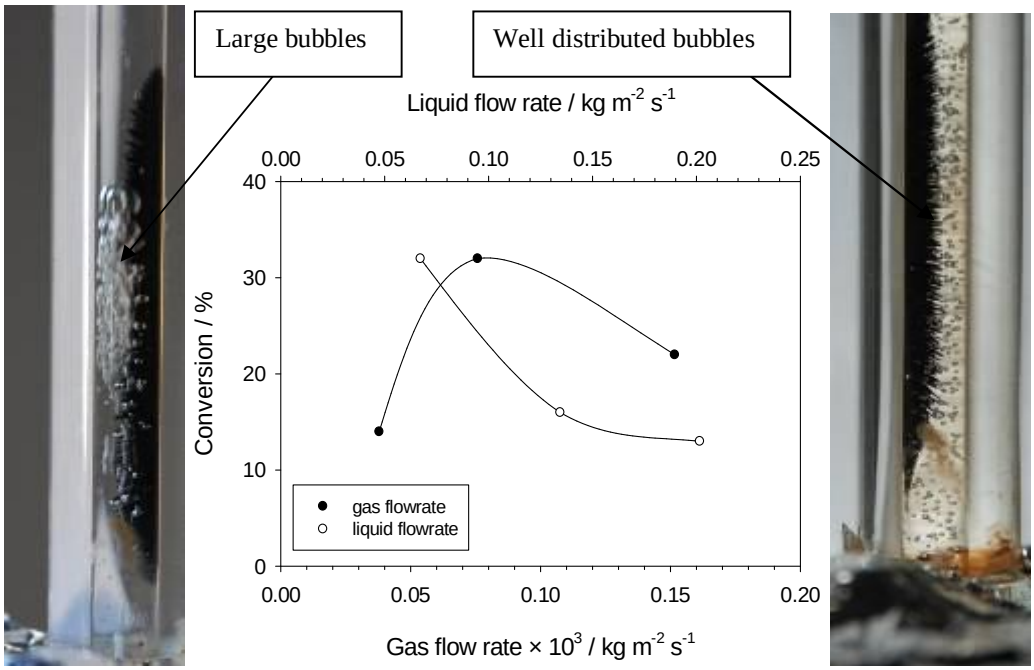


(a) (b)

Figure 36. The influence of liquid and gas flow rates on the rate of reaction (T = 303 K, p = atmospheric, $c_0$ = 0.1 kmol $m^{-3}$, n = 160 $min^{-1}$): (a) glass capillary reactor with a magnetically entrapped catalyst for hydrogenation with large hydrogen bubbles observed, (b) with well-distributed hydrogen bubbles.

To demonstrate the advantage of using a continuous capillary reactor, a semi-batch experiment using our standard initial conditions (T = 303 K, p = atmospheric, $\upsilon_G$ = 1 $cm^3$ $min^{-1}$, $c_0$ = 0.1 kmol $m^{-3}$) was carried out. The rate of reaction was around 15 times lower than in the continuous system ($1.38 \times 10^{-6}$ compared with $1.65 \times 10^{-5}$ mol $g_{cat}^{-1}$ $s^{-1}$). For synthetic details, see Appendix 2 sec. 3.30. The mass transfer between the gas-liquid and liquid-solid phases in a batch reactor is therefore very low, since there is a low interfacial area between the three phases.

### 3.2.2 Continuous Suzuki reaction in a flow reactor with magnetically entrapped and manipulated MNP/Pd(0)

A Suzuki coupling reaction (Scheme 42) of phenylboronic acid and 9-bromophenanthrene (9BP) has been chosen as model to characterise the reactor for monophasic reaction.

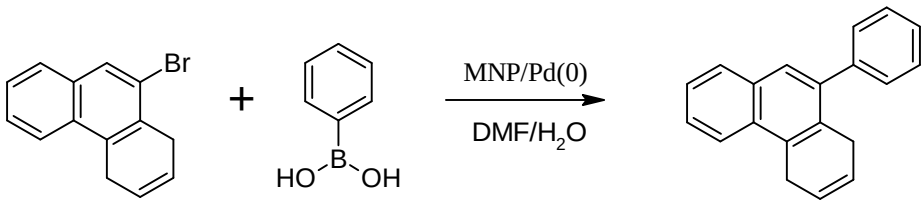


Scheme 42. Suzuki coupling of phenylboronic acid and 9-bromophenanthrene.

Figure 37a shows pictures of the reactor with the magnet at rest and with a rotating magnet (Figure 37b) for a one-phase liquid process. In the Figure 37b, a very good dispersion of MNP/Pd(0) was noted, and particles were observed in the whole volume of the capillary. These experiments were carried out in similar fashion to the hydrogenation of DMIT presented in Section 3.2.1. For synthetic details, see Appendix 2 sec. 3.31.

(a) (b)

Figure 37. Glass capillary reactor with magnetically entrapped catalyst for Suzuki reaction: (a) with resting external magnet, (b) with rotating external magnet.

Figure 38 shows the steady-state single-pass conversions obtained for various reactant flow rates. Reaction with 98 % conversion was obtained for a residence time of 20 min. Increasing the liquid flow rate resulted in lower conversion.

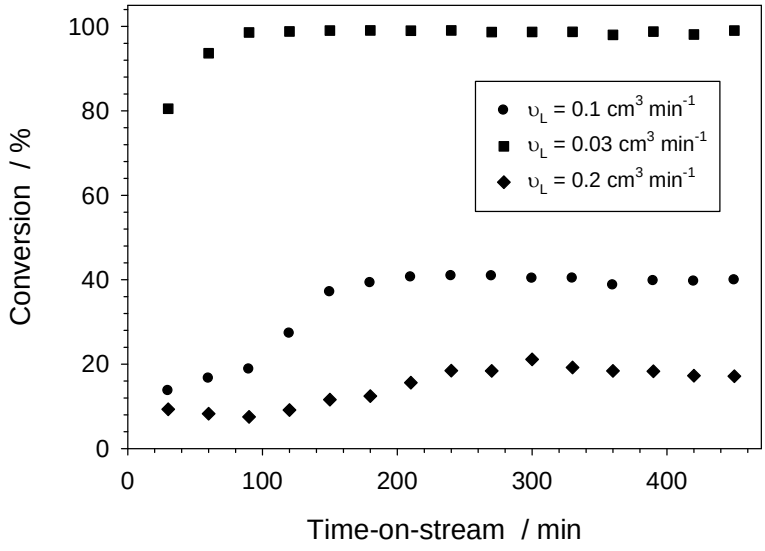


Figure 38. The evaluation of steady-state conversion in the reactor with magnetically entrapped catalyst for various reaction conditions (T = 383 K, p = atmospheric, n = 160 $min^{-1}$, $c_0$ = 0.025 kmol $m^{-3}$).

The relatively long time to reach steady-state conversion (90-120 min depending on the experimental conditions) may result from the slow reorganization of the

nanoparticle 'bed' in the rotating magnetic field, similarly to the hydrogenation of DMIT. In these experiments, the rotating magnet retained the catalyst nanoparticles in the space defined by the external magnetic field. AAS analysis of the product solution over the course of 8-10 h of reaction showed that the loss of catalyst was between 0 and 0.40 % (average 0.12 %) of the initial amount. It was mainly due to the catalyst being removed from magnetic field, while during the batch process no palladium leaching was observed.

The influence of the rotation rate of the magnet on the steady-state conversion and overall rate of reaction ($r_A$, Eq. 7) is shown in Figure 39. For an initial 9-bromophenanthrene concentration of 0.1 kmol $m^{-3}$ and liquid flow rate of 0.1 $cm^3$ $min^{-1}$ at 383 K, a 9 % conversion ($1.16 \times 10^{-6}$ mol $g_{cat}^{-1}$ $s^{-1}$) was obtained with the magnet at rest compared with a 33 % conversion ($4.30 \times 10^{-6}$ mol $g_{cat}^{-1}$ $s^{-1}$) obtained for the rotating catalytic bed. This could be explained by more efficient mixing in the presence of moving nanoparticles and better catalyst accessibility (Figure 37b). Varying the rotation rate over the range 120-200 rpm did not have a pronounced influence on the rate of hydrogenation.

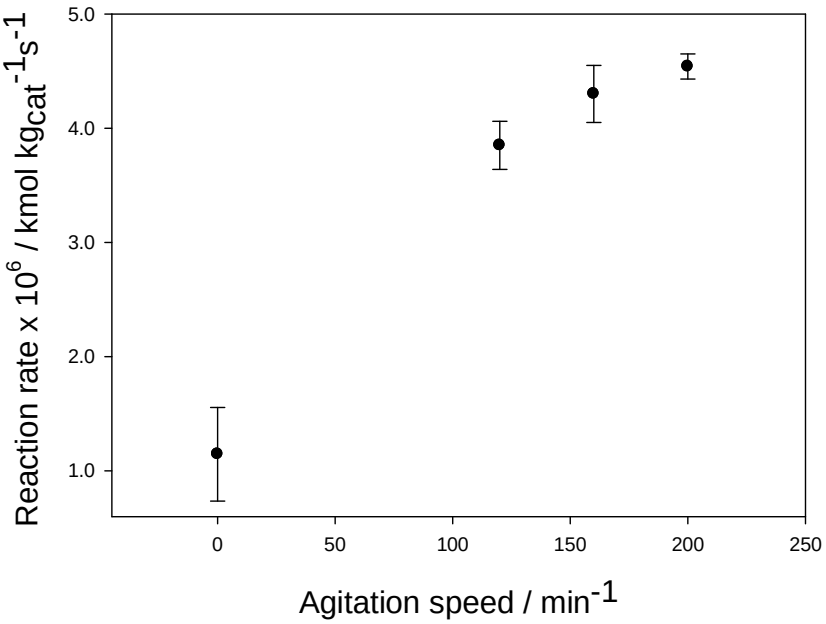


Figure 39. The influence of the agitation speed of the permanent magnet on the overall reaction rate (T = 383 K, p = atmospheric, $\upsilon_L$ = 0.1 $cm^3$ $min^{-1}$, $c_0$ = 0.025 kmol $m^{-3}$).

The influence of the initial 9-bromophenanthrene concentration on the overall rate of reaction is shown in Figure 40. A saturation-like isotherm was observed, suggesting a heterogeneous mechanism for the hydrogenation reaction using a magnetic nanocatalyst.

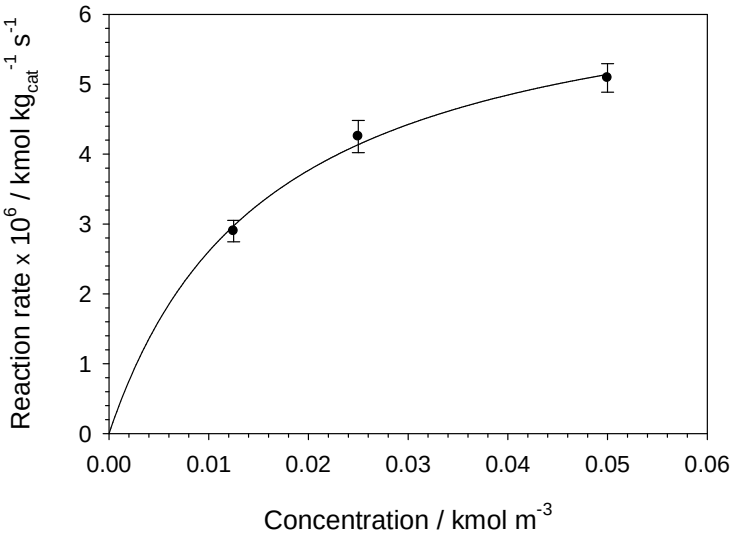


Figure 40. The influence of 9-bromophenanthrene concentration on the average rate of reaction (T = 383 K, p = atmospheric, $\upsilon_L$ = 0.1 $cm^3$ $min^{-1}$, n = 160 $min^{-1}$).

A linear relationship between the reaction rate and the inverse temperature was observed. The activation energy of the reaction was $\Delta E_A$ = 87.0 kJ $mol^{-1}$. This high value confirms the reaction limitation of the process (Figure 41) [9].

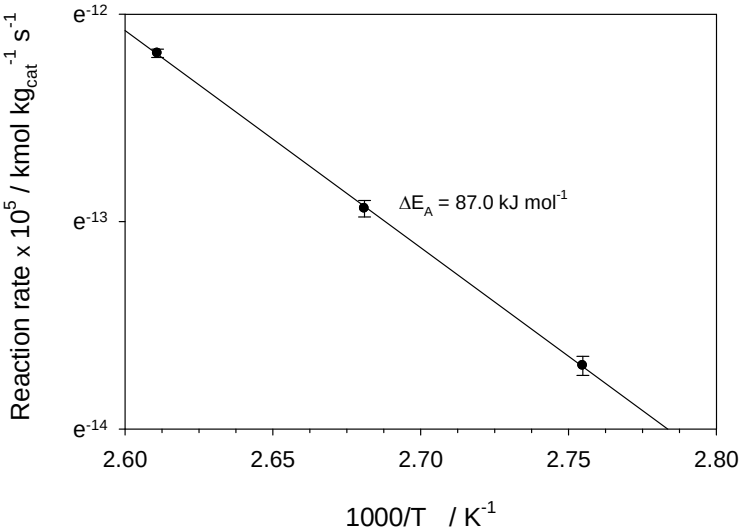


Figure 41. The influence of temperature on the average rate of reaction (p = atmospheric, $\upsilon_L$ = 0.1 $cm^3$ $min^{-1}$, $c_0$ = 0.025 kmol $m^{-3}$, n = 160 $min^{-1}$).

### 3.3 Conclusions

In conclusion, the successful hydrogenation of DMIT and a Suzuki cross coupling reaction in a continuous flow reactor with a rotating bed of nanocatalysts entrapped by the external magnetic field, represents the first demonstration of a potentially highly valuable new technology for performing chemical synthesis. Most significant was the ability of the magnetic field to hold the nanoparticles in the reactor without noticeable catalyst loss, even in two-phase flow. For the same conditions, the reaction rate for hydrogenation was at least an order of magnitude higher in the flow reactor than in a batch reactor. The possibility of a moving bed of nanocatalysts with its very high voidage in an open tube (98 % by vol., more than twice of that for traditional packed-bed reactors), without any additional separation devices inside the reactor, opens new avenues in the area of catalytic flow chemistry. Further optimization, including the exact correlation between the magnetic field strength, magnetic properties of the catalysts and the physical properties of the solvent is needed. In addition, further attention is needed on the design of efficient electromagnet systems to generate alternating magnetic fields to give a more elegant solution than the rotating permanent magnet used here.

# CHAPTER 4

## Utilization of magnetic nanocatalysts in microchannel reactors

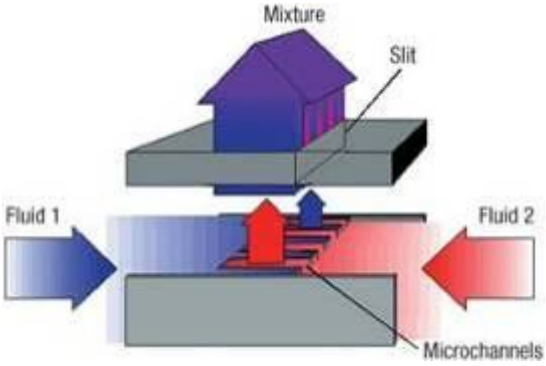


## 4 Introduction

Microreactor technology has become a strong focus in reactor engineering in recent years [140]. This is due to a number of advantages that it offers for chemical synthesis: enhanced mass and heat transfer, because of large surface area-to-volume ratio, which leads to another advantage, improved yield and selectivity [141-144]. Chemical synthesis in microreactors is typically more environmentally sustainable than traditional batch methods, because it is inherently less wasteful and because it provides unprecedented reaction control. Additionally, the small volume enables the safe use of highly toxic or explosive reactants [145]. One of the main distinguishing benefits of microreactor based chemistry is the ability for early-stage reaction optimization, and the ability for direct scale-up of the process [146]. In general, chemical transformations carried out in microreactors need a catalyst. Using a heterogeneous catalyst in a micro-size channel reactor is not an easy task, because of possible channel blockage. The other approach is the catalyst immobilization on the channel surface, which might be difficult in terms of uniform distribution of the active sites [147-150]. Although the utility of such reactors is very convenient, the problems arise from loading and unloading the catalytic metal before and after a continuous flow process. The superiority of the approach presented below is that the deactivated catalyst can easily be removed by the simple elimination of the magnetic field. It has been recently shown that there is the possibility for magnetic nanoparticle entrapment in a microreactor for bioapplication [151]. Theoretical work predicted that an alternating magnetic field can improve mixing efficiency [151]. Kim *et al.* has very recently described a microchemical system for continuous flow catalytic reactions with a flowing catalyst – immobilized on magnetic particles [153]. The system described first is based on catalyst entrapment and particle motion *via* a rotating magnetic field, and considers the reactor engineering and kinetics studies, which are crucial if these systems are to find wider application in manufacturing. The second system is similar to Kim's work and describes the investigation of the use of a silica coated magnetic nanoparticulate catalyst in the microreactor, in flow conditions for a two phase hydrogenation.

## 4.1 Continuous hydrogenation of nitrobenzene in a microreactor with magnetically entrapped and manipulated MNP/Pd(0)

This section will describe the MNP/Pd(0) catalyzed, two-phase hydrogenation reaction in a flow system, comprising a microreactor with the catalyst entrapped and moved by a permanent magnet (Scheme 43). This system combined a microreactor (XXL-ST-04 LTF GmbH), (Figure 42a, b), (channel size $2.2 \times 2.2$ mm, active volume of micromixers 4.5 ml) with a permanent magnet (surface magnetization 0.3 T**,** MMG MagDev, UK), which can rotate underneath the reactor syringe pump and MFC for hydrogen supply (Scheme 44).

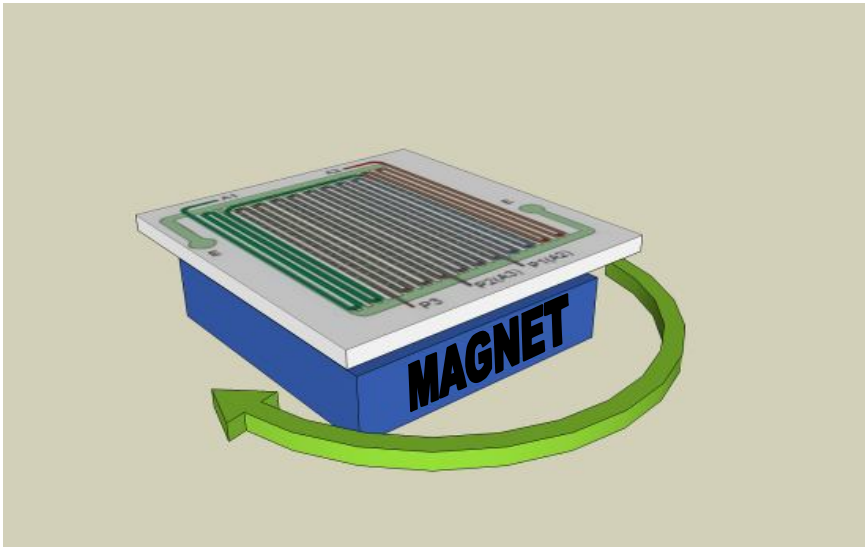


Scheme 43. Schematic of XXL-ST-04 microreactor with rotating external magnet underneath.

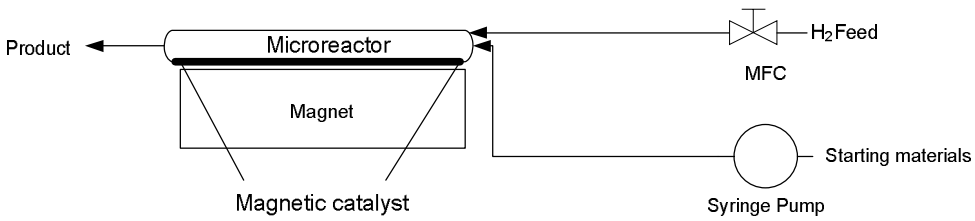


Scheme 44. Scheme of a microreactor unit with magnetically-entrapped and manipulated nanoparticle-supported catalysts.

The rotating magnet was thus able to entrap and move the MNPs inside the reactor. In this system, efficient, three-phase reactions might occur, because of the effective interaction between gas-liquid-solid, the large interfacial areas, and the short paths required for molecular diffusion in narrow channels. For this work, a MNP/Pd(0) catalyst was used. The method of preparation and characterization of this catalyst was described in Chapter 2. The hydrogenation of nitrobenzene (NB) (Scheme 42) was used to characterize the reactor by investigating the effect on conversion and overall rate of reaction (Eq. 7) of liquid and gas flow rates, reactant concentration and additional magnetic mixing. For synthetic details, see Appendix 2 sec. 3.32. In all experiments in this chapter gas flow rate was messured at NTP (Normal Temperature and Pressure).

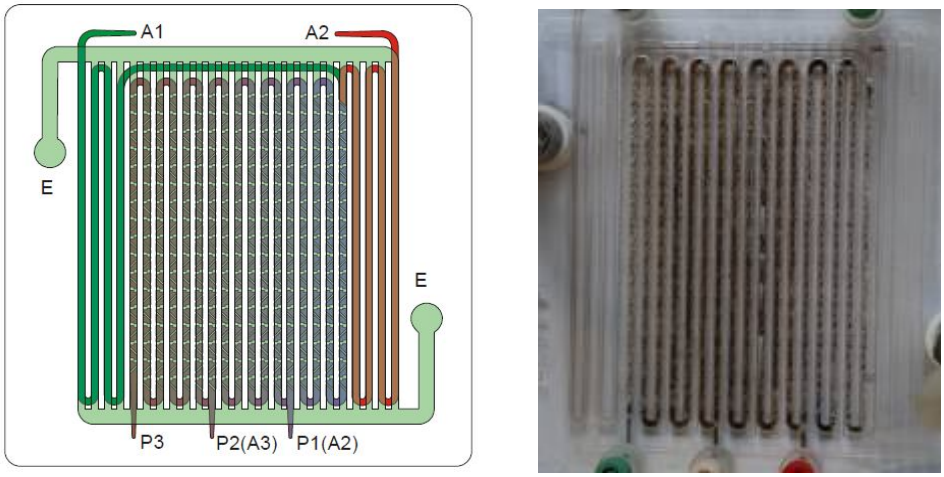


(a) (b)

Figure 42. (a) Schematic of XXL-ST-04 microreactor, (b) microreactor with magnetically entrapped catalyst for the hydrogenation.

Figure 43 shows the steady-state single-pass conversions obtained for various NB concentrations. Quantitative hydrogenation of NB was obtained for a liquid flow of 0.1 $cm^3$ $min^{-1}$ and $c_0$ = 0.05 kmol $m^{-3}$.

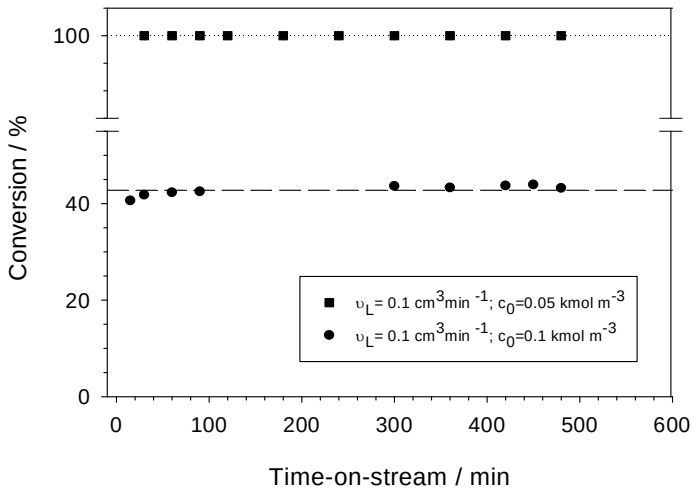


Figure 43. The evaluation of a steady-state conversion in the reactor with magnetically entrapped catalyst for initial reaction conditions (T = 303 K, p = atmospheric, $\upsilon_G$ = 0.8 $cm^3$ $min^{-1}$, n = 100 $min^{-1}$).

Increasing the concentration of NB resulted in a lower conversion of 43 % and was stable for 8 h, showing the catalyst stability. An important observation from these initial experiments was that the rotating magnet kept the catalyst nanoparticles inside of the microreactor even during two-phase bubble flow. AAS analysis of the product solution, over the course of 8 h of reaction, showed no palladium in the reaction product. The catalytic thin layer bed of MNPs was 22 microns high (1 % of the channel width) according to calculations, and was stable in a magnetic field.

The influence of the rotation of the magnet on the steady-state conversion and overall rate of reaction was investigated (Figure 44). The system was tested in two modes: with a resting magnet underneath the reactor, and with a rotating magnet (100 rpm). For an initial NB concentration of 0.1 kmol $m^{-3}$ and a liquid flow rate of 0.1 $cm^3$ $min^{-1}$ at 303 K, 34 % conversion was obtained ($5.90 \times 10^{-6}$ mol $g_{cat}^{-1}$ $s^{-1}$) with the magnet at rest, compared with 43 % conversion ($7.64 \times 10^{-6}$ mol $g_{cat}^{-1}$ $s^{-1}$) obtained for the experiment with the additional mixing caused by the magnet rotation.

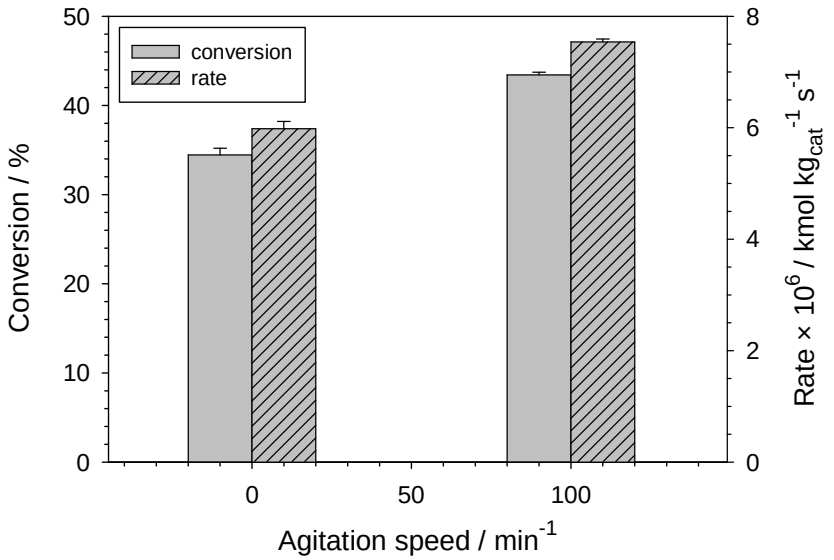


Figure 44. The influence of the agitation speed of the permanent magnet on the overall reaction rate and conversion (T = 303 K, p = atmospheric, $\upsilon_L$ = 0.1 $cm^3$ $min^{-1}$, $\upsilon_G$ = 0.8 $cm^3$ $min^{-1}$, $c_0$ = 0.1 kmol $m^{-3}$).

It was possible to observe the gentle motion of the particles inside the reactor during the magnet rotation. The positive influence of catalyst movement on the obtained conversion is shown in Figure 44. The increase in conversion could be explained by better catalyst accessibility and more efficient mass transfer of hydrogen into the liquid phase in the presence of moving nanoparticles [137].

The influence of the initial NB concentration on the overall rate of the reaction is shown in Figure 45. A saturation-like isotherm was observed, suggesting a heterogeneous mechanism for the hydrogenation reaction.

Increasing the liquid phase flow rate had no pronounced influence on the overall reaction rate (Figure 46). The effect of the gas flow was investigated; the unchanged NB conversion and the rate of the reaction could be explained by the competing effects of the NB/hydrogen ratio and the residence time. Gas flow rate was messured at NTP (Normal Temperature and Pressure).

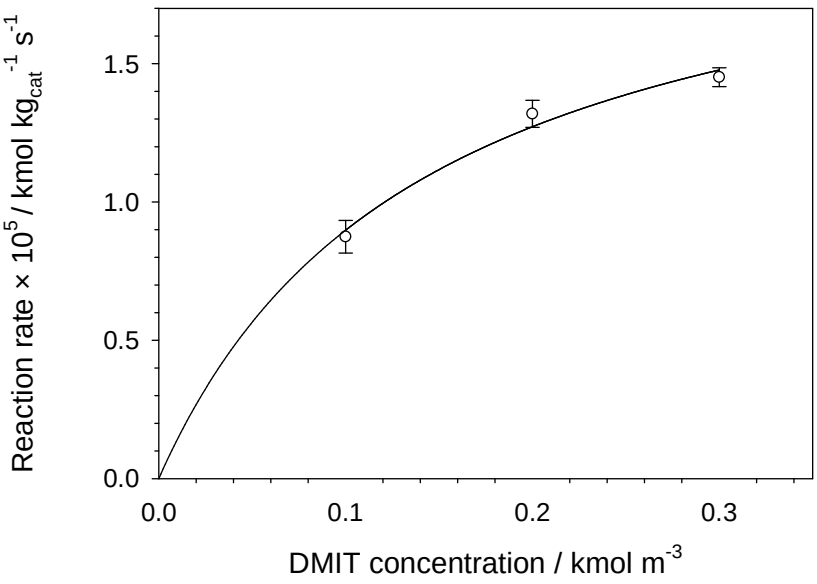


Figure 45. The influence of NB concentration on the average rate of reaction (T = 303 K, p = atmospheric, $\upsilon_L$ = 0.1 $cm^3$ $min^{-1}$, $\upsilon_G$ = 0.8 $cm^3$ $min^{-1}$, n = 100 $min^{-1}$).

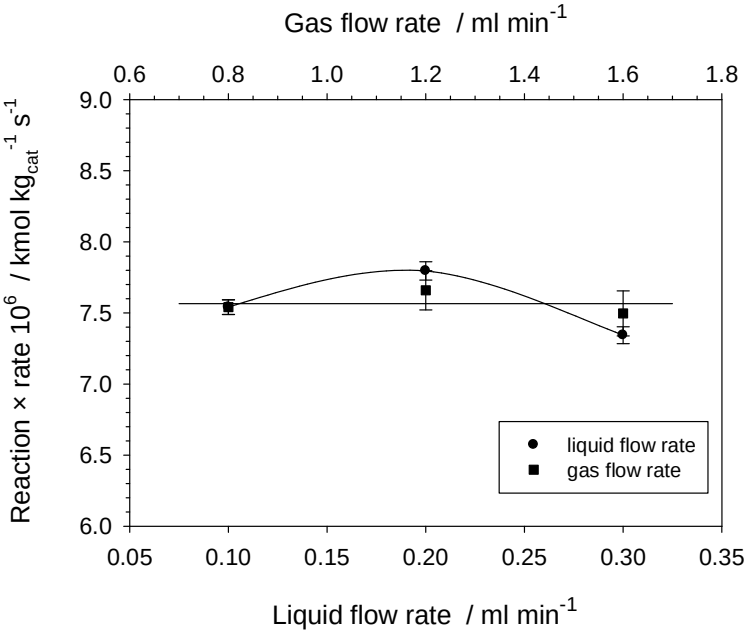


Figure 46. The influence of liquid and gas flow rates on the rate of reaction (T = 303 K, p = atmospheric, $c_0$ = 0.1 kmol $m^{-3}$, n = 100 $min^{-1}$).

## 4.2 Continuous hydrogenation of DMIT in a microreactor with magnetically entrapped and manipulated MNP/Pd(0)

To show the possibility of the extension of the presented catalytic system for other chemical transformations, the reactor was tested for the hydrogenation of an olefinic C=C bond. The hydrogenation of DMIT (dimethyl itaconte) (Scheme 38) was used to show the performance of the entrapped MNP/Pd(0) in a microchannel reactor. It was possible to carry out the reaction quantitatively for 8 h for a initial DMIT concentration of 0.05 kmol $m^{-3}$. For $c_0$ = 0.1 kmol $m^{-3}$, 57 % was achieved in a steady state and no catalyst deactivation was observed during the course of 8 h of the reaction (Figure 47). For synthetic details, see Appendix 2 sec. 3.33.

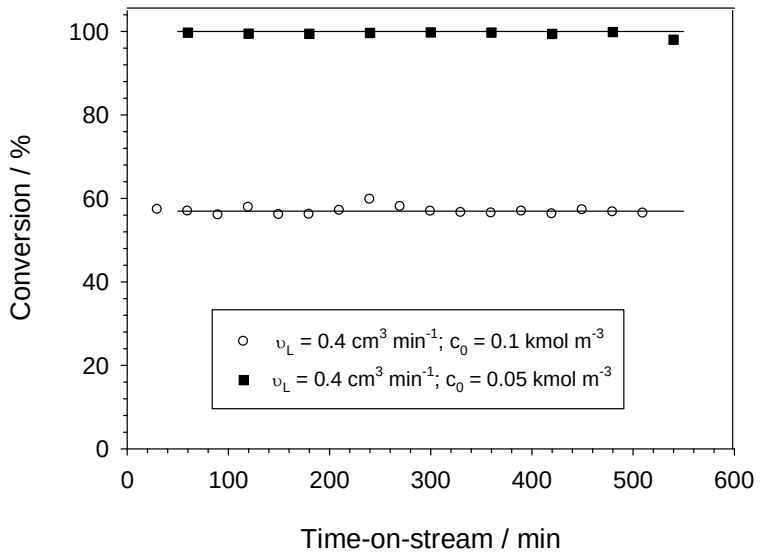


Figure 47. The evaluation of steady-state conversion in the reactor with a magnetically entrapped catalyst for DMIT hydrogenation (T = 303 K, p = atmospheric, $\upsilon_G$ = 1.6 $cm^3$ $min^{-1}$, $c_0$ = 0.1 kmol $m^{-3}$, n = 0 $min^{-1}$).

## 4.3 Continuous Knoevenagel - hydrogenation tandem reaction in microreactor with magnetically entrapped and manipulated MNP/Pd(0)

The initial experiments on the flow Knoevenagel - hydrogenation tandem reaction were carried out in the microreactor using toluene as a solvent; however, the collection of samples was impossible, due to high volatility of this solvent. Instead, the ethanol was chosen according to Postole *et al*. [154]. Although it is well known that Knoevenagel condensation proceeds faster in EtOH, this system was selected as a model reaction only. When the reactor was packed with the catalyst (approximately 1 % of the channel volume), two solutions (each containing one of the condensation reactant: benzaldehyde and ethyl cyanoacetate), were pumped using separate syringe pumps. The Knoevenagel reaction proceeded in the first section of the microreactor, which starts at inlet P 3 and ends at inlet P 2 (Figure 42) and has a total volume of 1.5 ml. For more details, see Appendix 2 sec. 3.34. The conversion of the condensation process was retained at >98 % during the whole experiment (Figure 48, Figure 49). The mixture containing the unsaturated Knoevenagel product was brought into contact with hydrogen in the second section of the microreactor (3 ml total volume), which starts at inlet P 2 (Figure 42). MNP/Pd(0) activity was stable for 4.5 h, giving a hydrogenation conversion of 73 %. A slow deactivation of the catalyst was observed after this time (Figure 48), however, 30 % of the hydrogenation conversion was still obtained even after 10 h of microreactor operation. After the experiment, the magnet was removed, the nanoparticles were simply washed out using solvent, and the reactor could be reloaded with fresh catalyst. Applying $Et_3N$ as a base, a stable concentration of the tandem reaction product was observed for a duration of 10 h, although with a lower conversion (*ca*. 45.1 ± 2.7 %) than for KOAc (Figure 49). These experiments confirmed the results obtained from the batch reactions in Section 2.1.8.

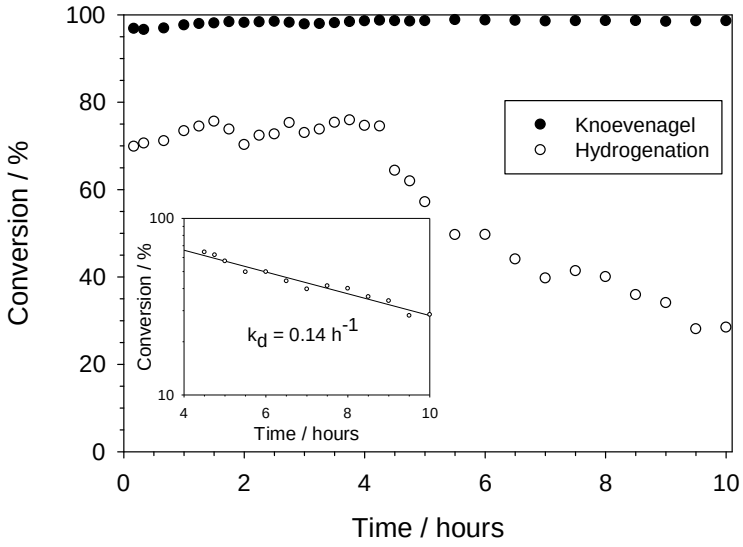


Figure 48. Kinetics of a continuous flow tandem Knoevenagel - hydrogenation process with KOAc used as a base.

Due to the change of the solvent, the semi-batch experiment was carried out under the same conditions to compare the efficiency of both processes. In both cases, the final reaction volume and amount of MNP/Pd(0) were the same. The calculated overall reaction rate for the semi-batch reaction system was one order of magnitude lower ($r_A$ = 6.11 x $10^{-7}$ and 6.08 x $10^{-8}$ mol $g_{cat}^{-1}$ $s^{-1}$ for the microreactor and the semi-batch processes respectively), confirming the advantages of using the microchannel reactor [155].

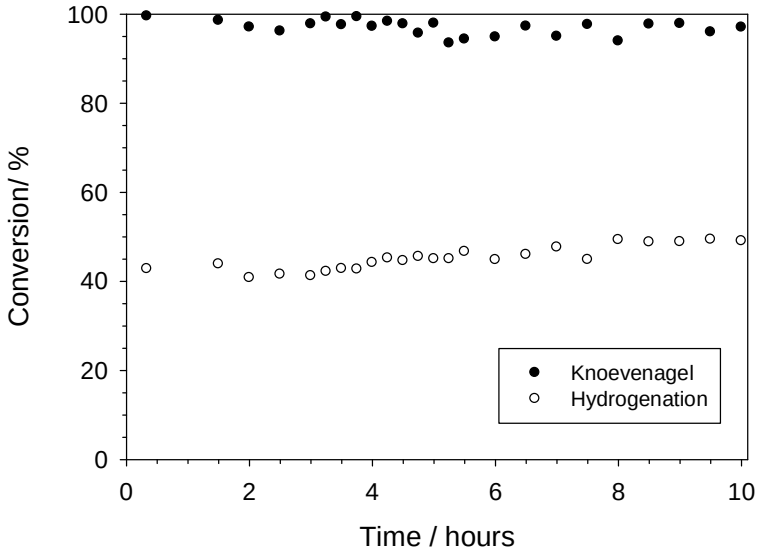


Figure 49. Kinetics of continuous flow tandem Knoevenagel - hydrogenation process with $Et_3N$ used as a base.

This simplified approach to continuous reactions using the MNP-based catalysts entrapped in a magnetic field can be applied to multiple nanoparticulate catalytic systems together for generating complex reactions in one flow process.

### 4.4 Continuous hydrogenation of DMIT in a flow reactor with MNP/$SiO_2$/Pd(0)

This section describes a two phase hydrogenation in a microreactor catalyzed by a magnetic highly dispersed nanocatalyst. This system combined a microreactor (XXL-ST-04 LTF GmbH) (Figure 50) immersed in ultrasonic bath, a peristaltic pump and a mass flow controller for the hydrogen supply (Scheme 45).

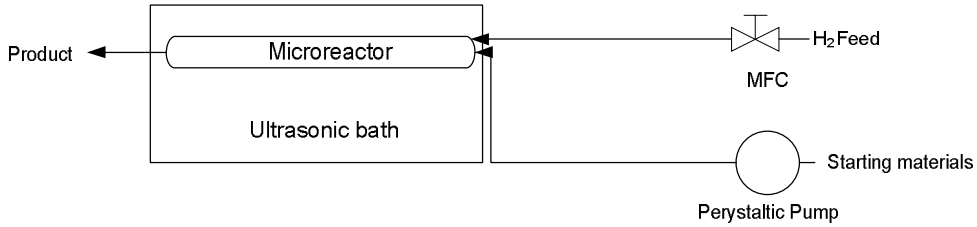


Scheme 45. Scheme of a microreactor unit for hydrogenation of DMIT using MNP/$SiO_2$/Pd(0) catalyst.

In this system efficient, three-phase reactions might occur, because of the effective interaction between gas-liquid, the highly dispersed nanoparticle catalyst, the large interfacial areas and the short paths required for molecular diffusion in the narrow channels. For this work, an MNP/$SiO_2$/Pd(0) catalyst was used. The method of preparation and characterization of this catalyst was described in Chapter 2. The hydrogenation of DMIT (Scheme 38) was used to characterize the reactor by investigating the effect on conversion and overall rate of the reaction (Eq. 7) of liquid and gas flow rates, temperatures, and catalyst loading. For more details, see Appendix 2 sec. 3.35.

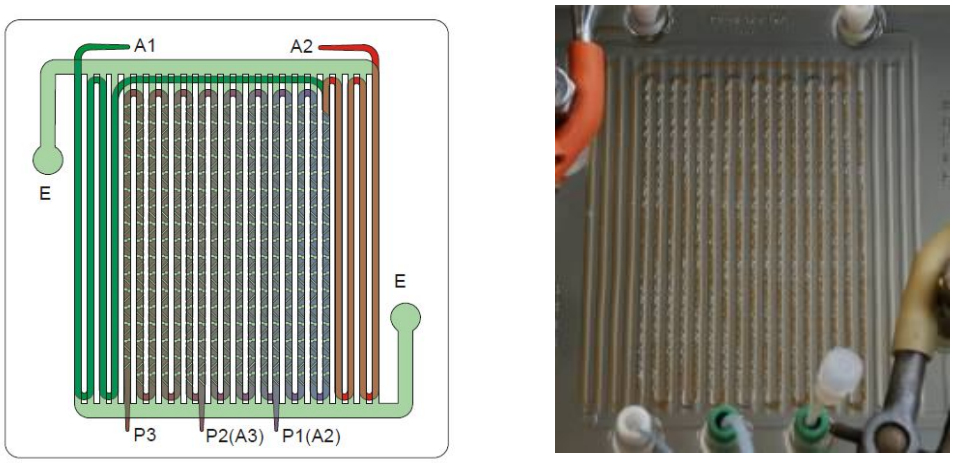


(a) (b)

Figure 50. (a) Schematic of microreactor (XXL-ST-04 LTF GmbH), (b) microreactor during the hydrogenation of DMIT with MNP/$SiO_2$/Pd(0).

Figure 51 shows the steady-state, single-pass conversions obtained for various catalyst concentrations. Decreasing the S/C ratio resulted in a higher conversion.

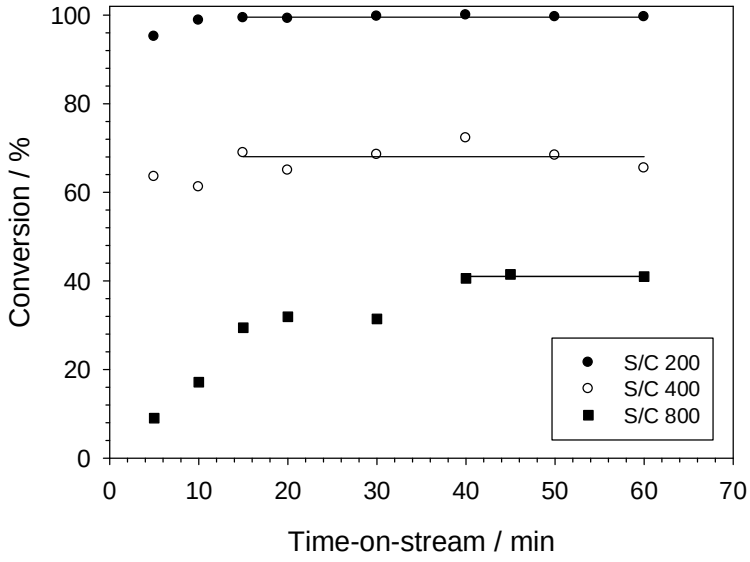


Figure 51. The evaluation of steady-state conversion in the reactor for initial reaction conditions (T = 293 K, p = atmospheric, $\upsilon_L$ = 1.0 $cm^3$ $min^{-1}$, $\upsilon_G$ = 2.4 $cm^3$ $min^{-1}$).

Quantitative hydrogenation of DMIT was obtained for S/C = 200 (S - substrate, C - catalyst) and liquid phase flow of 1 $cm^3$ $min^{-1}$. An important observation from these initial experiments was that the magnetic nanoparticulate catalysts enhanced by ultrasounds were not aggregating and were not sedimenting in

the reactor channels during the experiments. Increasing the concentration of the catalyst increased the conversion; but it had no influence on the rate of reaction (Figure 52).

Increasing the reaction temperature decreased the conversion of DMIT and the calculated rate of the reaction (Figure 53). This was caused by a decreased solubility of the hydrogen gas, resulting from a decrease in the hydrogen partial pressure in the gas bubbles due to methanol vaporization. The solubility of hydrogen in the methanol was calculated similarly to the method in Section 3.2.1. For details, see Appendix 2 sec. 2.3. The increase of the solubility of hydrogen in the liquid phase increased the rate of the reaction. A fuller explanation of the temperature influence would require rigorous mathematical modelling of the process.

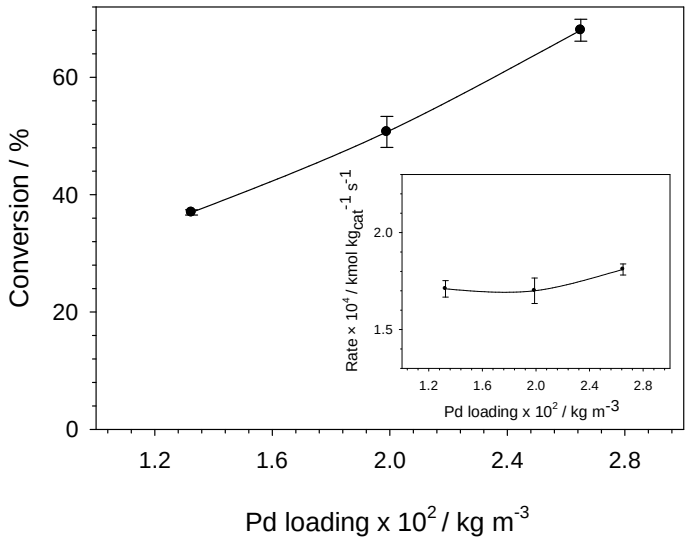


Figure 52. The influence of the catalyst loading on the conversion of DMIT. Insert: The influence of the catalyst loading on the reaction rate (T = 293 K, $c_0$ = 0.1 kmol m$^{-3}$, p = atmospheric, $\upsilon_L$ = 1.0 cm$^3$ min$^{-1}$, $\upsilon_G$ = 2.4 cm$^3$ min$^{-1}$).

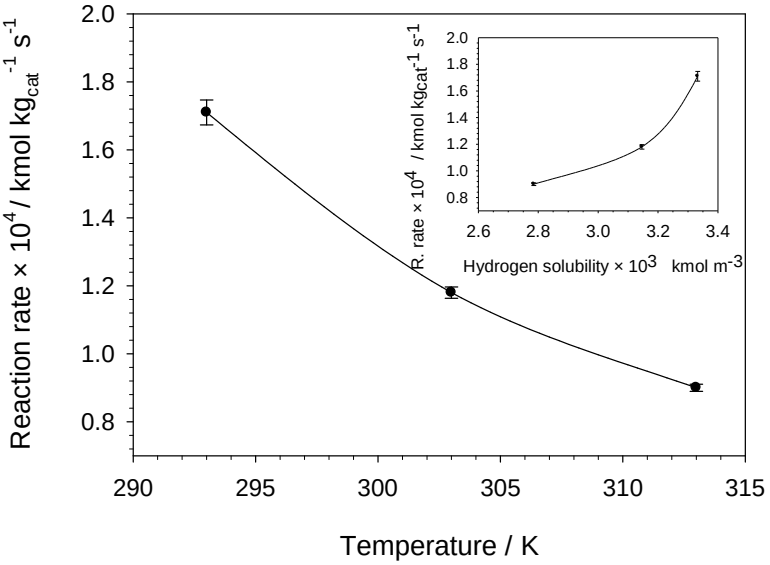


Figure 53. The influence of the temperature on the rate of the hydrogenation of DMIT. Insert: The influence of the hydrogen solubility in the organic phase on the reaction rate (p = atmospheric, $\upsilon_L$ = 1.0 $cm^3$ $min^{-1}$, $\upsilon_G$ = 2.4 $cm^3$ $min^{-1}$, $c_0$ = 0.1 kmol $m^{-3}$, S/C = 400).

Increasing the gas flow rate, (hence decreasing DMIT/hydrogen ratio and residence time ($\tau$) from 79.4 to 46.6 s), did not have a pronounced influence on the conversion (Figure 54). Stable conversion could be explained by compensation from two effects *i)* increased gas-liquid interfacial areas, (increase of the gas volumetric fraction inside the channel), decrease liquid volumetric fraction from 29.1 % to 17.2 %, and *ii)* shorter residence time of the liquid phase in the reactor.

To demonstrate the advantage of using a microreactor, a semi-batch experiment using the standard initial conditions (T = 303 K, p = atmospheric, $\upsilon_G$ = 2.4 $cm^3$ $min^{-1}$, $c_0$ = 0.1 kmol $m^{-3}$) was carried out. The rate of reaction was around 3 times lower than in the continuous system ($1.7 \times 10^{-4}$ compared with $6.3 \times 10^{-5}$ mol $g_{cat}^{-1}$ $s^{-1}$). The reaction rate was affected mainly by the less effective mass transfer of hydrogen in the semi-batch mode.

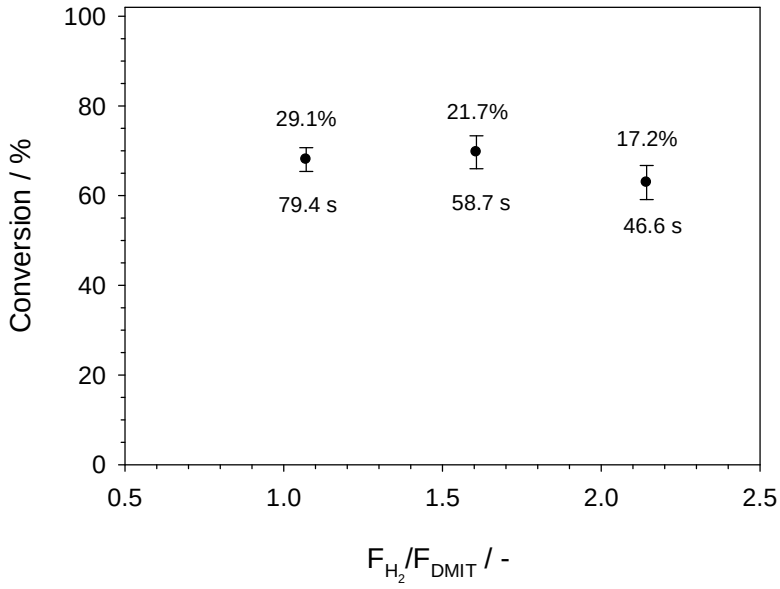


Figure 54. The influence of the molar flow ratio of $H_2$/DMIT on steady-state conversion in the reactor (T = 293 K, p = atmospheric, $\upsilon_L$ = 1.0 $cm^3$ $min^{-1}$, $c_0$ = 0.1 kmol $m^{-3}$, S/C = 400).

### 4.5 Conclusions

In conclusion, two systems based on microreactor were described. The first was based on catalyst entrapment and particle motion using a rotating magnetic field in a micoreactor. The second involved the application of silica-coated magnetic nanoparticulate catalyst for two phase hydrogenation in a microreactor. Hydrogenation of nitrobenzene in a microreactor, with a thin layer of nanocatalysts entrapped and moved by the external magnetic field represents the first demonstration of a potentially highly valuable new technology for performing chemical synthesis. The system was also successfully applied to the hydrogenation of diemthyl itaconate and to a tandem Knoevenagel condensation - hydrogenation process. Most significant was the ability of the magnetic field to hold the nanoparticles in the reactor without any noticeable catalyst loss, even in two-phase flow. Another advantage of this system is that the reaction can occur at low pressure and temperature, which is an important factor when considering the safety issues of hydrogen usage. The possibility of trapping and moving nanocatalysts without any

separation devices inside the reactor opens new avenues in the area of catalytic flow chemistry. The other superiority of the presented approach is that deactivated catalyst can easily be removed simply by elimination of the magnetic field. The second system involved the hydrogenation of dimethyl itaconate in a microreactor, using highly dispersed MNP/$SiO_2$/Pd(0). For the same conditions, the reaction rates were 3 times higher in the flow reactor than in a semi-batch reactor. As was the case with the first system, the reaction can occur at low pressures and temperatures. The magnetic nanocatalysts can be easily recovered from the product stream using the permanent magnet and can be recycled into the process.

Both concepts could be extended to other multiphase processes that use carbon dioxide or oxygen as a gas-phase reagent. Although one reactor can only produce a small amount of the product, it would be easy to scale-up the reactions by using a number of reactors in parallel.

# CHAPTER 5

Conclusions

and future work

## 5.1 Conclusions

The ultimate goal of this work was to study the possibilities of applying magnetic nanoparticle based catalysts in flow processes. In order to do that, many reactions in batch were screened using various MNP-based catalysts. Results of these experiments were described in Chapter 2. It was demonstrated that MNP/Ru(0) is a very promising catalyst for the dihydroxylation of styrene, dimethyl fumarte and dimethyl maleate. $NaIO_4$ was proven to be the most effective oxidising agent. MNP/Pd(0) catalyst was shown to be very effective and stable in catalysing the hydrogenation of DMIT. No loss of catalytic activity was observed over 4 cycles. The MNP/Pd(0) was also tested in the hydrogenation of nitrobenzene, and was shown to be a very efficient catalyst. The MNP/Pd(0) was reused in three more cycles with 100 % conversion to aniline. The application of iron oxide nanoparticles for accelerating the Knoevenagel condensation was also demonstrated. Moreover, impregnation of the MNPs with Pd(0) resulted in a system exhibiting excellent catalytic performance in tandem aldol condensation-hydrogenation processes, under mild conditions.

Another very interesting finding was that, silica coating was a very good method to prevent MNPs from aggregation. MNP/$SiO_2$ were easy to disperse in polar solvents from a dry powder, and were easy to separate (up to 5 min) using a standard permanent magnet. All of these results suggest that this material is suitable as a magnetically separable support for different catalysts. Varieties of catalysts were prepared using MNP/$SiO_2$ as a support, including Ru, Rh, Pd, Ag, and Au nanoparticles. MNP/$SiO_2$/Rh(0), MNP/$SiO_2$/Ru(0), and MNP/$SiO_2$/Pd(0) were very effective catalysts for DMIT hydrogenation.

Three different approaches to flow processes using MNP-based catalyst were described in Chapters 3 and 4. A new design for a capillary reactor with entrapped MNP/Pd(0) catalyst was presented in Chapter 3. The successful hydrogenation of DMIT and Suzuki cross coupling reaction in this reactor were carried out. The most significant was the ability of the magnetic field to hold the nanoparticles in the reactor without noticeable catalyst loss, even in two-phase gas-liquid flow. The

possibility of a moving bed of nanocatalysts with its very high voidage (98 vol %, more than twice of that for traditional packed-bed reactors), without any additional separation devices inside the reactor, opens new avenues in the area of catalytic flow chemistry. Kinetic studies showed possibilities of quantitative processes (100 % conversion), which suggest that this system could be a potentially highly valuable new technology for performing chemical synthesis.

Chapter 4 covered very successful experiments on the application of two kinds of nanoparticle-based catalysts in a microchannel reactor. First, a thin layer of MNP/Pd(0) nanocatalyst was entrapped and moved by the external magnetic field within the microreactor. This moving bed was able to catalyzed hydrogenation of nitrobenzene to aniline with good conversion up to 100 %. The system was also successfully applied for hydrogenation of DMIT and tandem Knoevenagel condensation - hydrogenation process. The superiority of presented approach is that the deactivated catalyst can be easily removed by simple elimination of magnetic field.

A second kind of nanoparticulate catalyst MNP/$SiO_2$/Pd(0) was used in a microreactor for the hydrogenation of DMIT with good results. The flowing catalyst was well dispersed in the liquid phase in channels of the microreactor and could be easily separated after the reaction. In all flow experiments, with the same conditions, reaction rates were higher than in batch process (Figure 55). Another advantage of these systems is that the reaction can occur at low pressure and temperature, which is an important factor, considering safety issues of hydrogen usage.

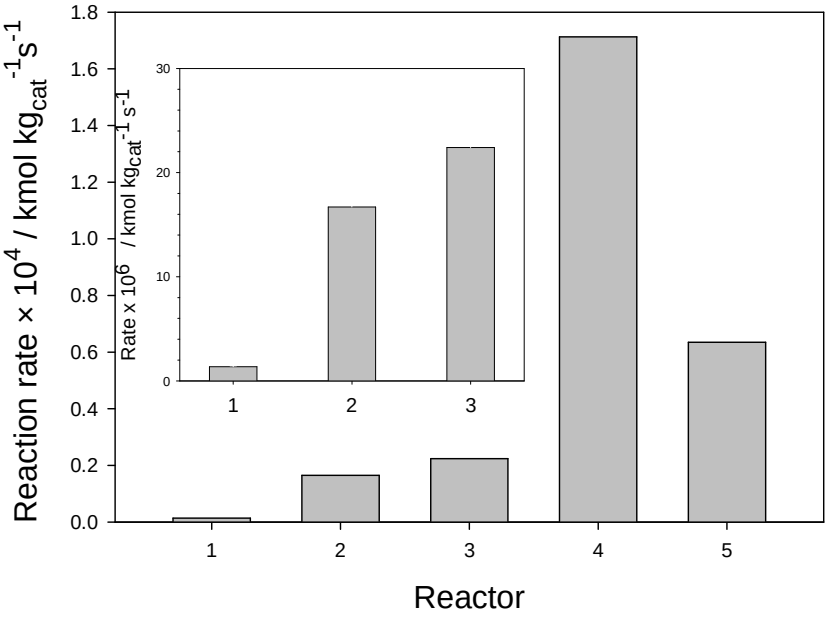


Figure 55. Comparison of reaction rates for various reactors, using different catalysts, for hydrogenation of DMIT: (1 - batch reactor using MNP/Pd(0), 2 - capillary reactor using MNP/Pd(0), 3 - microreactor using MNP/Pd(0), 4 - microreactor using MNP/ $SiO_2$/Pd(0), 5 - batch reactor using MNP/ $SiO_2$/Pd(0)).

In summary, using magnetic nanoparticles as a catalyst support, especially when expensive and toxic metals and ligands are employed offers high activity, selectivity, minimal loss, easy separation, recovery and reuse. These catalytic systems together with process intensification in different (micro)reactors could be of great economic and environmental importance in chemical and pharmaceutical industries; reducing costs and providing environmental protection benefits.

## 5.2 Future work

Several catalytic systems based on magnetic nanoparticulate support were investigated in this work. A very promising ruthenium catalyst MNP/Ru(0) for dihydroxylation of alkenes requires more investigations on catalyst stability. Kinetic studies should be carried out for the dihydrohylation of different alkenes using this catalyst. The MNP/Pd(0) catalyst showed potential for the Suzuki reaction. Further investigation of the efficiency of this catalyst for different C-C coupling reaction (Heck, Sonogashira, Negishi) should be carried out.

In terms of application of MNP-based catalysts in flow processes, further optimization, including the exact correlation between the magnetic field strength, magnetic properties of the catalysts and the physical properties of the solvent is needed. In addition, further attention is needed on the design of efficient electromagnet systems to generate alternating magnetic fields to give a more elegant solution than the rotating permanent magnet used here. Further studies in high pressure systems are needed to evaluate influence of higher pressure on the reaction rate and on the behaviour of the systems. The stability of the catalysts were evaluated in a maximum of 10 h long processes. Longer (up to 100 days) studies should be carried out, in order to prove long-term stability of these catalytic systems. A very interesting continuation of these studies would be an evaluation of different sizes of the channels for both capillary and micro-reactors in order to assess the influence of the size of the channels on reaction rate. The concept of MNP-catalyst entrapment in microsize channel reactors could be extended to other multiphase processes that use carbon dioxide or oxygen as gas-phase reagent. Although one reactor can produce only a small amount of the product, it would be easy to scale up reactions by using a number of reactors in parallel.

MNPs could also be applied in multimodal imaging. Preliminary results are described in Appendix 1.

# APPENDIX 1

## Bioapplication

## of magnetic nanoparticles

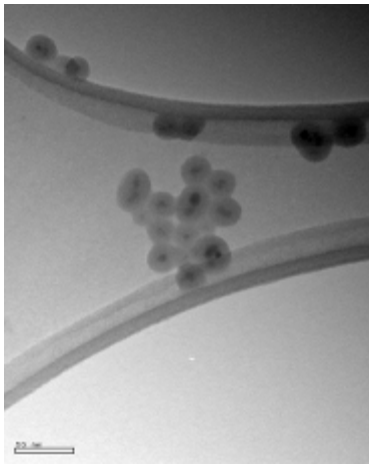

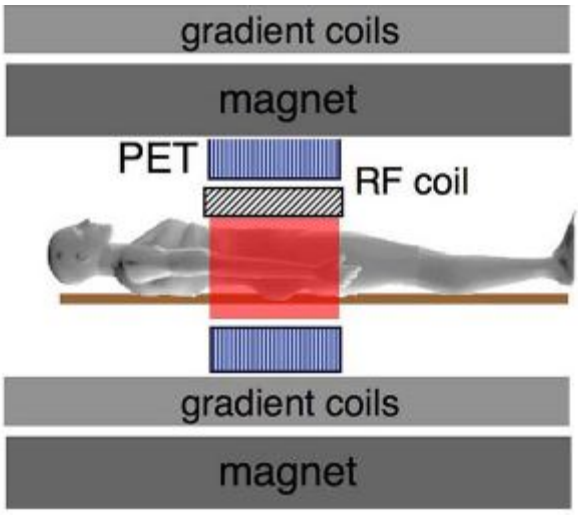

## 1 Introduction

Personalised medicine is currently considered the future of healthcare, and molecular imaging plays a key role towards this target. However, there is no single modality amongst molecular imaging techniques, which is ideal and adequate to gain all the essential information. For example, positron emission tomography (PET) has poor resolution, but a very high sensitivity, magnetic resonance imaging (MRI) has low sensitivity but excellent resolution, and optical fluorescence imaging is difficult to quantify. The combination of multiple molecular imaging techniques can therefore offer synergistic advantages over any modality alone, and can be an essential tool in state-of-the-art imaging research as well as standard practice in the clinic [156, 157].

One of the examples of multimodal imaging is the simultaneous PET-MRI technique. This new approach for functional and morphological imaging was first described by Judenhofer *et al*. [158]. The synergistic combination of PET and MRI holds promise for a successful next generation of dual-modality scanners in medical imaging. These instruments will provide us with accurate diagnoses, thanks to the sensitive and quantifiable signal of PET and the high soft-tissue resolution of MRI. Furthermore, patients will receive a lower radiation dose and will spend less time in the clinic. However, these new tools require new class of imaging probes. Therefore, there has been increasing interest in the development of dual(multi)-modality PET–MRI agents. The standard dual-modal PET-MRI imagine agent was based on PET isotope and gadolinium [159]. The second generation of dual(multi)-modal contrast agents are synthesised using MNPs, having a proven record of biocompatibility and a track record of extensive use in the clinic as MRI contrast agents [160, 161]. There are a few examples of dual(multi)-modality described in the literature, which use hybrid nanomaterial for PET/MRI or PET/MRI/NIRF (near infrared fluorescence). The preparation of serum albumin modified $MnFe_2O_4$ nanopaticles conjugated with $^{124}I$ was reported by Choi *et al*. [157]. Lee *et al*. described amino modified MNPs which were coupled to cyclic arginine-glycine-aspartic (RGD) peptides for integrin $\alpha_v\beta_3$ targeting and macrocyclic 1,4,7,10-tetraazacyclododecane-*N*,*N′*,*N″*,*N‴*,-tetraacetic acid (DOTA) chelators for PET and labelled with $^{64}Cu$ [162]. Jarrett *et al*. [163] developed the way of $^{64}Cu$ radiolabeling of dextran sulphate-coated superparamagnetic iron oxide nanoparticles. The labeling was done through

coordination of the $^{64}Cu$ to the chelating bifunctional ligand, *S*-2-(4-isothiocyanatobenzyl)-1,4,7,10-tetraazacyclododecane-1,4,7,10-tetraacetic acid (*p*-SCN-Bz-DOTA) and then conjugation to the nanoparticles. Devaraj *et al*. [164] reported the synthesis and *in vivo* characterization of $^{18}F$ modified trimodal MNPs ($^{18}F$-CLIO). This particle consisted of cross-linked dextran held together in a core-shell formation by a superparamagnetic iron oxide core, and functionalized with the radionuclide $^{18}F$ in high yields *via* click chemistry. Serum albumin MNPs, dually labeled with $^{64}Cu$-DOTA and Cy 5.5, were synthesised by Xie *et al*. [165] as a tri-modality imaging agent for PET/NIRF/MRI. Glaus *et al*. [166] reported synthesis of a probe consisting of a superparamagnetic iron oxide (SPIO) core coated with PEGylated phospholipids. The chelator 1,4,7,10-tetraazacyclo-dodecane-1,4,7,10-tetraacetic acid (DOTA) was conjugated to PEG termini to allow labelling with positron-emitting $^{64}Cu$. The radiolabeling of MNPs and anchoring of fluorescence dyes has been done in most of the cases presented, using complicated chemical conjugation. The isotope or dye might be bound relatively weakly to the surface of the MNPs, which might result in a lack of stability over time [167].

In the section below, efforts were focused on the incorporation of fluorescent and radioactive bodies in the silica shell, which should prevent leaching and sustain the stability. The results presented in Chapter 5 were obtained in collaboration with Dr. Sofia Pascu and Mr Rory Arrowsmith.

### 1.1 Dye doped silica coated MNPs

In this section, attention was focused on the encapsulation of fluorescent dyes in the silica shell of MNP/$SiO_2$. Based on methods proposed by Wu *et al*. [168] and Jacinto *et al*. [69], different dyes were used in order to obtain MNPs with fluorescent properties. In this synthesis, a one-step microemulsion process was applied. In a typical procedure, IGEPAL 520 (polyoxyethylene(5)isooctylphenyl) ether dispersed in cyclohexane was used as a surfactant. Then, $Fe_3O_4$ nanoparticles, dispersed in cyclohexane, were added. After this step, ammonium hydroxide saturated with the appropriated dye was added to form a reverse microemulsion. Tetraethylorthosilicate (TEOS) was used as a precursor of silica. The coating process, which consists of TEOS hydrolysis, catalyzed by ammonia, was carried out for 16 h. For synthetic details, see Appendix 2 sec. 3.36. Nanomaterials prepared in this way were separated

using a permanent magnet, and analyzed using the TEM technique and fluorescence spectroscopy. Unfortunately, none of the nanoparticles prepared using the aforementioned method exhibited fluorescence. It was suspected that the magnetic nanoparticulate core quenched the fluorescence. This is why, it was decided to repeat the coating procedure, but without using the NMP core. These experiments showed similar results - no fluorescence was observed in any of the samples. TEM images confirmed the size of the particles and that they were well dispersed. A very interesting result was observed when MB (methylene blue) was used. The MB dye was mostly distributed in the core of the silica shell (Figure 56b). Three other dyes (FL, Rubpy, rhodaimne B) were spread uniformly through the silica spheres (Figure 57b, Figure 58b, Figure 59b) or were not incorporated in the silica shell.

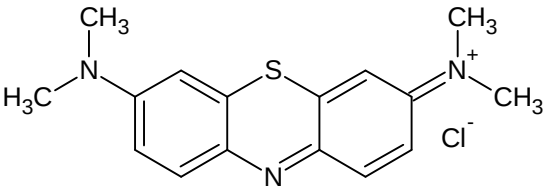


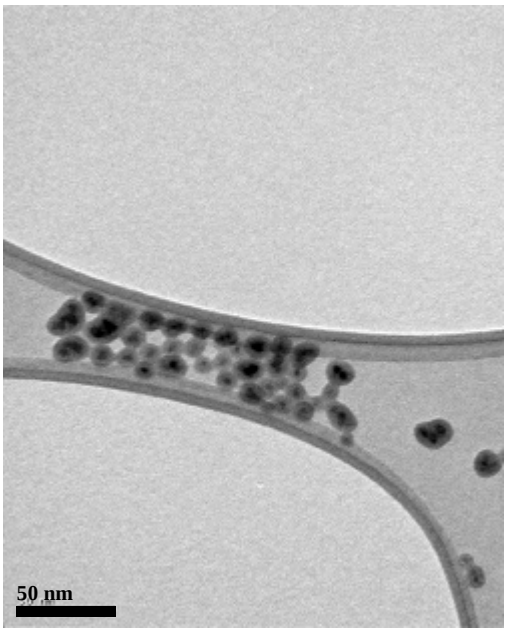


(a) (b)

Figure 56. (a) Structure of MB (methylene blue), (b) TEM micrograph of MB doped silica coated MNPs.

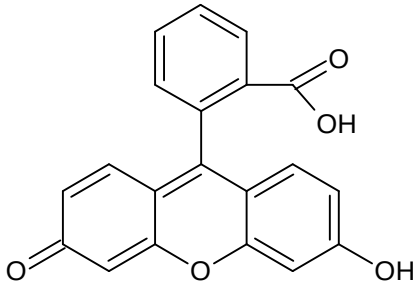


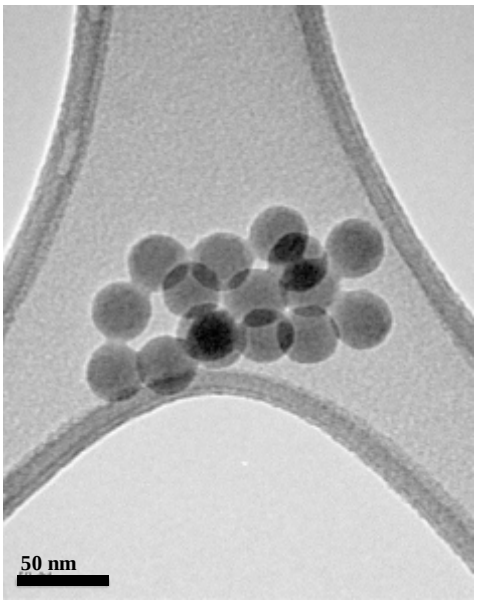


a) b)

Figure 57. (a) Structure of FL (fluorescein), (b) TEM micrograph of FL doped silica coated MNPs.

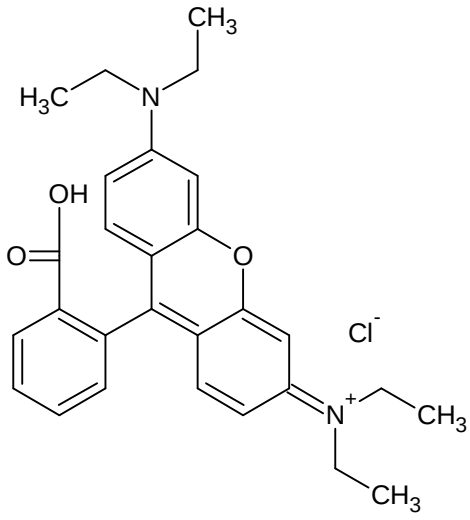


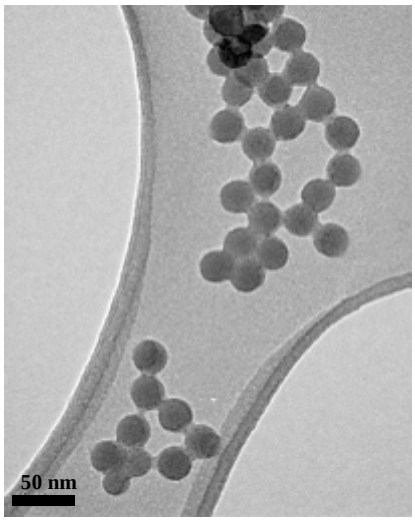


a) b)

Figure 58. (a) Structure of rhodamine B, (b) TEM micrograph of rhodamine B doped silica coated MNPs.

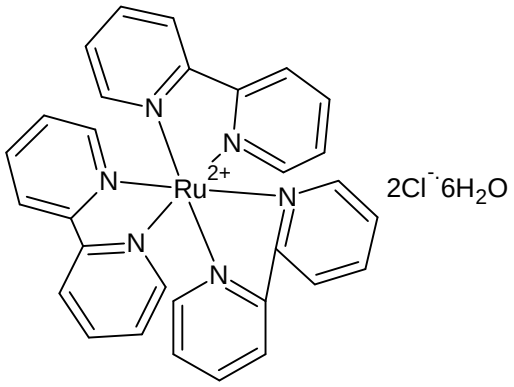


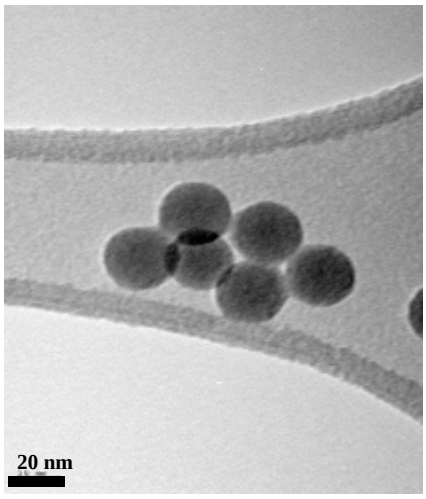


(a) (b)

Figure 59. (a) Structure of Rubpy (tris(2,2′-bipyridyl)ruthenium (II) chloride hexahydrate), (b) TEM micrograph of Rubpy doped silica coated MNPs.

Discouraged by the lack of fluorescent emission in dye-doped MNPs, it was decided to use QD (quantum dots).

**1.2 QD modified silica coated MNPs**

QD exhibit higher extinction co-efficient and comparable quantum yield to fluorescent dyes [169]. A very similar method, applied in last section, using reverse microemulison was empoyed. For synthetic details, see Appendix 2 sec. 3.37. QD (Lumidot CdSe 480) were purchased from Aldrich, and dispersed in cyclohexane, alongside with the MNPs. Nanoparticles prepared in this way were characterized using TEM techniques. The QD were visible (Figure 60), but detection by EDX analysis was not possible. To prove that the QD were encapsulated in the silica shell, an experiment with no MNP core presence was carried out. The results are shown in Figure 61, which clearly shows encapsulation of QD in silica shell. Unfortunately, nanocomposites prepared using aforementioned methodology did not exhibit fluorescent properties. Further experiments showed the sensitivity of QD to water, which was used in the process.

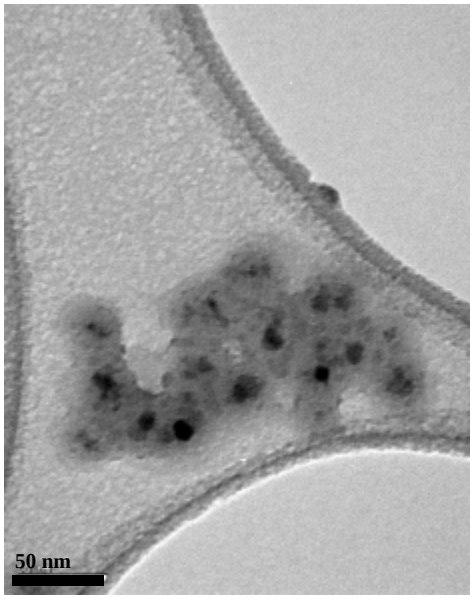


Figure 60. TEM micrograph of MNPs coated with silica and doped with CdSe QD.

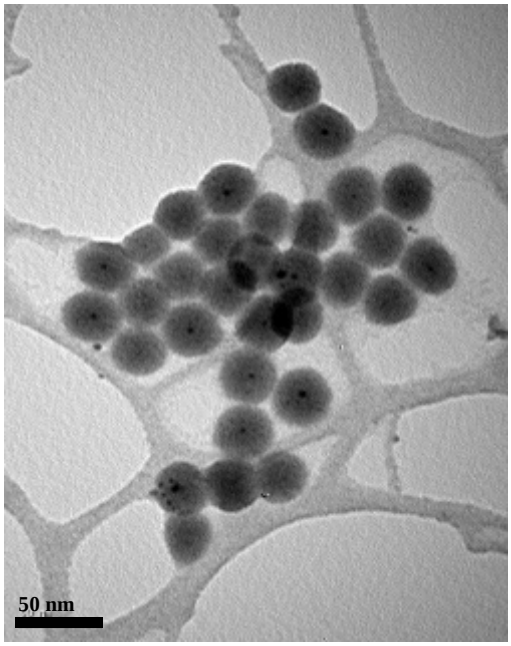


Figure 61. TEM micrograph of CdSe QD coated with silica shell.

Once the water sensitivity of Lumidots CdSe 480 was known, it was decide to use hydrophilic quantum dots (dispersed in water), kindly provided by Dr. Petra Cameron from the Department of Chemistry, University of Bath [170]. The earlier mentioned procedure, using a reverse microemulsion method was used to prepare the magnetic nanocomposites, using QD in water. For synthetic details, see Appendix 2 sec. 3.38. Nanocomposites prepared in this way exhibited high fluorescence. TEM

analysis showed aggregation of MNP/QD/$SiO_2$ (Figure 62). The aggregation of MNP/QD/$SiO_2$ was probably caused by the loss of reverse microemulsion stability.

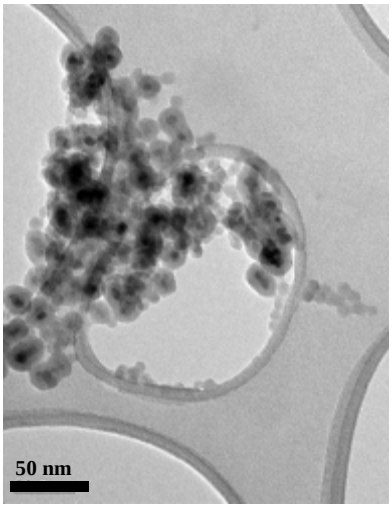


Figure 62. TEM micrograph of MNP/QD/$SiO_2$.

Encouraged by obtained result, it was decided to use this nanocomposite to evaluate the possibility whether this material is able to enter human cells.

### 1.2.1 *In vitro* fluorescence imaging of MNP/QD/$SiO_2$

FEK-4 human cells were cultured at 37 °C in a humidified atmosphere in air and were diluted once confluence had been reached. The culture occurred in Eagle's Minimum Essential Medium (EMEM) containing 15 % foetal calf serum (FCS), 0.5 % penicillin/streptomycin and 1 % L-glutamine. Surplus supernatant containing dead cell matter and excess protein was aspirated. The live adherent cells were then washed with 2 x 10 ml aliquots of phosphate buffer saline (PBS) solution to remove any remaining media containing FCS, which inactivates trypsin. Cells were resuspended in the solution by incubation in 3 ml of trypsin–PBS solution (0.25 % trypsin) for 5 min at 37 °C. After trypsinisation, 5 ml of medium containing the serum was added to inactivate the trypsin and the solution was centrifuged for 5 min (1000 rpm, 25 °C) to remove any remaining dead cell matter. The supernatant liquid was aspirated and 5 ml of medium was added to the cell matter left behind. Cells were counted using a haemocytometer and then seeded as 0.15 million cells in the absence of indicator dyes such as phenol red in Eagles Minimum Essential Medium

(15 % FCS), for 48 h in poly-D-lysine coated dishes. The cells were washed in serum free medium three times prior to the addition of the nanoparticles, and excited using a wavelength of 400 - 500 nm, on an Epi-fluorescent microscope and a laser scanning confocal microscope. For each experiment, images of cells were taken prior to addition, which indicate that cells were healthy, with low background fluorescence and therefore were suitable for nanoparticle addition. Nanoparticles in water (0.5 ml) were added to a doubly concentrated, serum free Eagle's Minimum Essential Medium (0.5 ml) and imaged at several points after initial incubation. Several identical batches of nanoparticles (A, B, and C) were incubated for the first experiment. Due to the relatively large size of the nanoparticles (caused by aggregation) cell uptake was slow and was not observed within 2 h. However, after 3 h it was possible to observe nanoparticles within the cell for batch A (Figure 64). For both A and B the nanoparticles could be seen either attached to the cell surface or within the cell after 4 h incubation followed by washing twice with Phosphate Buffered Saline (PBS) (Figure 66) and (Figure 69). The nanoparticles had not entered all of the cells at this point, indicating that the process of uptake was not rapid and was likely inhibited by poor diffusion (Figure 65). Cell morphology was affected little during the time observed, indicating low toxicity caused by the nanoparticles. These experiments therefore suggest that the nanoparticles have potential to enter cells and to act as MRI imaging agents, but that attachment and entry to cells is slow and further work would be to make smaller, more lipophillic nanoparticles that would have better entry into the cell.

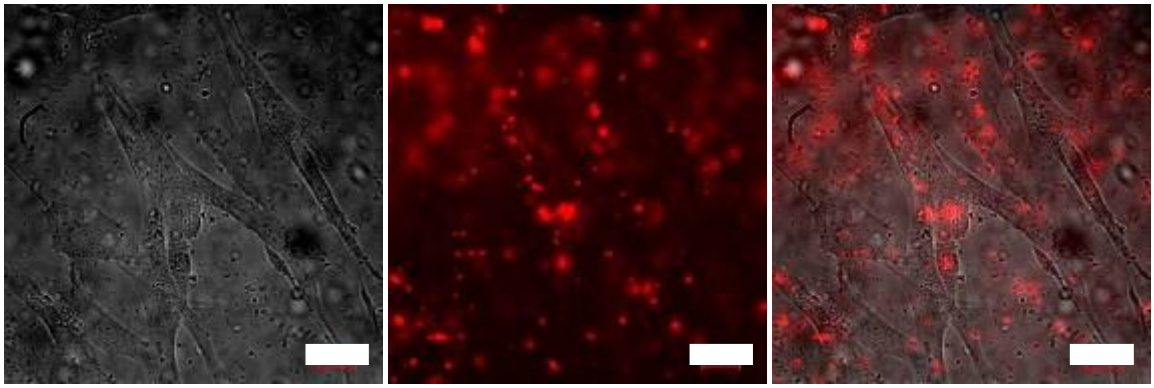

(a) (b) (c)

Figure 63. Nanoparticles from batch A incubated for 30 minutes where (a) is brightfield image, (b) is the fluorescence channel and (c) is an overlay of (a) and (b). Scalebar: 20 µm; image was taken using the Epi-fluorescent microscope.

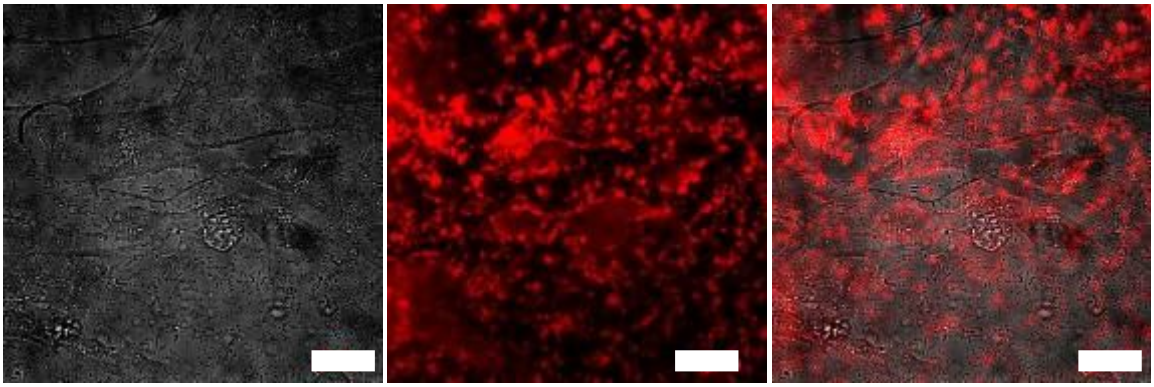

(a) (b) (c)

Figure 64. Nanoparticles from batch A incubated for 3 h indicating uptake into cells where (a) is brightfield image, (b) is the fluorescence channel and (c) is an overlay of (a) and (b). Scalebar: 20 µm; image was taken using the Epi-fluorescent microscope.

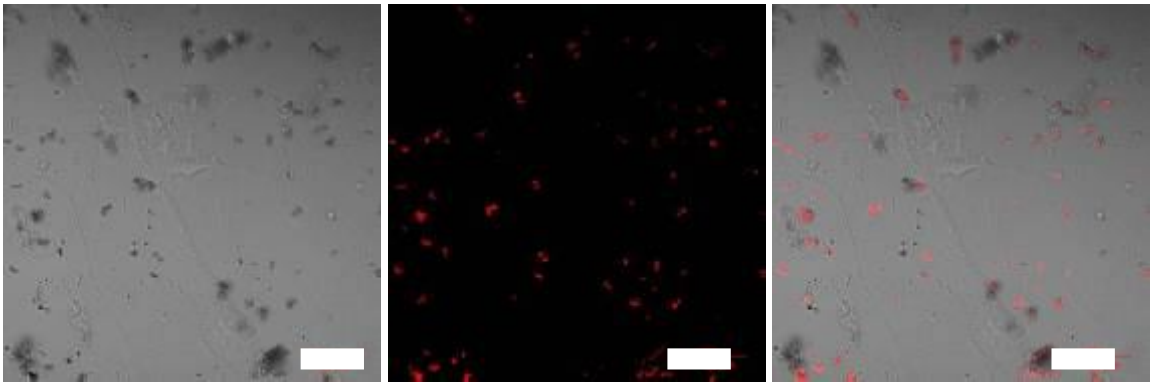

(a) (b) (c)

Figure 65. Nanoparticles from batch A incubated for 4 h, washed twice with PBS and returned to serum free medium where (a) is DIC image, (b) is the fluorescence channel and (c) is an overlay of (a) and (b). Scalebar: 20 µm; image was taken using the laser scanning microscope.

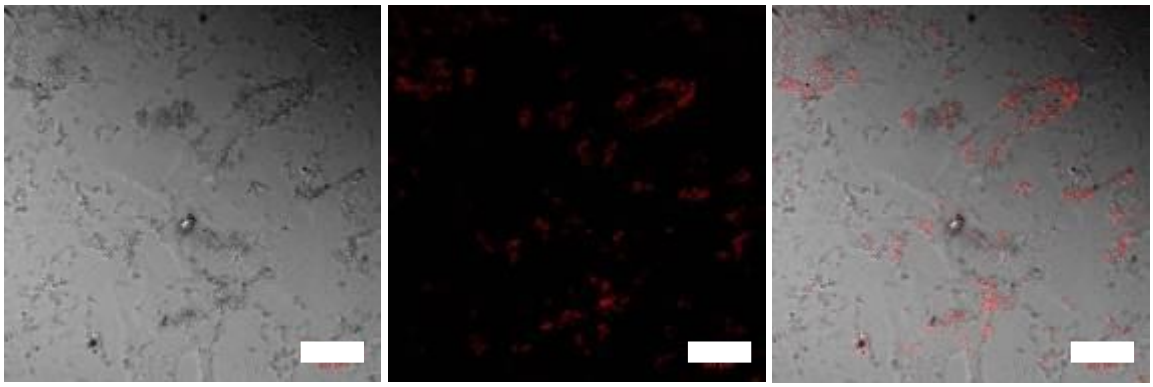

(a) (b) (c)

Figure 66. Nanoparticles from batch A incubated for 4 h, washed twice with PBS and returned to serum free medium where (a) is DIC image, (b) is the fluorescence channel and (c) is an overlay of (a) and (b). Scalebar: 20 µm; image was taken using the laser scanning microscope.

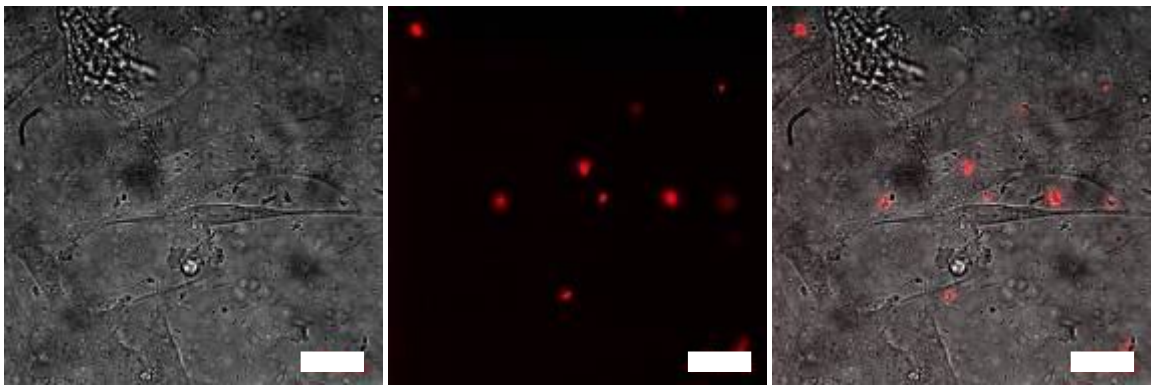

(a) (b) (c)

Figure 67. Nanoparticles from batch B incubated for 30 minutes where (a) is brightfield image, (b) is the fluorescence channel and (c) is an overlay of (a) and (b). Scalebar: 20 µm; image was taken using the Epi-fluorescent microscope.

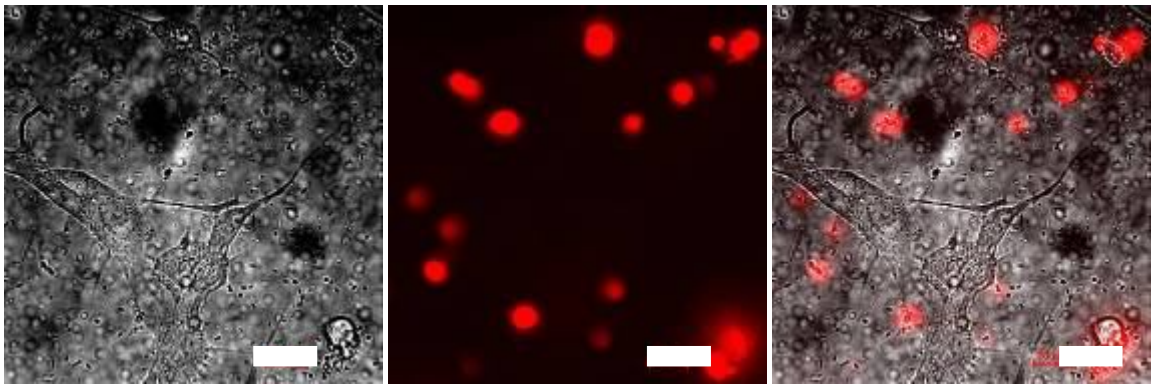

(a) (b) (c)

Figure 68. Nanoparticles from batch B incubated for 60 minutes where (a) is brightfield image, (b) is the fluorescence channel and (c) is an overlay of (a) and (b). Scalebar: 20 µm; image was taken using the Epi-fluorescent microscope**.**

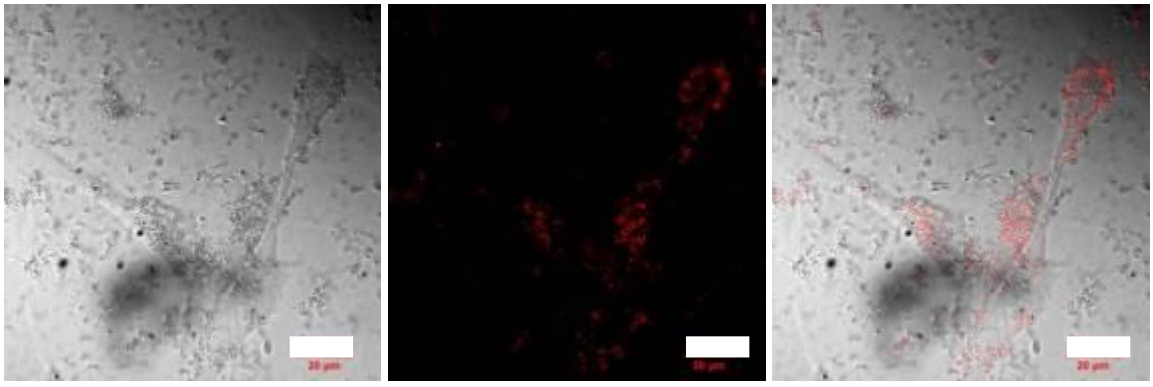

(a) (b) (c)

Figure 69. Nanoparticles from batch B incubated for 4 h, washed twice with PBS and returned to serum free medium where (a) is DIC image, (b) is the fluorescence channel and (c) is an overlay of (a) and (b). Scalebar: 20 µm; image was taken using the laser scanning microscope.

A second experiment under identical conditions was carried out with a third batch of nanoparticles (batch C). For up to 6 h of incubation, the cells appeared healthy, with little nanoparticle cell attachment or uptake.

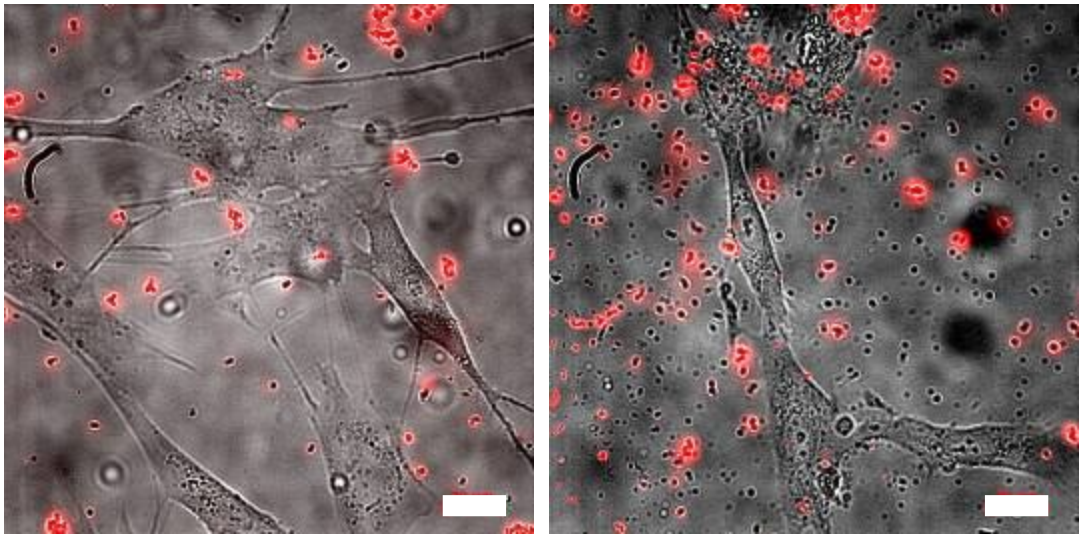

(a) (b)

Figure 70. Nanoparticles from batch C where (a) is the overlay of the brightfield image and fluorescence channel after 40 minutes of incubation and (b) is the overlay of the brightfield image and fluorescence channel after 6 h of incubation followed by washing twice with PBS. Scalebar: 20 µm; image was taken using the Epi-fluorescent microscope.

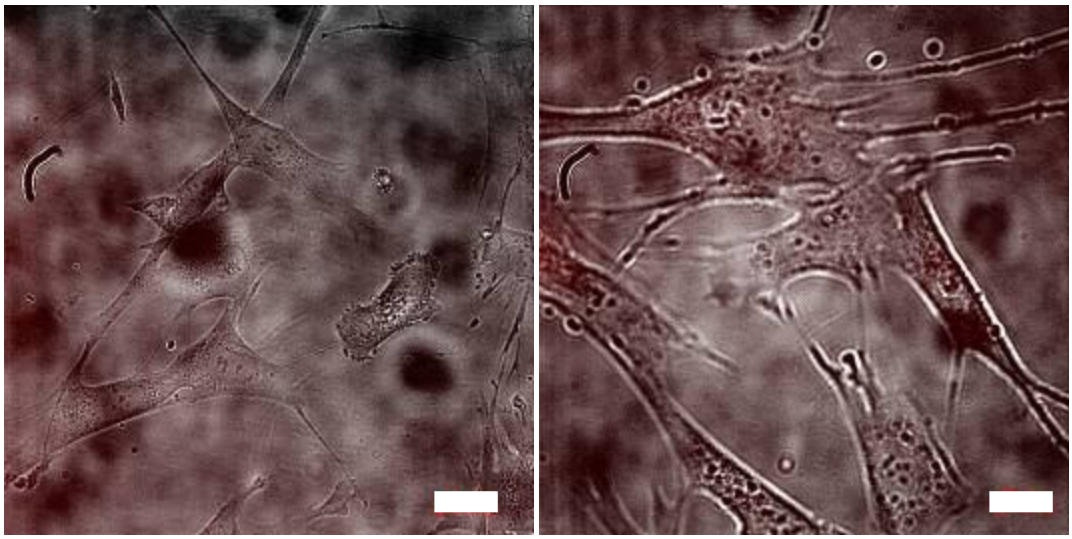

(a) (b)

Figure 71. Control experiments before the addition of nanoparticles (a) is representative of the first experiment and (b) of the second experiment. Scalebar: 20 µm; image was taken using the Epi-fluorescent microscope.

### 1.3 Rhenium modified silica coated MNPs

To prove the possibility of incorporating radioactive metal into the silica shell during the coating process, an experiment with nonradioactive metal salt was carried out. Ammonium perrhenate ($NH_4ReO_4$) was added to cyclohexane during the coating process, and was slowly transferred to the water droplets in the microemulsion and incorporated into the silica shell as it was being formed. For synthetic details, see Appendix 2 sec. 3.39.T EM analysis was carried out, in which slightly agglomerated particles were observed (Figure 72). EDX analysis showed a weak signal for Re in the silica shell (Figure 73). $NH_4ReO_4$ was used as a model for a well-known medical radiotracer ($^{99}TcO_4^-$ and $^{86}ReO_4^-$ ), used for SPECT (single-photon emission computed tomography) or PET imaging.

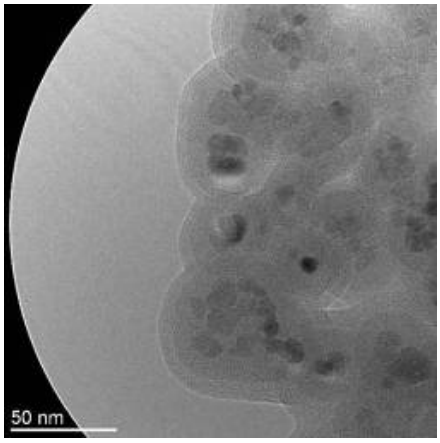


Figure 72. TEM micrograph of rhenium doped silica coated MNPs.

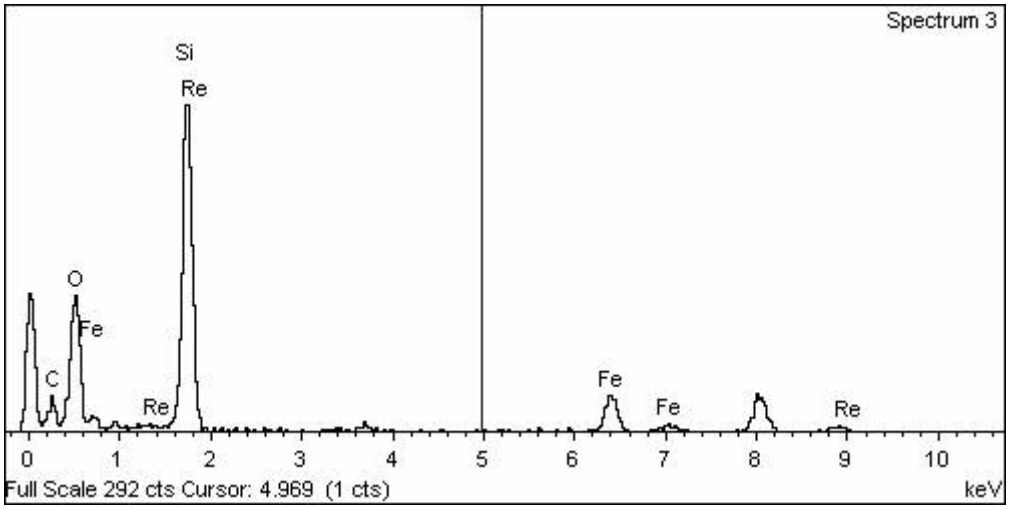


Figure 73. EDX spectrum of Re modified MNP/$SiO_2$ (taken in TEM mode covering a wide area approx. equivalent to the area shown in Figure 72).

### 1.4 $^{64}$Cu modified silica coated MNPs

Based on this result, it was decided to test the possibility for encapsulation of $^{64}$Cu (also know radiotracer for PET techniques). In this experiment radioactive $^{64}Cu(OAc)_2$ (kindly prepared by Dr. Frank Aigbirhio from Wolfson Brain Imaging Centre in Cambridge) was used in order to incorporate radioactive material in a silica shell of MNP/$SiO_2$. Different amounts of $^{64}Cu(OAc)_2$ were added in different orders during the coating microemulsion process in order to optimize the conditions. For synthetic details, see Appendix 2 sec. 3.40. The preparation procedures for $^{64}$Cu modified MNPs are shown in Table 4.

Table 4. The procedures of preparation of $^{64}$Cu modified MNPs.

| Sample | A | B | C | D | E | F |
|---|---|---|---|---|---|---|
| Cyclohexane / ml | 3.5 | 3.5 | 3.5 | 3.5 | 3.5 | 3.5 |
| IGEPAL 520 / g | 0.223 | 0.223 | 0.223 | 0.223 | 0.223 | 0.223 |
| $Fe_3O_4$ / µl | 50 | 50 | 50 | 50 | 50 | 50 |
| Ammonia / µl | 25 | 35 | 5 | 45 | 45 | 45 |
| $^{64}Cu(OAc)_{2(aq)}$ / µl | 40 | 100 | 50 | - | - | - |
| TEOS / µl | 39 | 39 | 39 | 15 | 15 | 15 |
| Time / h | - | - | - | 2 | 2 | 2 |
| $^{64}Cu(OAc)_{2(aq)}$ / µl | - | - | - | 50 | 25 | 100 |
| TEOS / µl | - | - | - | 24 | 24 | 24 |
| Total time / h | 7 | 7 | 7 | 7 | 7 | 7 |

The magnetic nanomaterials resulting from this were separated using a permanent magnet and washed twice with methanol and once with water. The radiolabeled nanoparticles, dispersed in a water solution, were tested for radioactivity after 7 h of encapsulation. Taking into account the half life (12.701 h) of $^{64}$Cu nuclide, encapsulation factors for all samples were calculated. Very promising results are summarized in Table 5. There is a difference between samples A-C and D-F. The smaller encapsulation factors for samples D-F can simply be explained by the shorter reaction time of $^{64}Cu(OAc)_2$ in the reverse microemulsion system.

Table 5. Encapsulation factors for radiolabeling of MNPs.

| Sample | A | B | C | D | E | F |
|---|---|---|---|---|---|---|
| Encapsulation factor | 88 % | 91 % | 94 % | 53 % | 84 % | 78 % |

All samples were characterized using the TEM technique (Figure 74). In comparison to the unchanged reverse microemulsion method, the addition of an aqueous solution of $^{64}Cu(OAc)_2$ has significant influence on the size, shape and agglomeration state of the prepared nanocomposites. The samples A-C were very aggregated, and in the majority of particles, no clear magnetic core was observed. Better results were obtained when a $^{64}Cu(OAc)_2$ solution was added after a precoating period (samples D-F). The best quality nanoparticles (sample E) were obtained for the smallest amount of added $^{64}Cu(OAc)_2$.

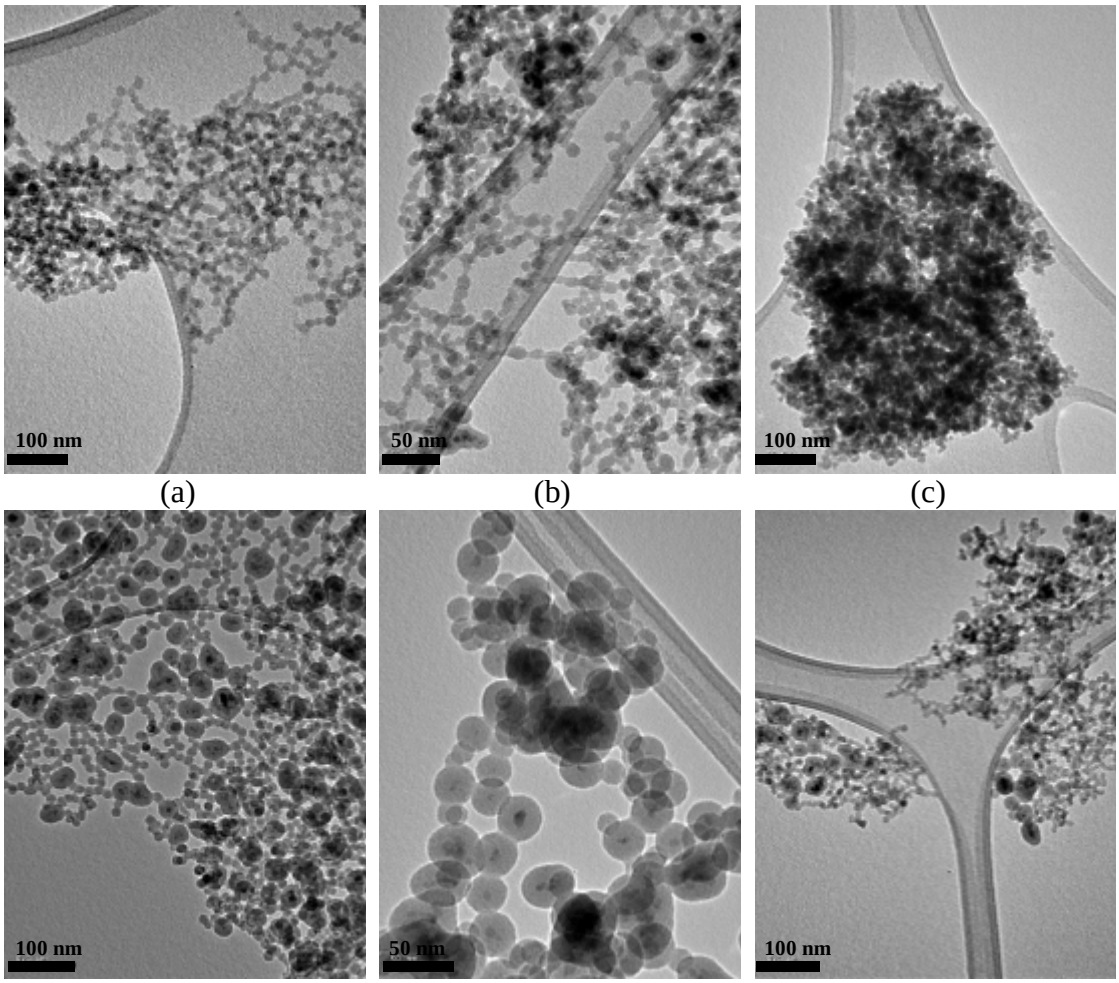


Figure 74. TEM micrographs of silica coated MNPs with addition of $^{64}Cu(OAc)_2$. (a) – sample A, (b) – sample B, (c) – sample C, (d) – sample D, (e) – sample E, (f) – sample F.

In summary, taking into account the encapsulation results and TEM images, sample E is the most promising candidate for future investigation on encapsulation of a $^{64}Cu$ radiotracer.

### 1.5 Conclusions

In conclusion, a method of synthesis for QD-modified, silica-coated magnetic nanoparticles was presented. *In vitro* experiments suggested that the nanoparticles have the potential to enter cells and to act as MRI imaging agents. It was possible to radiolabel the MNPs with $^{64}Cu$ nuclide, which was incorporated in a silica shell. An easy and effective way of incorporating fluorescent and radioactive bodies in the silica shell was shown. This should prevent leaching and sustain the stability of this nanocomposite. Having all necessary entities for multiomodal imaging agents inside

of silica shell there is space for chemistry surface studies on choosing appropriate targeting agents. These results prove the possibility for synthesis of stable tri-modal imaging agent. Chapter 5 described an easy and effective way of incorporating fluorescent quantum dots and radioactive molecules in to the silica shell of nanoparticles. *In vitro* experiments suggested that the nanoparticles have the potential to enter human cells. It was possible to radiolabel the MNPs with $^{64}Cu$ nuclide, which was incorporated in a silica shell. These results proved the possibility for synthesis of a stable multimodal imaging agent. To verify the multimodal imaging capability of nanoparticles, samples should undergo microPET/microMRI scans. Biodistribution and histological studies should be considered to investigate the *in vivo* behaviour and determine nanoparticle uptake by different organs.

# APPENDIX 2

## Materials and methods

## 1 Chemicals

**From Fluka**

ruthenium (III) chloride hydrate purum, ~41 % as Ru

gold (III) chloride hydrate ~50 % as Au

2-butanol

DMF (98 %)

phenylboronic acid

**From Sigma-Aldrich**

benzylaldehyde

benzyl alcohol

diethyl phosphate

ethylene glycol (99 %)

dimethyl fumarate (97 %)

dimethyl maleate ( 96 %)

1-decene (97 %)

sulfuric acid, fuming (20 % $SO_3$)

dimethyl methylsuccinate (98 %)

dimethyl (R)-(+)-methylsuccinate (99 %)

$[Rh(cod)Cl]_2$ (98 %),

R-BINAP - (R)-(+)-(1,1'-Binaphthalene-2,2'-diyl)bis(diphenylphosphine)

dimethyl itaconate (99 %)

ammonium hydroxide (28 % $NH_3$ in water)

hydrochloric acid (37 %)

iron (II) chloride tetrahydrate (99 %),

iron (III) chloride hexahydrate (99 %),

tetramethylammonium hydroxide pentahydrate (99 %),

styrene (99 %)

sodium citrate

sodium periodate

palladium chloride

nitrobenzene (99 %)
ethyl cyanoacetate
potassium acetate
methylene blue
fluorescein
rhodamine B
QD (Lumidot CdSe 5 mg $ml^{-1}$)
aluminum chloride
sodium borohydride
Lutrol® F 127
Pluronic® P-123
furfuryl alcohol
tetraethyl orthosilicate
oleic acid
IGEPAL® CA-520
rhodium (III) chloride
silver nitrate
9-bromophenanthrene

**From Alfa Aesar**

(R)-(+)-2,2',6,6'-Tetramethoxy-4,4'-bis(diphenylphosphino)-3,3'-bipyridine
(R)-(+)-2,2',6,6'-Tetramethoxy-4,4'-bis(di(3,5-xylyl)phosphino)-3,3'-bipyridine

**From Fisher Scientific**

ethanol (96 %)
methanol (HPLC grade)
ethyl acetate (LRG)
hexane (LRG)
MeCN (LRG)
tetrahydrofurane (LRG)
dichloromethane (LRG)
sulphuric acid
2-propanol (LRG)
cyclohexane (LRG)

**2 Instrumentation and exemplar calculations**

The microanalysis was carried out using the Elemental Analyzer CE–440 (EAI External Analytical INC).

The size and morphology of the nanoparticles was characterized by transmission electron microscopy. TEM images were recorded on a JEOL JEM-1200EX II Transmission Electron Microscope (JEOL, Tokyo, Japan) equipped with the Gratan Digital Camera & Digital Micrograph 3.4 Software (Gattan, Oxon, UK).

X-ray diffraction data were obtained using a Philips 4 kW X-ray generator (PW1730) with a CuKa X-ray source (k = 1.54060 Å) and a diffractometer goniometer (PW1820) controlled *via* Philips (PW1877 PC-APD) software.

The metal contents in the supernatants were detected by atomic absorption spectrophotometry (AAS) with a Perkin Elmer Analyst 100 atomic absorption spectrophotometer.

Gas chromatography analyses were carried out on an Agilent Technologies 6890N Network GC System equipped with an HP-5 column 30 m 0.320 mm.

NMR spectra were obtained in $CDCl_3$ and $D_2O$ on a Bruker Avance 300 spectrometer operating at 300 MHz.

X-ray photoelectron spectroscopy (XPS) measurements were performed on a Kratos HSi instrument equipped with an Al Kα monochromated X-ray source and charge neutraliser. High-resolution spectra were recorded at normal emission using analyser pass energy of 40 eV and an X-ray power of 225 W. Energy referencing was performed using the valence band and adventicious carbon at 285 eV.

## 2.1 Example of NMR spectrum interpretation

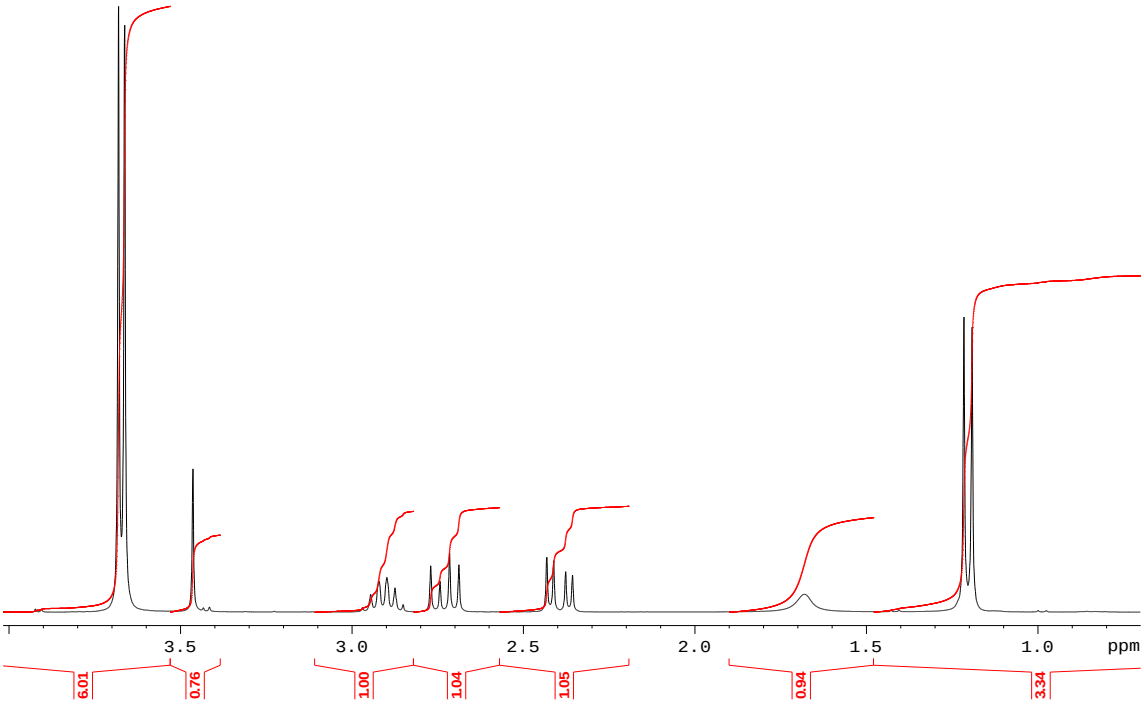


Figure 75. NMR spectrum of the product of hydrogenation of DMIT.

$^1$H NMR ($CDCl_3$): δ = 1.2 (d, 3H, $CH_3$), δ = 2.4 (dd, 1H, CH), δ = 2.7 (dd, 1H, CH) , δ = 2.9 (m, 1H, $CH_3$), δ = 3.6 (2s, 6H, $CH_3$)

## 2.2 Example of GC chromatogram

Conversion was calculated from equation below:

$$X_{NB} = \frac{C_{AN}}{C_{NB} + C_{AN}} 100\%$$

$$X_{NB} = \frac{28868}{66951 + 28868} 100\% = 30\%$$

$X_{NB}$ – conversion of nitrobenzene

$C_{AN}$ –concentration of aniline

$C_{NB}$ – concentration of nitrobenzene

Retention time for aniline 1.905 min, Area of the pick = $C_{AN}$ = 28868

Retention time for nitrobenzene 2.497 min, Area of the pick =$C_{NB}$ = 66951

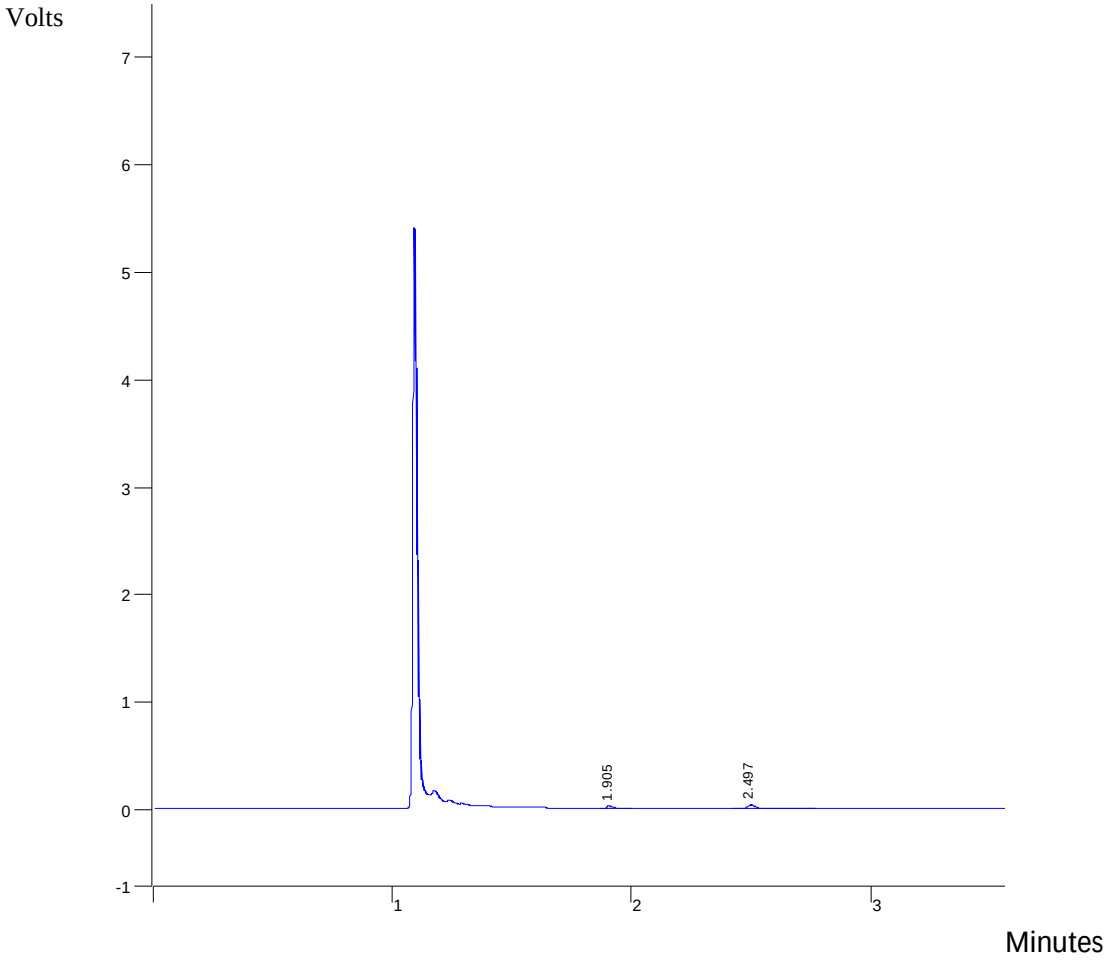


Figure76. GC chromatogram of the product of hydrogenation of nitrobenzene.

**2.3 Example of hydrogen solubility calculations**

$T = 20\ °C$

$log_{10} p_{MeOH} = A - \frac{B}{C+T}$ Antoine equation

*A, B, C* - Antoine coefficients

*A=8.09126*

*B=1582.91*

*C=239.096*

$p_{MeOH} = 0.1279\ bar$

$p_{TOTAL} = p_{H2} + p_{MeOH} = 1bar$

$p_{H2} = p_{TOTAL} - p_{MeOH}$

$p_{H2} = 0.8721\ bar$

$p_{H2} = H\, x_{H2}$ Henry's law

*H* - Hery's constant

$x_{H2}$ - molar fraction of hydrogen in methanol

Henry's constant was calculated from the correlation

$ln(H/MPa) = 122.3 - 4815.6/T(K) - 17.5\ ln(T/K) + 1.4 \times 10^{-7}(P/Pa)$

$H = 648.645\ MPa$

$x_{H2} = 0.000134$

$$x_{H2} = \frac{n_{H2}}{n_{H2} + n_{MeOH}} \approx \frac{n_{H2}}{n_{MeOH}}; \quad n_{H2} << n_{MeOH}$$

$$x_{H2} = \frac{\frac{n_{H2}}{V}}{\frac{n_{MeOH}}{V}} = \frac{c_{H2}}{c_{MeOH}}$$

$C_{H2} = C_{MeOH}\ x_{H2}$

$$C_{MeOH} = \frac{d_{MeOH}}{M_{MeOH}}$$

$C_{H2} = 0.003325\ kmol\ m^{-3}$

## 3 Experimental procedures

### 3.1 Synthesis of iron oxide nanoparticles

$FeCl_3 \cdot 6H_2O$ (5.4 g, 20 mmol) and $FeCl_2 \cdot 4H_2O$ (2.0 g, 10 mmol) were dissolved under $N_2$ in an acidic solution (10.3 mmol HCl in 25 ml $H_2O$), such that $Fe^{3+}$ to $Fe^{2+}$ molar ratio was 2. The prepared solution was added dropwise to 250 ml of a deoxygenated 1.5 M $NH_4OH$ with vigorous stirring. The black precipitate was isolated from the solvent *via* magnetic decantation. The washing-decantation procedure was repeated three times followed by washing twice with 100 ml of 0.1 M TMAOH. The suspension was precipitated with acetone and methanol, and the precipitate dried in vacuum overnight and over $CaCl_2$.

### 3.2 Synthesis of MNP/[R-BINAS-Rh(cod)$Cl_2$]

0.5 g of R-BINAP was dissolved in concentrated sulphuric acid with dropping 20 % $SO_3$ in concentrated sulphuric acid in 50ml round bottom flask and stirring for 3 days at 10 °C under argon. The reaction was quenched by pouring the solution into 100 ml ice-cold water. The product was neutralized by dropwise addition of aqueous sodium hydroxide (50 wt % NaOH) until pH = 7 was reached. The mixture was left for 16 h. The volume of the solution was reduced to 30 ml in a vacuum and 100 ml of methanol was added. Sulfonated R-BINAP (R-BINAS) was recovered as a solid by vacuum drying the filtered methanolic solution.

A round bottom flask was charged with 0.100 g of $[Rh(cod)Cl_2]_2$, 0.03304 g of R- BINAS and 30 ml of pure THF at room temperature and stirred for 1.5 h under argon. THF was evaporated. The flask was charged with 80 ml of methanol and 1.22 g of $Fe_3O_4$ nanoparticles. Immobilization was taken for 3 h in ultrasonic bath. After that, catalyst was washed 3 times with methanol. Catalyst was dried under vacuum for 3 days and over $CaCl_2$.

$^1$H NMR ($D_2O$): δ = 6.8-7.5 (m, 24H, Ar), δ = 7.7 (d, 2H, ArH), δ = 7.9 (d, 2H, ArH), δ = 8.7 (d, 2H, ArH)

$^{31}$P NMR($D_2O$): δ = 14.57

elementary analysis:
Cal: %C = 36.7 %, %H = 1.68 %,
Found: %C = 37.0 %, %H = 2.62 %

### 3.3 Hydrogenation of DMIT on MNP/[R-BINAS-Rh(cod)$Cl_2$]

50 $cm^3$ high pressure stainless steel reactor was charged with 0.791 g of DMIT, 20 ml of methanol and 0.58 g of MNP/[R-BINAS-Rh(cod)$Cl_2$]. It was alternatively purged with $N_2$ and $H_2$ four times and finally filled with $H_2$ up to the pressure of 3.5 bar. The reaction mixture was stirred at 50 °C for 4 h. After the reaction time, the reactor was cooled to room temperature and depressurized to atmospheric pressure. The catalyst was separated by magnetic decantation, washed three times with MeOH and used for the subsequent reaction without further purification. The reaction mixture and supernatants after catalyst washing were collected and solvent evaporated under vacuum.

### 3.4 Synthesis of MNP/[R-P-Phos-Rh(cod)$Cl_2$]

Round bottom flask was charged with 0.0045 g of [Rh(cod)$Cl_2$]$_2$, 0.01 g R-(+)-P-Phos((R)-(+)-2,2',6,6'-Tetramethoxy-4,4'-bis(diphenylphosphino)-3,3'-bipyridine) and 30 ml of pure THF at room temperature and stirred for 1.5 h under argon. THF was evaporated. The flask was charged with 80 ml of methanol and 0.5 g of $Fe_3O_4$ nanoparticles. Immobilization was taken for 3 h in ultrasonic bath. After that, catalyst was washed 3 times with methanol. Catalyst was dried under vacuum for 3 days and over $CaCl_2$.

### 3.5 Synthesis of NP-[R-P-Xyl-Phos-Rh(cod)$Cl_2$]

Round bottom flask was charged with 0.00325 g of [Rh(cod)$Cl_2$]$_2$, 0.01 g of R-(+)-P-Xyl-Phos-((R)-(+)-2,2',6,6'-Tetramethoxy-4,4'-bis(di(3,5-

xylyl)phosphino)3,3'bi-pyridine) and 30 ml of pure THF at room temperature and stirred for 1.5 h under argon. THF was evaporated. The flask was charged with 80 ml of methanol and 0.5 g of $Fe_3O_4$ nanoparticles. Immobilization was taken for 3 h in ultrasonic bath. After that, catalyst was washed 3 times with methanol. Catalyst was dried under vacuum for 3 days and over $CaCl_2$.

### 3.6 Synthesis of MNP/Au(0)

1.00 g of $Fe_3O_4$ nanoparticles were dispersed in 50 ml of 0.1 M TMAOH in two-neck round bottom flask. Solution was diluted using 150 ml of water and stirred with 50 ml of 0.1 M sodium citrate for 10 min. Alternately 0.2 M ammonium hydroxide and 1 % water solution of gold (III) chloride hydrate ($HAuCl_4$) was added incrementally, with a 10 minute break between each addition (Table 6).

Table 6. Alternate addition of ammonium hydroxide ($NH_4OH$) and 1 % water solution of gold(III) chloride hydrate ($HAuCl_4$).

| Iteration | 0.2 M $NH_4OH$ (mL) | 1 % $HAuCl_4$ (mL) |
|---|---|---|
| 1 | 8 | 8 |
| 2 | 3 | 5.5 |
| 3 | 3 | 5.5 |
| 4 | 3 | 5.5 |
| 5 | 3 | 5.5 |
| 6 | 3 | 5.5 |
| 7 | 3 | 5.5 |
| 8 | 3 | 5.5 |
| 9 | 3 | 5.5 |
| 10 | 3 | 5.5 |

### 3.7 Oxidation of alcohols using $H_2O_2$ on MNP/Au(0)

Tubes were charged with dried appropriate amount of MNP/Au(0) catalyst (S/C = 100, 0.14 g; 300, 0.046 g; 600, 0.023 g) and different alcohols 1.11 g of 2-butanol and 1.62 g of benzyl alcohol. Each tube was charged with 0.34 g $H_2O_2$.

Reactions were carried out in 90 °C for 24 h. Catalysts were separated using magnetic decantation.

### 3.8 Oxidation of benzyl alcohol using $O_2$ MNP/Au(0)

Round bottom flask was charged with 0.22 g of benzyl alcohol 10 ml of toluene and 0.073 g of MNP/Au(0) catalyst. The resulting mixture was stirred at 90 °C under $O_2$ flow for 24 h.

### 3.9 Preparation of MNP/Ru(0) catalyst – polyol method

0.025 g of $RuCl_3 \cdot nH_2O$ was dissolved under $N_2$ in 50 ml of ethylene glycol. 1.50 g of dry $Fe_3O_4$ nanoparticles were added and the mixture was heated under reflux to 180 °C for 3 h. Ethylene glycol mixture was then cooled to a room temperature and diluted with 450 ml of 0.3 M $NaNO_{3(aq)}$ solution. The solid was collected by magnetic decantation, washed twice with acetone and dried in air and then in a vacuum and over $CaCl_2$.

### 3.10 Dihydroxylation of alkenes using $NaIO_4$ on MNP/Ru(0)

642 mg (3mmol) of $NaIO_4$ was dissolved in 2 ml of 0.21 M sulphuric acid at 45 °C. The solution was cooled down to 0 °C and 0.247 g of the MNP/Ru(0) was added followed by 12 ml mixture of EtOAc - MeCN (1:1). The mixture was stirred for additional 5 min. Then, 2 mmol of alkenes was added (0.229 ml of styrene, 0.288 g of dimethyl fumarate, 0.250 ml of dimethyl maleate). Excess of acid and $NaIO_4$ was quenched using saturated $NaHCO_3$ solution. The catalyst was separated by magnetic decantation, and supernatant was extracted 3 times using 15 ml of EtOAc.

### 3.11 Dihydroxylation of alkenes using $O_2$ on MNP/Ru(0)

0.2 mmol of alkene (0.229 ml of styrene, 0.288 g of dimethyl fumarate, 0.250 ml of dimethyl maleate, 0.247 g of 1-decene) were diluted in 5 ml of *tert*-butanol and 12.5 ml of aqueous buffer solution (pH = 10). 0.247 g of MNP/Ru(0) was then added. The mixture was stirred at 50 °C under $O_2$ flow for 24 h.

### 3.12 Dihydroxylation of alkenes using $H_2O_2$ on MNP/Ru(0)

0.2 mmol of olefins (0.229 ml of styrene, 0.288 g of dimethyl fumarate, 0.247 g of 1-decene) were dissolved in a mixture of water : acetone (2.48 ml : 7.52 ml). 0.247 g of MNP/Ru(0) and 32 µl of $H_2O_2$ were added. The reaction mixture was stirred for 24 h at room temperature.

### 3.13 Synthesis of MNP/Pd(0)

500 mg of dry $Fe_3O_4$ MNPs were dispersed in 75 ml $H_2O$ and sonicated for 30 min. 26.6 mg (0.15 mmol) $PdCl_2$ was dissolved in 50 µl of HCl in 10 ml of $H_2O$ and added to the dispersion. 25 ml of EtOH (5:1, v/v) was added and solution was stirred for 1 h under the nitrogen. Freshly prepared water solution of $NaBH_4$ (0.04 M) was added dropwise; over 30 min. The mixture was stirred overnight to complete the reaction. MNP/Pd(0) catalyst was separated using magnet, washed with water and ethanol, and dried under vacuum and over $CaCl_2$.

### 3.14 Hydrogenation of DMIT on MNP/Pd(0)

50 $cm^3$ high pressure stainless steel reactor was charged with 1.185 g of DMIT, 20 ml of methanol and 0.25 g of MNP/Pd(0). It was alternatively purged with $N_2$ and $H_2$ four times and finally filled with $H_2$ up to the pressure of 3.5 bar. The reaction mixture was stirred at 50 °C for 4 h. After the reaction time, the reactor was

cooled to room temperature and depressurized to atmospheric pressure. The catalyst was separated by magnetic decantation, washed three times with MeOH and used for the subsequent reaction without further purification. The reaction mixture and supernatants after catalyst washing were collected and solvent evaporated under vacuum.

### 3.15 Hydrogenation of NB on MNP/Pd(0)

50 $cm^3$ high pressure stainless steel reactor was charged with 0.923 g of NB, 20 ml of methanol and 0.25 g of MNP/Pd(0). It was alternatively purged with $N_2$ and $H_2$ four times and finally filled with $H_2$ up to the pressure of 3.5 bar. The reaction mixture was stirred at 50 °C for 4 h. After the reaction time, the reactor was cooled to room temperature and depressurized to atmospheric pressure. The catalyst was separated by magnetic decantation, washed three times with MeOH and used for the subsequent reaction without further purification. The reaction mixture and supernatants after catalyst washing were collected and solvent evaporated under vacuum.

### 3.16 Knoevenagel condensation on MNP/Pd(0)

In the reaction flask (Carousel 12 Reaction Station, Radleys Discovery Technologies, UK), the catalyst (150 mg or 3 mol % Pd) and base (2.25 mmol) were placed and the flask was sealed and purged with argon. 5 ml of dry toluene was added and the suspension was heated to 80 °C. Benzyl aldehyde (1.5 mmol) and ethyl cyanoacetate (1.5 mmol, 170 mg) were dissolved in 0.4 ml of toluene and added *via* syringe to the reaction flask. Samples of reaction mixture were taken at time intervals and analysed by GC. After completion, the reaction mixture was cooled, separated by magnetic decantation, poured into water (10 ml) and extracted with ethyl acetate (3 × 5 ml). The collected organic layers and washing supernatants were washed with water (10 ml) and brine (10 ml) then dried over $MgSO_4$.

### 3.17 Hydrogenation of Knoevenagel condensation product

When quantitative conversion of the condensation reaction was achieved, the reaction temperature was decreased and the hydrogenation was started by bubbling hydrogen through the reaction mixture under stirring at 50 °C. The reaction was monitored by GC and the reaction conversion was calculated on a basis of product amount detected by GC.

### 3.18 Coating of MNPs with an alumina shell

Isotropic solutions were prepared by dissolving $AlCl_3 \cdot 6H_2O$ (0.26 g) precursor and block copolymer F-127 (0.09 g) in EtOH (23 ml) or P-123 (0.10 g) in EtOH (14 ml), and $H_2O$ (20 ml), and 0.3 g of $Fe_3O_4$ nanoparticles was added. 0.45 ml 26-28 % $NH_3 \cdot H_2O$ solution was added dropwise. The solution was refluxed for 1 h. The resulting solution was then aged at 20-22 °C for 20 h. After that, alumina coated nanoparticles were dried and then calcined at 1000 °C for 2 h.

### 3.19 Coating of MNPs with a carbon shell (pluronic method)

0.2 g of $Fe_3O_4$ nanoparticles were suspended in 30 ml of dry toluene. Afterwards, the MNPs were mixed with 1.0 g of Pluronic surfactant P-123 for 4 h. After separation MNPs were dried, and the solid was thermally treated at 850 °C for 2 h under a flow of nitrogen to achieve carbon-protected nanoparticles.

### 3.20 Coating of MNPs with a carbon shell (furfuryl alcohol method)

0.2 g of $Fe_3O_4$ nanoparticles were mixed with 5 ml of furfuryl alcohol in the presence of 0.2g of oxalic acid. The polymerization was carried out at 90 °C for 8 h. After separation MNPs were dried, and the solid was thermally treated at 850 °C for 2 h under a flow of nitrogen to achieve carbon-protected nanoparticles.

### 3.21 Preparation of MNPs and coating of MNPs with a silica shell

$FeCl_3 \cdot 6H_2O$ (2.162 g, 8 mmol) and $FeCl_2 \cdot 4H_2O$ (0.8 g, 4 mmol) were dissolved under $N_2$ in an acidic solution (0.125 ml HCl in 10 ml of $H_2O$). The prepared solution was added dropwise to 100 ml of a deoxygenated 1.5 M $NH_4OH$ with vigorous stirring. The black precipitate was isolated from the solvent *via* magnetic decantation. The washing–decantation procedure was repeated three times followed by adding 100 ml of 0.1 M TMAOH and sonicating for 30 min. 500 ml of 2-propanol was then added and solution was sonicated for additional 1 h. Suspension was heated up to 50 °C and stirred mechanically and 20 ml of ammonia was added following by 4 ml of TEOS (1 ml every 30 min). The mixture was stirred for 4 h and magnetic nanoparticles coated with silica were magnetically separated and washed 3 times with 100 ml of water and 3 times with 100 ml of ethanol. Particles were dried at 50 °C for 1 h and under vacuum overnight.

### 3.22 Synthesis of iron oxide nanoparticles for microemulsion method of coating

10 ml of 1 M of $FeCl_3$ were mixed with 2.5 ml of 2 M $FeCl_2$ dissolved in 2 M HCl. Both solutions were freshly prepared with deoxygenated water before use. Immediately after being mixed under nitrogen, the solution containing the iron chlorides was added to 125 ml of ammonium hydroxide solution (0.7 M) under vigorous mechanical stirring, and under nitrogen atmosphere. After 30 min, the black precipitated formed was separated magnetically and redispersed in a new portion of water (3 × 250 ml). Oleic acid (5 mmol) dissolved in 5 ml of acetone was dropwise added.

### 3.23 Coating of MNPs with a silica shell using microemulsion method

In a typical experiment, 44.60 g of polyoxyethylene(5)isooctylphenyl ether was dispersed in 700 ml of cyclohexane. Then, 200 mg of $Fe_3O_4$ nanoparticles dispersed in cyclohexane (20 mg $ml^{-1}$) was added. The mixture was stirred until it

became transparent. After this step, 9.44 ml of ammonium hydroxide (29 % aqueous solution) was added to form a reverse microemulsion. Finally, 7.70 ml of tetraethylorthosilicate (TEOS) was added. The solution was gently stirred for 16 h. The nanocomposite was precipitated with methanol and separated by magnetic decantation.

### 3.24 Synthesis of metal nanoparticulate catalysts supported on MNP/$SiO_2$

Metal precursors (5.8 mg of $RuCl_3$, 5.9 mg of $RhCl_3$, 4.9 mg of $PdCl_2$, 4.7 mg of $AgNO_3$, 11.1 mg of $HAuCl_4 \cdot 3H_2O$) were dissolved in water. In the case of $PdCl_2$, a 20 µl of HCl (37 %) was added. The solution was heated until the metal salt was completely dissolved. 0.1 g of MNP/$SiO_2$ suspended in 90 ml of water was added. Suspension was agitated using magnetic stirrer and 5 ml of 0.04 M $NaBH_4$ solution was slowly injected over 6 h. Catalyst was separated using magnet washed 3 times with water and once with methanol and then dried in 50 °C and in a vacuum.

### 3.25 Oxidation of benzyl alcohol using $O_2$ on MNP/$SiO_2$/Au(0)

Round bottom flask was charged with 0.22 g of benzyl alcohol 10 ml of toluene and 0.10 g of MNP/$SiO_2$/Au(0) catalyst. The resulting mixture was stirred at 90 °C under $O_2$ flow for 24 h.

Round bottom flask was charged with 10 ml of cyclohexane and 0.10 g of MNP/$SiO_2$/Au(0) catalyst. The resulting mixture was stirred at 80 °C under $O_2$ flow for 6 h.

### 3.26 Epoxidation of benzyl alcohol using $O_2$ on MNP/$SiO_2$/Ag(0)

1.14 ml (10 mmol) of styrene in toluene was mixed with 0.1 g of MNP/$SiO_2$/Ag. and refluxed for 0.5 h in a three-necked flask under magnetic stirring. Then, 6 ml of TBHP in 4 ml of toluene was added dropwise to the mixture in the flask.

### 3.27 Dehydrogenation of benzyl alcohol on MNP/$SiO_2$/Ag(0)

0.1 g of MNP/$SiO_2$/Ag was mixed with 1mmol of benzyl alcohol in 5 ml of p-xylene. The reaction mixture was heated up to 130 °C with continuous stirring under argon atmosphere.

### 3.28 Hydrogenation of DMIT on MNP$SiO_2$/Pd(0), MNP$SiO_2$/Rh(0), MNP$SiO_2$/Ru(0)

50 $cm^3$ high pressure stainless steel reactor was charged with 1.185 g of DMIT, 20 ml of methanol and 0.1 g of MNP$SiO_2$/Pd(0) or MNP$SiO_2$/Rh(0), or MNP$SiO_2$/Ru(0). It was alternatively purged with $N_2$ and $H_2$ four times and finally filled with $H_2$ up to the pressure of 3.5 bar. The reaction mixture was stirred at 50 °C for 4 h. After the reaction time, the reactor was cooled to room temperature and depressurized to atmospheric pressure. The catalyst was separated by magnetic decantation, washed three times with MeOH and used for the subsequent reaction without further purification. The reaction mixture and supernatants after catalyst washing were collected and solvent evaporated under vacuum.

### 3.29 Continuous hydrogenation of DMIT in a flow reactor with magnetically entrapped and manipulated MNP/Pd(0)

The usual procedure was to pump the reaction solution through the capillary until it was level with the bottom of the magnet. Hydrogen gas was injected *via* a HPLC frit from the bottom of the reactor. 1 ml of a suspension containing 0.1 g of MNP/Pd(0) in methanol was then injected using a needle. When the catalyst agglomerated in the magnetic field the rotation of the magnet was started. The initial conditions used for hydrogenation of DMIT were: initial concentration, $C_{DMIT}$ = 0.1 kmol $m^{-3}$, flow rate of methanol solution $\upsilon_L$ = 0.1 $cm^3$ $min^{-1}$, T = 303 K and hydrogen gas flow rate, $\upsilon_{H2}$ = 1 $cm^3$ $min^{-1}$. The usual total reaction time was 8 h. The progress of the reaction was followed by gas chromatographic analysis on samples taking from the level of the top of rotating magnet.

### 3.30 Hydrogenation of DMIT in batch reactor on MNP/Pd(0)

Semi-batch experiment was conducted in 50 ml round bottom flask equipped with tubing for hydrogen delivery. The flask was charged with 0.2 g of MNP/Pd(0) and 30 ml of 0.1 M DMIT solution in methanol. The reaction mixture was heated up to 30 °C with continuous stirring and flow of 1 $cm^3$ $min^{-1}$ of hydrogen was started.

### 3.31 Continuous Suzuki reaction in flow reactor with magnetically entrapped and manipulated MNP/Pd(0)

The usual procedure was to pump the reaction solution through the capillary until it was level with the bottom of the magnet. 1 ml of a suspension containing 0.1 g of MNP/Pd(0) in reaction mixture (DMF/water:70 ml/10 ml, 0.514 g of 9-bromophenanthrene, 0.268 g of $PhB(OH)_2$, 0.1 g of $K_2CO_3$), was then injected using a needle. When the catalyst agglomerated in the magnetic field the rotation of the magnet was started. The initial conditions used were: initial concentration, $C_{9BP}$ = 0.025 kmol $m^{-3}$, flow rate of liquid solution $\upsilon_L$ = 0.1 $cm^3$ $min^{-1}$, T = 383 K. The usual total reaction time was 8 h. The progress of the reaction was followed by gas chromatographic analysis on samples taking from the level of the top of rotating magnet.

### 3.32 Continuous hydrogenation of NB in a microreactor with magnetically entrapped and manipulated MNP/Pd(0)

The glass XXL-ST-04 micromixer-type reactor (channel size 2.2 × 2.2 mm, active volume of micromixers 4.5 ml) was charged with 0.3 g of MNP/Pd(0) suspended in 4.5 ml of the reaction mixture (methanolic solution of NB (0.1 M), *via* the inlet P 3. Then, the permanent magnet (MagDev, UK, surface magnetisation 0.3 T) was placed under the reactor in order to trap the catalytic nanoparticles. After the magnetic sedimentation of the MNP/Pd(0), the catalyst bed was flushed 3 times with the reaction mixture. Then 0.1 M solution of NB was pumped *via* the inlet A 1

using syringe pumps. The inlet A 2 was supplied with the hydrogen Samples were collected from the outlet P 3 and analysed using GC. The initial conditions used for hydrogenation of nitrobenzene were: initial concentration, $c_0$ = 0.1 kmol $m^{-3}$, flow rate of methanol solution $\upsilon_L$ = 0.1 $cm^3$ $min^{-1}$, T = 303 K and hydrogen gas flow rate, $\upsilon_{H2}$ = 0.8 $cm^3$ $min^{-1}$.

**3.33 Continuous hydrogenation of DMIT in a microreactor with magnetically entrapped MNP/Pd(0)**

The glass XXL-ST-04 micromixer-type reactor (channel size 2.2 × 2.2 mm, active volume of micromixers 4.5 ml) was charged with 0.2 g of MNP/Pd(0) suspended in 4.5 ml of the reaction mixture (methanolic solution of DMIT (0.1 M), *via* the inlet P 3. Then, the permanent magnet (MagDev, UK, surface magnetisation 0.3 T) was placed under the reactor in order to trap the catalytic nanoparticles. After the magnetic sedimentation of the MNP/Pd(0), the catalyst bed was flushed 3 times with the reaction mixture. Then 0.1 M solution of DMIT was pumped *via* the inlet A 1 using syringe pumps. The inlet A 2 was supplied with the hydrogen. Samples were collected from the outlet P 3 and analysed using GC. The initial conditions used for hydrogenation of DMIT were: initial concentration, $c_0$ = 0.1 kmol $m^{-3}$, flow rate of methanol solution $\upsilon_L$ = 0.4 $cm^3$ $min^{-1}$, T = 303 K and hydrogen gas flow rate, $\upsilon_{H2}$ = 1.6 $cm^3$ $min^{-1}$.

**3.34 Continuous Knoevenagle-hydrogenation tandem reaction in microreactor with magnetically entrapped MNP/Pd(0).**

The glass XXL-ST-04 micromixer-type reactor (channel size 2.2 × 2.2 mm, active volume of micromixers 4.5 ml) was charged with 0.2 g of MNP/Pd(0) suspended in 4.5 ml of the reaction mixture (ethanolic solution of benzaldehyde (0.1 M), ethyl cyanoacetate (0.1 M), and potassium acetate (0.15 M)) *via* the inlet P 3. Then, the permanent magnet (MagDev, UK, surface magnetisation 0.3 T) was placed under the reactor in order to trap the catalytic nanoparticles. After the

magnetic sedimentation of the MNP/Pd(0), the catalyst bed was flushed 3 times with the reaction mixture. Then 0.1 M solution of benzaldehyde containing 1.5 equiv. KOAc; and 0.1 M solution of ethyl cyanoacetate were pumped (0.05 ml $min^{-1}$ each) *via* the inlet P 3 using two separate syringe pumps. The inlet P 2 (A 3) was supplied with the hydrogen with the flow controlled on the level 0.3 ml $min^{-1}$. Samples were collected from the outlet A 1 and analysed using GC. Temperature of reaction was controlled at 50 °C by the flow of heating medium throughout heat exchange channels.

### 3.35 Continuous hydrogenation of DMIT in microreactor on MNP/$SiO_2$/Pd(0)

In a typical experiment 250 ml of 0.1 M DMIT solution containing 223.2 mg MNP/$Si_2O$/Pd(0) was pumped through the inlet A 1 and contacted with hydrogen pumped through inlet A 2. Reactor was immersed in ultrasonic bath (30 kHz, 50 W). Samples were collected from outlet P 3. Catalyst was separated using a permanent magnet (surface magnetization 0.3 T, MMG MagDev, UK). Samples were analyzing using gas chromatographic analysis. The final product with 100 % conversion was additionally characterized using NMR. The initial conditions used for hydrogenation of DMIT were: initial concentration, $c_0 = 0.1$ kmol $m^{-3}$, flow rate of methanol solution $\upsilon_L$ = 1.0 $cm^3$ $min^{-1}$, T = 293 K and hydrogen gas flow rate, $\upsilon_{H2} = 2.4$ $cm^3$ $min^{-1}$.

### 3.36 Dye-doped silica coated MNPs

In a typical experiment 0.223 g of polyoxyethylene(5)isooctylphenyl ether was dispersed in 3.5 ml of cyclohexane. Then, 1.0 mg of $Fe_3O_4$ dispersed in cyclohexane (20 mg $ml^{-1}$) was added. The mixture was stirred until it became transparent. After this step, 45 µl of ammonium hydroxide (29 % aqueous solution), (containing different amounts of dye: methylene blue 10 mg $ml^{-1}$ fluorescein 20 mg $ml^{-1}$, rhodamine B 10 mg $ml^{-1}$, Rubpy 40 mg $ml^{-1}$) was added to form a

reverse microemulsion. Finally, 39 µl of TEOS was added. The solution was gently stirred for 16 h. The nanocomposite was precipitated with methanol and separated by magnetic decantation.

### 3.37 Hydrophobic QD modified silica coated MNPs

In a typical experiment, 0.223 g of polyoxyethylene(5)isooctylphenyl ether was dispersed in 3.5 ml of cyclohexane. Then, 1.0 mg of $Fe_3O_4$ dispersed in cyclohexane (20 mg $ml^{-1}$) was added, followed by 50 µl of QD (Lumidot CdSe 5 mg $ml^{-1}$). The mixture was stirred until it became transparent. After this step, 45 µl of ammonium hydroxide (29 % aqueous solution) was added to form a reverse microemulsion. Finally, 39 µl of TEOS was added. The solution was gently stirred for 16 h. The nanocomposite was precipitated with methanol and separated by magnetic decantation.

### 3.38 Hydrophilic QD modified silica coated MNPs

In a typical experiment, 0.223 g of polyoxyethylene(5)isooctylphenyl ether was dispersed in 3.5 ml of cyclohexane. Then, 1.0 mg of $Fe_3O_4$ dispersed in cyclohexane (20 mg $ml^{-1}$) was added, followed by 50 µl of QD (water soluble). The mixture was stirred until it became transparent. After this step, 45 µl of ammonium hydroxide (29 % aqueous solution) was added to form a reverse microemulsion. Finally, 39 µl of TEOS was added. The solution was gently stirred for 16 h. The nanocomposite was precipitated with methanol and separated by magnetic decantation.

### 3.39 Rhenium modified silica coated MNPs

In a typical experiment, 0.223 g of polyoxyethylene(5)isooctylphenyl ether was dispersed in 3.5 ml of cyclohexane. Then, 1.0 mg of $Fe_3O_4$ dispersed in cyclohexane (20 mg $ml^{-1}$) was added. The mixture was stirred until it became transparent. After this step, 45 µl of ammonium hydroxide (29 % aqueous solution) was added to form a reverse microemulsion. Finally, 39 µl of TEOS was added. The

solution was gently stirred for 16 h. The nanocomposite was precipitated with methanol and separated by magnetic decantation.

### 3.40 $^{64}$Cu modified silica coated MNPs

In a typical experiment 0.223 g of polyoxyethylene(5)isooctylphenyl ether was dispersed in 3.5 ml of cyclohexane. Then, 1.0 mg of $Fe_3O_4$ was dispersed in cyclohexane (20 mg $ml^{-1}$). The mixture was stirred until it became transparent. After this step, 45 µl of ammonium hydroxide (29 % aqueous solution) was added to form a reverse microemulsion, followed by 15 µl of TEOS. Reaction was carried out for 2 h and 25 µl of $^{64}Cu(OAc)_{2(aq)}$ was added and additional 24 µl of tetraethylorthosilicate (TEOS). The solution was gently stirred for 5 h. The nanocomposite was precipitated with methanol and separated by magnetic decantation.

**References**


1. http://en.wikipedia.org/wiki/Charles_Holland_Duell, 07.02.2012.
2. Yadugiri, V. T., Malhotra, R., *Plenty of room - fifty years after the Feynman lecture.* Current Science, 2010. 99: p. 900-907.
3. Ozin, G.S., Arsenault, A.C., *Nanochemistry*. 2005, Cambridge: The Royal Society of Chemistry.
4. Fendler, J.H., *Nanoparticles and Nanostructured Films.* 1998, Weinheim: Wiley-VCH.
5. Drexler, K.E., *Engines of creation.* 1990, London: Fourth Estate.
6. Grunes, J., Zhu, J., Somorjai, A., *Catalysis and Nanoscience.* Chemical Communitations, 2003. 10: p. 2257-2260.
7. Astruc, D., Lu, F., Aranzaes, J.R., *Nanoparticles as Recyclable Catalysts:The Froniter Between Homogeneous and Hetergeneous Catalysis.* Angewandte Chemie Int. Ed., 2005. 44: p. 7852-7872.
8. Hagen, J., *Industrial Catalysis.* 1999, Weinheim: Wiley-VCH.
9. Thomas, J.M., Thomas, W.J., *Principal and Practice of Heterogeneous Catalysis.* 1996, Weinheim: Wiley-VCH.
10. Hermann, W.A., Cornils, B., *Applied Homogeneous Catalysis with Organometallic Compounds*. 2000, Weinheim: Wiley-VCH.
11. Bell, A.T., *The Impact of Nanoscience on Heterogeneous Catalysis.* Science, 2003. 299: p. 1688-91.
12. Ertl, G., *Handbook of Heterogeneous Catalysis*. Vol. 1. 1997, Weinheim: Wiley-VCH.
13. Jiménez-González, C., Constable, D. J. C., *Green Chemistry and Engineering: A Practical Design Approach.* 2011: Wiley-VCH.
14. Cole-Hamiltone, D.J., *Homogeneous catalysis - new approaches to catalyst separation,recovery and recycling.* Science, 2003. 299: p. 1702-1706.
15. Mansoori, G.A., *Principles of nantechnology*. 2005, Singapore: World Scienctific.
16. Gu, H.W., Xu, K.M., Xu, C.J., Xu, B., *Biofunctional magnetic nanoparticles for protein separation and pathogen detection.* Chemical Communications, 2006 (9): p. 941-949.

17. Bonnemain, B., *Superparamgnetic agents in magnetic resonance imaging: physiochemical characteristics an clinical applications.* Journal of Drug Targeting, 1998. 6: p. 167-174.
18. Corrnell, R.M., Schwertmann, U., *The Iron Oxides: structure, properties, reactions, occurrences and uses.* 2003, Weinheim: Wiley-VCH.
19. Sun, S., Zeng, H., *Size-Controlled Synthesis of Magnetite Nanoparticles.* Journal of the American Chemical Society, 2002. 124 (28): p. 8204-8205.
20. Gupta, A.K., Wells, S., *Surface-modified superparamagnetic nanoparticles for drug delivery: Preparation, characterization, and cytotoxicity studies.* IEEE Transactions on Nanobioscience, 2004. 3 (1): p. 66-73.
21. Gupta, A.K., Gupta, M., *Synthesis and surface engineering of iron oxide nanoparticles for biomedical applications.* Biomaterials, 2005. 26 (18): p. 3995-4021.
22. Lu, A.H., Salabas, E.L., Schuth, F., *Magnetic nanoparticles: Synthesis, protection, functionalization, and application.* Angewandte Chemie-Int. Ed., 2007. 46 (8): p. 1222-1244.
23. Rosensweig, R.E., *Ferrohydrodynamics.* 1997, Cambridge: Cambridge University Press.
24. Koch, C.C., *Nanostructured materials: processing, properties and potential applications.* 2002, Norwich: William Andrew Publishing.
25. Berkovski, B., *Magnetic fluid and application handbook.* 1996, New York: Begell House.
26. Alexandrescu, R., Morjan, I., Crunteanu, A., Cojocaru, S., Petcu, S., Teodorescu, V., Huisken, F., Kohn, B., Ehbrecht, M., *Iron-oxide-based nanoparticles produced by pulsed infrared laser pyrolysis of $Fe(CO)_5$.* Material Chemistry and Physics, 1998. 55: p. 115-121.
27. Rinaldi, C., *Dekker Encyclopedia of Nanoscience and Nanotechnology*. 2004: New York: *Marcel Dekker Inc.*
28. Kim, D.K., Zhang, Y., Voit, W., Rao, K.V., Muhammed, M., *Synthesis and characterization of surfactant-coated superparamagnetic monodispersed iron oxide nanoparticles.* Journal of Magnetism and Magnetic Materials, 2001. 225 (1-2): p. 30-36.

29. Sun, S., Zeng, H., Robinson, D.B., Raoux, S., Rice P.M., Wang, S.X., Li G.X., *Monodisperse $MFe_2O_4$ (M = Fe, Co, Mn) nanoparticles.* Journal of the American Chemical Society, 2004. 126 (1): p. 273-279.
30. Jana, N.R., Chen, Y.F., Peng, X.G., *Size- and shape-controlled magnetic (Cr, Mn, Fe, Co, Ni) oxide nanocrystals via a simple and general approach.* Chemistry of Materials, 2004. 16 (20): p. 3931-3935.
31. Hyeon, T., *Chemical synthesis of magnetic nanoparticles.* Chemical Communications, 2003 (8): p. 927-934.
32. Li, Z., Sun, Q., Gao M.Y., *Preparation of water-soluble magnetite nanocrystals from hydrated ferric salts in 2-pyrrolidone: Mechanism leading to $Fe_3O_4$.* Angewandte Chemie Int. Ed., 2005. 44 (1): p. 123-126.
33. Wang, X., Zhuang, J., Peng, Q., Li, Y.D., *A general strategy for nanocrystal synthesis.* Nature, 2005. 437 (7055): p. 121-124.
34. Deng, H., Li, X.L., Peng, Q., Wang, X., Chen, J.P., Li, Y.D., *Monodisperse magnetic single-crystal ferrite microspheres.* Angewandte Chemie Int. Ed., 2005. 44 (18): p. 2782-2785.
35. Rosano, H.L., *Microemulsion Systems.* 1987. New York: *Marcel Dekker Inc.*
36. Gobe, M., Konno, K., Kandori, K., Kitahara, A., *Preparation and characterization of monodisperse magnetite sols in W/O microemulsion.* Journal of Colloid and Interface Science 1983. 93: p. 293-295.
37. Yaacob, I.I., Nunes, A.C., Bose, A., Shah, D.O., *Synthesis and characterization of magnetic nanoparticles in spontaneously generated vesicles.* Journal of Colloid and Interface Science, 1994. 168: p. 289-301.
38. Igartua, M., Saulnier, P., Heurtault, B., Pech, B., Proust, J.E., Pedraz, J.L., Benoit, J.P., *Development and characterization of solid lipid nanoparticles loaded with magnetite.* International Journal of Pharmaceutics, 2002. 233: p. 149-157.
39. Raj, K., Moskowitz, B., Casciari, R., *Advances in ferrfluid technology.* Journal of Magnetism and Magnetic Materials, 1995. 149: p. 174-180.
40. Vekas, L., Bica, D., *Magnetic nanoparticles and concentrated magnetic nanofluids: Synthesis properties and some applications.* China Particuology, 2007. 5: p. 43-49.

41. Kaloni, P.N., Venkatasubramanian, S., *Flow of a magnetic fluid between eccentric rotating disks.* Journal of Magnetism and Magnetic Materials, 2007. 320: p. 142-149.
42. Chino, N., Tanaka, Y., Fukumura, K., Hiraki, Y., *Magnetic liquid.* 1989: U.S. Patent US 4831961.
43. Papell, S.S., *Low viscosity magnetic fluid obtained by the colloidal suspension of magnetic particles.* 1965. U.S. Patent US32155721965.
44. http://en.wikipedia.org/wiki/Ferrofluid, 24.09.2011.
45. Guin, D., Baruwati, B., Manorama, S.V., *Pd on Amine-Terminated Ferrite Nanoparticles: A Complete Magnetically Recoverable Facile Catalyst for Hydrogenation Reactions.* Organic Letters, 2007. 9 (7): p. 1419-1421.
46. Fan, J., Gao, Y., *Nanoparticle-supported catalysts and catalytic reactions - a mini-review.* Journal of Experimental Nanoscience, 2006. 1 (4): p. 457-475.
47. Tsang, S.C., Caps, V., Paraskevas, I., Chadwick, D., Thompsett, D., *Magnetically Separable, Carbon-Supported Nanocatalysts for the Manufacture of Fine Chemicals.* Angewandte Chemie, 2004. 116 (42): p. 5763-5767.
48. Hu, A., Yee, G.T., Lin, W., *Magnetically Recoverable Chiral Catalysts Immobilized on Magnetite Nanoparticles for Asymmetric Hydrogenation of Aromatic Ketones.* Journal of the American Chemical Society, 2005. 127 (36): p. 12486-12487.
49. Stevens, P.D., Fan, J.D., Gardimalla, H.M.R., Yen, M., Gao, Y., *Superparamagnetic nanoparticle-supported catalysis of Suzuki cross-coupling reactions.* Organic Letters, 2005. 7 (11): p. 2085-2088.
50. Stevens, P.D., Li, G.F., Fan, J.D., Yen, M., Gao, Y., *Recycling of homogeneous Pd catalysts using superparamagnetic nanoparticles as novel soluble supports for Suzuki, Heck, and Sonogashira cross-coupling reactions.* Chemical Communications, 2005 (35): p. 4435-4437.
51. Zheng, Y., Stevens, P.D., Gao Y., *Magnetic nanoparticles as an orthogonal support of polymer resins: Applications to solid-phase Suzuki cross-coupling reactions.* Journal of Organic Chemistry, 2006. 71 (2): p. 537-542.
52. Duanmu, C., Saha, I., Zheng, Y., Goodson, B.M., Gao, Y., *Dendron-functionalized superparamagnetic nanoparticles with switchable solubility in organic and aqueous media: Matrices for homogeneous catalysis and*

*potential MRI contrast agents.* Chemistry of Materials, 2006. 18 (25): p. 5973-5981.

53. Wang, Z.F., Shen, B., Zou, A.H., He, N.Y., *Synthesis of $Pd/Fe_3O_4$ nanoparticle-based catalyst for the cross-coupling of acrylic acid with iodobenzene.* Chemical Engineering Journal, 2005. 113 (1): p. 27-34.
54. Laska, U., Frost, C.G., Price, G.J., Plucinski, P.K., *Easy-separable magnetic nanoparticle-supported Pd catalysts: Kinetics, stability and catalyst re-use.* Journal of Catalysis, 2009. 268 (2): p. 318-328.
55. Zhu, Y.H., Peng, S.C., Emi, A., Zhenshun, S., Monalisa, M., Kemp, R.A., *Supported ultra small palladium on magnetic nanoparticles used as catalysts for suzuki cross-coupling and heck reactions.* Advanced Synthesis & Catalysis, 2007. 349 (11-12): p. 1917-1922.
56. Lv, G.H., Mai, W.P., Jin, R., Gao, L.X., *Immobilization of dipyridyl complex to magnetic nanoparticle via click chemistry as a recyclable catalyst for Suzuki cross-coupling reactions.* Synlett, 2008 (9): p. 1418-1422.
57. Chouhan, G., Wang, D., Alper, H., *Magnetic nanoparticle-supported proline as a recyclable and recoverable ligand for the CuI catalyzed arylation of nitrogen nucleophiles.* Chemical Communications, 2007 (45): p. 4809-4811.
58. Baruwati, B., Guin, D., Manorama, S.V., *Pd on Surface-Modified $NiFe_2O_4$ Nanoparticles: A Magnetically Recoverable Catalyst for Suzuki and Heck Reactions.* Organic Letters, 2007. 9 (26): p. 5377-5380.
59. Laska, U., Frost, C.G., Plucinski, P.K., Price, G.J., *Rhodium containing magnetic nanoparticles: Effective catalysts for hydrogenation and the 1,4-addition of boronic acids.* Catalysis Letters, 2008. 122 (1-2): p. 68-75.
60. Polshettiwar, V., Baruwati, B., Varma, R.S., *Self-Assembly of Metal Oxides into Three-Dimensional Nanostructures: Synthesis and Application in Catalysis.* ACS Nano, 2009. 3 (3): p. 728-736.
61. Polshettiwar, V., Nadagouda, M.N., Varma, R.S., *The synthesis and applications of a micro-pine-structured nanocatalyst.* Chemical Communications, 2008 (47): p. 6318-6320.
62. Liu, J.M., Peng, X.G., Sun, W., Zhao, Y.W., Xia, C.G., *Magnetically Separable Pd Catalyst for Carbonylative Sonogashira Coupling Reactions for the Synthesis of Alkynyl Ketones.* Organic Letters, 2008. 10 (18): p. 3933-3936.

63. Kim, J., Lee, J.E., Lee, J., Jang, Y., Kim, S.W., An, K., Yu, H.H., Hyeon, T., *Generalized Fabrication of Multifunctional Nanoparticle Assemblies on Silica Spheres.* Angewandte Chemie Int. Ed., 2006. 45 (29): p. 4789-4793.

64. Luo, S.Z., Zheng, X.X., Xu, H., Mi, X.L., Zhang, L., Cheng, J.P., *Magnetic Nanoparticle-Supported Morita–Baylis–Hillman Catalysts.* Advanced Synthesis & Catalysis, 2007. 349 (16): p. 2431-2434.

65. Shylesh, S., Schunemann, V., Thiel, W.R., *Magnetically Separable Nanocatalysts: Bridges between Homogeneous and Heterogeneous Catalysis.* Angewandte Chemie Int. Ed., 2010. 49(20): p. 3428-3459.

66. Jun, C.H., Park, Y.J., Yeon, Y.R., Choi, J.R., Lee, W.R., Ko, S.J., Cheon, J., *Demonstration of a magnetic and catalytic Co@Pt nanoparticle as a dual-function nanoplatform.* Chemical Communications, 2006 (15): p. 1619-1621.

67. Yi, D.K., Lee, S.S., Ying, J.Y., *Synthesis and Applications of Magnetic Nanocomposite Catalysts.* Chemistry of Materials, 2006. 18 (10): p. 2459-2461.

68. Rossi, L.M., Silva, F.P., Vono, L.L.R., Kiyohara, P.K., Duarte, E.L., Itri, R., Landers, R., Machado, G., *Superparamagnetic nanoparticle-supported palladium: a highly stable magnetically recoverable and reusable catalyst for hydrogenation reactions.* Green Chemistry, 2007. 9 (4): p. 379-385.

69. Jacinto, M.J., Kiyohara, P.K., Masunaga, S.H., Jardim, R.F., Rossi, L.M., *Recoverable rhodium nanoparticles: Synthesis, characterization and catalytic performance in hydrogenation reactions.* Applied Catalysis A: General, 2008. 338 (1-2): p. 52-57.

70. Jacinto, M.J. Santos, O.H.C.F., Jardim, R.F., Landers, R., Rossi, L.M., *Preparation of recoverable Ru catalysts for liquid-phase oxidation and hydrogenation reactions.* Applied Catalysis A: General, 2009. 360 (2): p. 177-182.

71. Polshettiwar, V., Baruwati, B., Varma, R.S., *Nanoparticle-supported and magnetically recoverable nickel catalyst: a robust and economic hydrogenation and transfer hydrogenation protocol.* Green Chemistry, 2009. 11 (1): p. 127-131.

72. Baruwati, B., Polshettiwar, V., Varma, R.S., *Magnetically recoverable supported ruthenium catalyst for hydrogenation of alkynes and transfer hydrogenation of carbonyl compounds.* Tetrahedron Letters, 2009. 50 (11): p. 1215-1218.

73. Kotani, M., Koike, T., Yamaguchi, K., Mizuno, N., *Ruthenium hydroxide on magnetite as a magnetically separable heterogeneous catalyst for liquid-phase oxidation and reduction.* Green Chemistry, 2006. 8 (8): p. 735-741.

74. Zhang, J.L., Wang, Y., Ji, H., Wei, Y.G., Wu, N.Z., Zuo, B.J., Wang, Q.L., *Magnetic nanocomposite catalysts with high activity and selectivity for selective hydrogenation of ortho-chloronitrobenzene.* Journal of Catalysis, 2005. 229 (1): p. 114-118.

75. Abu-Reziq, R., Wang, D., Post, M., Alper, H., *Platinum nanoparticles supported on ionic liquid-modified magnetic nanoparticles: Selective hydrogenation catalysts.* Advanced Synthesis & Catalysis, 2007. 349 (13): p. 2145-2150.

76. Wang, Y. Lee, J. K., *Recyclable nano-size Pd catalyst generated in the multilayer polyelectrolyte films on the magnetic nanoparticle core.* Journal of Molecular Catalysis A: Chemical, 2007. 263 (1-2): p. 163-168.

77. Panella, B., Vargas, A., Baiker, A., *Magnetically separable Pt catalyst for asymmetric hydrogenation.* Journal of Catalysis, 2009. 261 (1): p. 88-93.

78. Li, J., Zhang, Y.M., Han, D.F., Gao, Q., Li, C., *Asymmetric transfer hydrogenation using recoverable ruthenium catalyst immobilized into magnetic mesoporous silica.* Journal of Molecular Catalysis A: Chemical, 2009. 298 (1-2): p. 31-35.

79. Zhang, S., Zhao, X., Niu, H., Shi, Y., Cai, Y., Jiang, G., *Superparamagnetic $Fe_3O_4$ nanoparticles as catalysts for the catalytic oxidation of phenolic and aniline compounds.* Journal of Hazardous Materials, 2009. 167 (1-3): p. 560-566.

80. Arai, T., Sato, T., Kanoh, H., Kaneko, K., Oguma, K., Yanagisawa, A., *Organic-inorganic hybrid polymer-encapsulated magnetic nanobead catalysts.* Chemistry-A European Journal, 2008. 14 (3): p. 882-885.

81. Shi, F., Tse, M.K., Pohl, M.M., Bruckner, A., Zhang, S.M., Beller, M., *Tuning Catalytic Activity between Homogeneous and Heterogeneous*

*Catalysis: Improved Activity and Selectivity of Free Nano-$Fe_2O_3$ in Selective Oxidations.* Angewandte Chemie, 2007. 119 (46): p. 9022-9024.

82. Polshettiwar, V., Varma, R.S., *Nanoparticle-supported and magnetically recoverable palladium (Pd) catalyst: a selective and sustainable oxidation protocol with high turnover number.* Organic & Biomolecular Chemistry, 2009. 7 (1): p. 37-40.
83. Tong, J.H., Bo, L.L., Li, Z., Lei, Z.Q., Xia, C.G., *Magnetic $CoFe_2O_4$ nanocrystal: A novel and efficient heterogeneous catalyst for aerobic oxidation of cyclohexane.* Journal of Molecular Catalysis A: Chemical, 2009. 307 (1-2): p. 58-63.
84. Aschwanden, L., Panella, B., Rossbach, P., Keller, B., Baiker, A., *Magnetically Separable Gold Catalyst for the Aerobic Oxidation of Amines.* ChemCatChem, 2009. 1 (1): p. 111-115.
85. Mori, K., Kanai, S., Hara, T., Mizugaki, T., Ebitani, K., Jitsukawa, K., Kaneda, K., *Development of Ruthenium Hydroxyapatite-Encapsulated Superparamagnetic $Fe_2O_3$ Nanocrystallites as an Efficient Oxidation Catalyst by Molecular Oxygen.* Chemistry of Materials, 2007. 19 (6): p. 1249-1256.
86. Schatz, A., Grass, R.N., Stark, W.J., Reiser, O., *TEMPO Supported on Magnetic C/Co-Nanoparticles: A Highly Active and Recyclable Organocatalyst.* Chemistry-A European Journal, 2008. 14 (27): p. 8262-8266.
87. Shokouhimehr, M., Piao, Y.Z., Kim, J., Jang, Y.J., Hyeon, T., *A magnetically recyclable nanocomposite catalyst for olefin epoxidation.* Angewandte Chemie Int. Ed., 2007. 46 (37): p. 7039-7043.
88. Tang, H.L.,Yu, C.H., Oduoro, W., He, H.Y., Tsang, S.C., *Engineering of a Monodisperse Core Shell Magnetic Ti-O-Si Oxidation Nanocatalyst.* Langmuir, 2008. 24 (5): p. 1587-1590.
89. Shylesh, S., Schweizer, J., Demeshko, S., Schunemann, V., Ernst, S., Thiela, W.R., *Nanoparticle Supported, Magnetically Recoverable Oxodiperoxo Molybdenum Complexes: Efficient Catalysts for Selective Epoxidation Reactions.* Advanced Synthesis & Catalysis, 2009. 351 (11-12): p. 1789-1795.
90. Zhang, D.H., Li, G.D., Li, J.X., Chen, J.S., *One-pot synthesis of Ag-$Fe_3O_4$ nanocomposite: a magnetically recyclable and efficient catalyst for epoxidation of styrene.* Chemical Communications, 2008 (29): p. 3414-3416.

91. Mori, K., Sugihara, K., Kondo, Y., Takeuchi, T., Morimoto, S., Yamashita, H., *Synthesis and Characterization of Core Shell FePt@Ti-Containing Silica Spherical Nanocomposite as a Catalyst Carrier for Liquid-Phase Reactions.* The Journal of Physical Chemistry C, 2008. 112 (42): p. 16478-16483.

92. Yoon, T.G., Lee, W., Oh. Y.S., Lee, J.K., *Magnetic nanoparticles as a catalyst vehicle for simple and easy recycling.* New Journal of Chemistry, 2003. 27 (2): p. 227-229.

93. Abu-Reziq, R., Alper, H., Wang, D., Post, M.L., *Metal Supported on Dendronized Magnetic Nanoparticles: Highly Selective Hydroformylation Catalysts.* Journal of the American Chemical Society, 2006. 128 (15): p. 5279-5282.

94. Shi, Y.L., Qiu, W., Zheng, Y., *Synthesis and characterization of a POM-based nanocomposite as a novel magnetic photocatalyst.* Journal of Physics and Chemistry of Solids, 2006. 67 (11): p. 2409-2418.

95. Gleeson, O., Tekoriute, R., Gunko Y.K., Connon S.J., The *First Magnetic Nanoparticle-Supported Chiral DMAP Analogue: Highly Enantioselective Acylation and Excellent Recyclability.* Chemistry-A European Journal, 2009. 15 (23): p. 5669-5673.

96. ODálaigh, C., Corr, S.A., Gunko. Y.K., Connon. S.J., *A Magnetic-Nanoparticle-Supported 4-N,N-Dialkylaminopyridine Catalyst: Excellent Reactivity Combined with Facile Catalyst Recovery and Recyclability.* Angewandte Chemie, 2007. 119 (23): p. 4407-4410.

97. Lee, D., Lee, J., Lee, H., Jin, S., Hyeon, T., Kim, B., *Filtration-Free Recyclable Catalytic Asymmetric Dihydroxylation Using a Ligand Immobilized on Magnetic Mesocellular Mesoporous Silica.* Advanced Synthesis & Catalysis, 2006. 348 (1-2): p. 41-46.

98. Polshettiwar, V., Varma, R.S., *Nanoparticle-Supported and Magnetically Recoverable Ruthenium Hydroxide Catalyst: Efficient Hydration of Nitriles to Amides in Aqueous Medium.* Chemistry-A European Journal, 2009. 15 (7): p. 1582-1586.

99. Martinez, R., Ramon, D.J., Yus, M., *Unmodified nano-powder magnetite catalyzes a four-component Aza-Sakurai reaction.* Advanced Synthesis & Catalysis, 2008. 350 (9): p. 1235-1240.

100. Phan, N.T.S., Jones, C.W., *Highly accessible catalytic sites on recyclable organosilane-functionalized magnetic nanoparticles: An alternative to functionalized porous silica catalysts.* Journal of Molecular Catalysis A-Chemical, 2006. 253 (1-2): p. 123-131.

101. Ding, S., Xing, Y., Radosz, M., Shen, Y., *Magnetic nanoparticle supported catalyst for atom transfer radical polymerization.* Macromolecules, 2006. 39 (19): p. 6399-6405.

102. Hara, T., Kaneta, T., Mori, K., Mitsudome, T., Mizugaki, T., Ebitani, K., Kaneda, K., *Magnetically recoverable heterogeneous catalyst: Palladium nanocluster supported on hydroxyapatite-encapsulated* $\gamma$*-*$Fe_2O_3$ *nanocrystallites for highly efficient dehalogenation with molecular hydrogen.* Green Chemistry, 2007. 9 (11): p. 1246-1251.

103. Jiang, Y., Guo, C., Xia, H., Mahmood, I., Liu, C., Liu, H., *Magnetic nanoparticles supported ionic liquids for lipase immobilization: Enzyme activity in catalyzing esterification.* Journal of Molecular Catalysis B-Enzymatic, 2009. 58 (1-4): p. 103-109.

104. Gardimalla, H.M.R., Mandal, D., Stevens, P.D., Yen, M., Gao, Y., *Superparamagnetic nanoparticle-supported enzymatic resolution of racemic carboxylates.* Chemical Communications, 2005 (35): p. 4432-4434.

105. Zheng, Y., Duanmu, C., Gao, Y., *A Magnetic Biomimetic Nanocatalyst for Cleaving Phosphoester and Carboxylic Ester Bonds under Mild Conditions.* Organic Letters, 2006. 8 (15): p. 3215-3217.

106. Neuberger, T., Schopf, B., Hofmann, H., Hofmann, M., Vonrechenberg, B., *Superparmagnetic nanoparticles for biomedical applications. Possibilities and limitations of new drug delivery system.* Journal of Magnetism and Magnetic Materials, 2005. 293: p. 483-496.

107. McBain, S.C.; Yiu, H.H.P., Dobson, J., *Magnetic nanoparticles for gene and drug delivery.* International Journal of Nanomedicine, 2008. 3 (2): p. 169-180.

108. Zhang, Y., Zhang, J., *Surface modification of monodisperse magnetite nanoparticles for improved intracellular uptake to breast cancer cells.* Colloid and Interface Science, 2005. 283: p. 352-357.

109. Berry, C.C., Curtis, A.S.G., *Functionalisation of magnetic nanoparticles for applications in biomedicine.* Journal of Physics D, 2003. 36: p. 198-206.

110. Tomasovicova, N., Koneracka, M., Kopcansky, P., Timko, M., Zavisova, V., *Infared study of biocompatible magnetic nanoparticles.* Measurement Science Review, 2006. 6: p. 32-35.

111. Babincova, M., Sourivong, P., Leszczynska, D., Babinec, P., *Blood-specific whole-body electrmagnetic hyperthermia.* Medical Hypotheses, 2000. 66: p. 459-460.

112. Moore, A., Marecos, E., Bogdanov, A., Weissleder, R., *Tumoral distribution of long-circulating dextran-coated iron oxide nanoparticles in a rodent model.* Radiology, 2000. 214: p. 586-574.

113. Gupta, A., Naregalkar, R.R., *Recent advances on surface engineering of magnetic iron oxide nanoparticles and their biomedical applications.* Nanomedicine, 2007. 2: p. 23-29.

114. Lubbe, A., Alexiou, C., *Clinical applications of magnetic drug targeting.* Journal of Surgical Research, 2000. 95: p. 200-206.

115. Bonnadonna, G., Gianni, L., *Drugs ten years later: epirubicin.* Annals of Oncology, 1993. 4(359).

116. Hilger, I., Andra, W., Hergt, R., Hiergeist, R., Schubert, H., Kaiser, W.A., *Electromagnetic Heating of Breast Tumors in Interventional Radiology: In Vitro and in Vivo Studies in Human Cadavers and Mice.* Radiology, 2001. 218: p. 570-575.

117. Lyon, J. L., Fleming, D. A., Stone, M. B., Schiffer, P., Williams, M. E. *Synthesis of Fe oxide core/Au shell nanoparticles by iterative hydroxylamine seeding.* Nano Letters, 2004. 4 (4): p. 719-723.

118. Wan, K.T., Davis, M., *Asymmetric Hydrogenation in Water by a Rhodium Complex of Sulfonated 2,2'-Bis( dipheny1phosphino)-I ,I '-binaphthyl (binap).* Chemical Communitations, 1993: p. 1263.

119. Ohta, T., Takaya, H. and Noyori, R., *BINAP-Ruthenium(II) Dicarboxylate Complexes: New, Highly Efficient Catalysts for Asymmetric Hydrogenations.* Inorganic Chemistry, 1988. 27 p. 566-569.

120. Zhang, S., Gao, S., Xi, Z., Xu, J. *Solvent-free oxidation of alcohols catalyzed by an efficient and reusable heteropolyphosphatotungstate.* Catalysis Communications, 2007. 8: p. 531-534.

121. Nishimura, T., Onoue, T., Ohe, K., Uemura, S., *Palladium (II)-Catalyzed Oxidation of Alcohols to Aldehydes and Ketones by Molecular Oxygen. The* Journal of Organic Chemistry, 1999, 64 (18), p. 6750–6755.

122. Kurihara, L.K., Chow, G.M., Schoen, P.E., *Nanocrystalline Metallic Powders and Films Produced by the Polyol Method.* Nano Structured Materials, 1995. 5: p. 607-6013.

123. Ho, C.M., Yu, W.Y., Che, C.M, *Ruthenium Nanoparticles Supported on Hydroxyapatite as an Efficient and Recyclable Catalyst for cis-Dihydroxylation and Oxidative Cleavage of Alkenes.* Angewandte Chemie, 2004. 43: p. 3303-3307.

124. Dobler C., Mehltretter, G.M., Sundermeier, U., Beller, M., *Dihydroxylation of olefins using air as the terminal oxidant.* Journal of Organometallic Chemistry, 2001. 621: p. 70-76.

125. Jonsson, S.Y., Farnegardh, K., Backvall, J.E., *Osmium-Catalyzed Asymmetric Dihydroxylation of Olefins by $H_2O_2$ Using a Biomimetic Flavin-Based Coupled Catalytic System.* Journal of the American Chemical Society, 2001. 123: p. 1365 -1371.

126. Smith, M.B., March, J., Smith, B., *March's Advanced Organic Chemistry: Reactions, Mechanisms, and Structure*. Wiley-Interscience. 2007.

127. Lu, Y., Yin, Y.D., Mayers, B.T., Xia, Y.N., *Modifying the surface properties of superparamagnetic iron oxide nanoparticles through a sol-gel approach.* Nano Letters, 2002. 2 (3): p. 183-186.

128. Wan, L.J., Fu, H.G., Shi, K.Y., Tian, X.Q., *Simple synthesis of mesoporous alumina thin films.* Materials Letters, 2008. 62 (10-11): p. 1525-1527.

129. Lu, A. H., Li, W. C., Matoussevitch, N., Spliethoff, B., Bonnemann, H. Schuth, F., *Highly stable carbon-protected cobalt nanoparticles and graphite shells.* Chemical Communications, 2005 (1): p. 98-100.

130. Almeida, C., Zarbin, A.J.G., *Hollow porous carbon microspheres obtained by the pyrolysis of $TiO_2$/poly(furfuryl alcohol) composite precursors.* Carbon, 2006. 44 (14): p. 2869-2876.

131. Nakao, Y., Kaeriyama, K., *Preparation of Noble-Metal Sols in the Presence of Surfactants and Their Properties.* Journal of Colloid and Interface Science, 1986. 110 (1): p. 82-87.

132. Zhu, K.K., Hu, J.C., Richards, R., *Aerobic oxidation of cyclohexane by gold nanoparticles immobilized upon mesoporous silica.* Catalysis Letters, 2005. 100 (3-4): p. 195-199.

133. Mitsudome, T., Mikami, Y., Funai, H., Mizugaki, T., Jitsukawa, K., Kaneda, K., *Heterogeneous catalysis - Oxidant-free alcohol dehydrogenation using a reusable hydrotalcite-supported silver nanoparticle catalyst.* Angewandte Chemie Int. Ed., 2008. 47 (1): p. 138-141.

134. Saaby, S., Knudsen, K.R., Ladlow, M., Ley, S.V., *The use of a continuous flow-reactor employing a mixed hydrogen-liquid flow stream for the efficient reduction of imines to amines.* Chemical Communications, 2005 (23): p. 2909-2911.

135. Kirschning, A., Solodenko, W., Mennecke, K., *Combining enabling techniques in organic synthesis: Continuous flow processes with heterogenized catalysts.* Chemistry-A European Journal, 2006. 12 (23): p. 5972-5990.

136. Schatz, A., Grass, R. N., Kainz, Q., Stark, W. J., Reiser, O., *Cu(II)-Azabis(oxazoline) Complexes Immobilized on Magnetic Co/C Nanoparticles: Kinetic Resolution of 1,2-Diphenylethane-1,2-diol under Batch and Continuous-Flow Conditions.* Chemistry of Materials, 2010. 22 (2): p. 305-310.

137. Olle, B., Bucak, S., Holmes, T. C., Bromberg, L., Hatton, T. A., Wang, D. I., *Enhancement of oxygen mass transfer using functionalized magnetic nanoparticles.* Industrial & Engineering Chemistry Research, 2006. 45 (12): p. 4355-4363.

138. d'Angelo, J.V.H., Francesconi, A.Z., *Gas-liquid solubility of hydrogen in n-alcohols (1<= n <= 4) at pressures from 3.6 MPa to 10 MPa and temperatures from 298.15 K to 525.15 K.* Journal of Chemical and Engineering Data, 2001. 46 (3): p. 671-674.

139. Lange, N.A., *Handbook of Chemistry*. 2005, New York: McGraw-Hill.

140. Jensen, K.F., *Microreaction engineering - is small better?* Chemical Engineering Science, 2001. 56 (2): p. 293-303.

141. Ahmed-Omer, B., Brandt, J.C., Wirth, T., *Advanced organic synthesis using microreactor technology.* Organic & Biomolecular Chemistry, 2007. 5 (5): p. 733-740.

142. Watts, P., Haswell, S.J., *The application of micro reactors for organic synthesis.* Chemical Society Reviews, 2005. 34 (3): p. 235-246.

143. Geyer, K., Codee, J.D.C., Seeberger, P.H., *Microreactors as tools for synthetic chemists - The chemists' round-bottomed flask of the 21st century?* Chemistry-A European Journal, 2006. 12 (33): p. 8434-8442.

144. Watts, P., Wiles, C., *Recent advances in synthetic micro reaction technology.* Chemical Communications, 2007 (5): p. 443-467.

145. Mason, B. P., Price, K. E., Steinbacher, J. L., Bogdan, A. R., McQuade, D.T., *Greener approaches to organic synthesis using microreactor technology.* Chemical Reviews, 2007. 107 (6): p. 2300-2318.

146. Frost, C.G., Mutton, L., *Heterogeneous catalytic synthesis using microreactor technology.* Green Chemistry, 2010. 12 (10): p. 1687-1703.

147. Navascuel, N., Escuin, M., Rodas, Y., Irusta, S., Mallada, R., Santamari, J., *Combustion of Volatile Organic Compounds at Trace Concentration Levels in Zeolite-Coated Microreactors.* Industrial & Engineering Chemistry Research. 49 (15): p. 6941-6947.

148. Kobayashi, J., Mori, Y., Kobayashi, S., *Triphase hydrogenation reactions utilizing palladium-immobilized capillary column reactors and a demonstration of suitability for large scale synthesis.* Advanced Synthesis & Catalysis, 2005. 347 (15): p. 1889-1892.

149. Wang, N.W., Matsumoto, T., Ueno, M., Miyamura, H., Kobayashi, S., *A Gold-Immobilized Microchannel Flow Reactor for Oxidation of Alcohols with Molecular Oxygen.* Angewandte Chemie Int. Ed., 2009. 48 (26): p. 4744-4746.

150. Hwang, S.M., Kwon, O.J., Ahn, S.H., Kim, J.J., *Silicon-based micro-reactor for preferential CO oxidation.* Chemical Engineering Journal, 2009. 146 (1): p. 105-111.

151. Liu, J.Y., Lin, S., Qi, D.W., Deng, C.H., Yang, P.Y., Zhang, X.M., *On-chip enzymatic microreactor using trypsin-immobilized superparamagnetic nanoparticles for highly efficient proteolysis.* Journal of Chromatography A, 2007. 1176 (1-2): p. 169-177.

152. Wei, Z.H., Lee, C.P., Lai, M.F., *Magnetic Force Switches for Magnetic Fluid Micromixing.* Japanese Journal of Applied Physics, 2010. 49 (1).

153. Park, C.P., Kim, D.P., *A Microchemical System with Continuous Recovery and Recirculation of Catalyst-Immobilized Magnetic Particles.* Angewandte Chemie Int. Ed., 2010. 49 (38): p. 6825-6829.

154. Karmakar, B., Chowdhury, B., Banerji, J., *Mesoporous titanosilicate Ti-TUD-1 catalyzed Knoevenagel reaction: An efficient green synthesis of trisubstituted electrophilic olefins.* Catalysis Communications. 11 (7): p. 601-605.

155. Ehrfeld, W., Hessel, V., Löwe, H., *Microreactors: New Technology for Modern Chemistry*. 2000, Weinheim: WILEY-VCH.

156. Jennings, L.E., Long, N.J., *'Two is better than one'-probes for dual-modality molecular imaging.* Chemical Communications, 2009 (24): p. 3511-3524.

157. Choi, J.S., Park, J.C., Nah, H., Woo, S., Oh, J., Kim, K.M., Cheon, G.J., Chang, Y., Yoo, J., Cheon, J., *A Hybrid Nanoparticle Probe for Dual-Modality Positron Emission Tomography and Magnetic Resonance Imaging.* Angewandte Chemie, 2008. 120 (33): p. 6355-6358.

158. Judenhofer, M.S., Wehrl, H.F., Newport, D.F., Catana, C., Siegel, S.B., Becker, M.,; Thielscher, A., Kneilling, M., Lichy, M.P., Eichner, M., Klingel, K., Reischl, G., Widmaier, S., Rocken, M., Nutt, R.E., Machulla, H.J., Uludag, K., Cherry, S.R., Claussen, C.D., Pichler, B.J., *Simultaneous PET-MRI: a new approach for functional and morphological imaging.* Nat Med, 2008. 14 (4): p. 459-465.

159. Frullano, L., Catana, C., Benner, T., Sherry, A.D., Caravan, P., *Bimodal MR–PET Agent for Quantitative pH Imaging.* Angewandte Chemie Int. Ed., 49 (13): p. 2382-2384.

160. Fang, C., Zhang, M., *Multifunctional magnetic nanoparticles for medical imaging applications.* Journal of Materials Chemistry, 2009. 19 (35): p. 6258-6266.

161. Kim, J., Piao, Y., Hyeon, T., *Multifunctional nanostructured materials for multimodal imaging, and simultaneous imaging and therapy.* Chemical Society Reviews, 2009. 38 (2): p. 372-390.

162. Lee, H.Y., Li, Z., Chen, K., Hsu, A.R., Xu, C.J., Xie, J., Sun, S.H., Chen, X.Y., *PET/MRI Dual-Modality Tumor Imaging Using Arginine-Glycine-Aspartic (RGD)-Conjugated Radiolabeled Iron Oxide Nanoparticles.* Journal of Nuclear Medicine, 2008. 49 (8): p. 1371-1379.

163. Jarrett, B.R., Gustafsson, B., Kukis, D.L., Louie, A.Y., *Synthesis of 64Cu-Labeled Magnetic Nanoparticles for Multimodal Imaging.* Bioconjugate Chemistry, 2008. 19 (7): p. 1496-1504.

164. Devaraj, N.K., Keliher, E.J., Thurber, G.M., Nahrendorf, M., Weissleder, R., *$^{18}$F Labeled Nanoparticles for in Vivo PET-CT Imaging.* Bioconjugate Chemistry, 2009. 20 (2): p. 397-401.

165. Xie, J., Chen, K., Huang, J., Lee, S., Wang, J.H., Gao, J., Li, X.G., Chen, X., *PET/NIRF/MRI triple functional iron oxide nanoparticles.* Biomaterials. 31 (11): p. 3016-3022.

166. Glaus, C., Rossin, R., Welch, M.J., Bao, G., *In Vivo Evaluation of 64Cu-Labeled Magnetic Nanoparticles as a Dual-Modality PET/MR Imaging Agent.* Bioconjugate Chemistry. 21 (4): p. 715-722.

167. de Rosales, R.T.M., Tavare, R., Paul, R.L., Jauregui-Osoro, M., Protti, A., Glaria, A., Varma, G., Szanda, I., Blower, P.J., *Synthesis of 64CuII–Bis (dithiocarbamatebisphosphonate) and Its Conjugation with Superparamagnetic Iron Oxide Nanoparticles: In Vivo Evaluation as Dual-Modality PET–MRI Agent.* Angewandte Chemie Int. Ed., 2011. 50 (24): p. 5509-5513.

168. Wu, H., Huo, Q.S., Varnum, S., Wang, J., Liu, G.G.; Nie, Z.M., Liu, J., Lin, Y.H., *Dye-doped silica nanoparticle labels/protein microarray for detection of protein biomarkers.* Analyst, 2008. 133 (11): p. 1550-1555.

169. Michalet, X., Pinaud, F.F., Bentolila, L.A., Tsay, J.M., Doose, S., Li, J.J., Sundaresan, G., Wu, A.M., Gambhir, S.S., Weiss, S., *Quantum Dots for Live Cells, in Vivo Imaging, and Diagnostics.* Science, 2005. 307 (5709): p. 538-544.

170. Cameron, P.J., Zhong, X.H., Knoll, W., *Monitoring the covalent binding of quantum dots to functionalized gold surfaces by surface plasmon resonance spectroscopy.* Journal of Physical Chemistry C, 2007. 111 (28): p. 10313-10319.